AUTOPHAGY REGULATES SEX STEROID SYNTHESIS IN HUMAN OVARY

by

Françesko Hela

A Dissertation Submitted to the
Graduate School of Health Sciences in Partial
Fulfillment of the Requirements for the Degree
of

Doctor of Philosophy

in

Molecular and Cellular Medicine

January 25, 2022

AUTOPHAGY REGULATES SEX STEROID SYNTHESIS IN HUMAN OVARY

Koc University

Graduate School of Health Sciences

This is to certify that I have examined this copy of a doctoral dissertation by

Françesko Hela

and have found that it is complete and satisfactory in all respects,
and that any and all revisions required by the final
examining committee have been made.

Committee Members:

Prof. Dr. Özgür Öktem (Advisor)

Prof. Dr. Afsun Şahin

Assist. Prof. Serçin Karahüseyinoğlu

Prof. Dr. Süleyman Nezih Hekim

Assoc. Prof. Gamze Tanrıverdi

Date: _____

"Science, my lad, is made up of mistakes, but they are mistakes which it is useful to make, because they lead little by little to the truth."

Jules Verne

Dedicated to the most important women in my life: My grandmother and my mom. Their love and dedication made me who I am today.

ABSTRACT

AUTOPHAGY REGULATES SEX STEROID SYNTHESIS IN HUMAN OVARY

Autophagic process is evolutionarily conserved process that aims to maintain the energy homeostasis of the cell by recycling long-lived proteins and organelles. Emerging data indicates that autophagy also regulates lipid metabolism in a process called lipophagy. Here we describe a novel role of autophagy in steroid biosynthesis in human ovary. Pharmacological inhibition or genetic interruption of autophagic process through silencing of autophagy genes (Beclin1 and ATG5) via siRNA and shRNA technologies significantly compromised steroidogenesis and resulted in a dose-dependent and progressive decline in basal and gonadotropin-stimulated estradiol (E_2) and progesterone (P_4) production of the explant cultures of corpus luteum and the primary and immortalized human granulosa cells. Blockage of autophagy was also associated with a marked cytoplasmic accumulation of the lipid droplets (LDs), which strongly co-localized with autophagy substrates (LC3 and SQSTM1/p62) and lysosome. Furthermore, we found that the expression of the autophagy genes, the co-localization of the LDs with autophagosome and lysosome are defective and, autophagy-mediated steroidogenesis are compromised in the corpora luteae of the patients who had clinically documented luteal phase defect due to their inability to produce P_4 in sustainable levels to maintain pregnancy and prevent miscarriage. More interestingly, pharmacological induction of autophagy with rapamycin together with luteotropic hCG administration had a synergistic effect on steroidogenesis and autophagy and drastically corrected defective P_4 production in the luteal GCs of these patients in vitro. Taken collectively these findings suggest that autophagy plays a pivotal role in basal and gonadotropin-stimulated steroidogenesis by promoting the association of the LDs with lysosome to deliver the lipid cargo within the LDs to lysosomes for degradation in order to release free cholesterol required for steroid synthesis in human ovary. Given that P_4 hormone is essential for preparation of endometrium for implantation and maintenance of pregnancy, our findings may have significant clinical implications and open a new avenue in the treatment of infertility, pregnancy-related complications, and miscarriages in human.

Keywords: Autophagy, Steroidogenesis, Corpus luteum, Ovary, IVF.

ÖZET

OTOFAJİ INSAN YUMURTALIĞINDA SEKS STEROID SENTEZINI DÜZENLER

Otofaji, yaşlanmış ve bozulmuş protein ve organeller gibi hücre yapılarını geri dönüştürerek hücrenin enerji homeostazını korumayı amaçlayan evrimsel olarak korunan bir süreçtir. Ortaya çıkan veriler, otofajinin ayrıca lipofaji adı verilen bir süreçle lipit metabolizmasını da düzenlediğini göstermektedir. Bu çalışmada, insan yumurtalığındaki steroid biyosentezinde otofajinin yeni bir rolünü tanımlıyoruz. Otofaji genlerinin (Beclin1 ve ATG5) siRNA ve shRNA teknolojileri kullanılarak susturulması yoluyla otofajik sürecin farmakolojik inhibisyonu veya genetik olarak kesintiye uğraması, steroidogenezi önemli ölçüde baskıladı; bu korpus luteumun eksplant kültürlerinin, primer ve ölümsüzleştirilmiş insan granüloza hücrelerinin bazal ve gonadotropin ile uyarılan estradiol (E2) ve progesteron (P4) üretiminde doza bağlı ve ilerleyici bir düşüşle sonuçlandı. Otofajinin bloke edilmesi, güçlü bir şekilde otofaji substratları (LC3 ve SQSTM1/p62) ve lizozom ile birlikte lokalize olan lipid damlacıklarının (LD'ler) belirgin bir sitoplazmik birikimi ile de ilişkilendirildi. Ayrıca, otofaji genlerinin ekspresyonunun, LD'lerin otofagozom ve lizozom ile birlikte lokalizasyonlarının kusurlu olduğunu bulduk ve klinik olarak belgelenmiş luteal faz defekti olan hastaların korpuslarında otofaji aracılı steroidogenez, gebeliği sürdürmek ve düşük yapmayı önlemek için sürdürülebilir seviyelerde P4 üretememeleri nedeniyle tehlikeye girer. Daha ilginç olarak, luteotropik hCG ile birlikte rapamisin uygulamasıyla otofajinin farmakolojik indüksiyonu, bu hastaların in vitro luteal GC'lerinde steroidogenez ve otofaji üzerinde sinerjistik bir etkiye ve büyük ölçüde düzeltilmiş kusurlu P4 üretimine sahipti. Toplu olarak ele alındığında bu bulgular, otofajinin, insan yumurtalığında steroid sentezi için gerekli serbest kolesterolü serbest bırakmak amacıyla LD'ler içindeki lipid yükünü lizozomlara iletmek üzere LD'lerin lizozom ile birleşmesini teşvik ederek bazal ve gonadotropin ile uyarılan steroidogenezde çok önemli bir rol oynadığını göstermektedir. P4 hormonunun, endometriumun implantasyonu ve gebeliğin sürdürülmesi için hazırlanmasında gerekli olduğu göz önüne alındığında, bulgularımız önemli klinik etkilere sahip olabilir ve insanda kısırlık, gebelikle ilgili komplikasyonlar ve düşüklerin tedavisinde yeni bir yol açabilir.

Keywords: Otofaji, Steroidogenez, Korpus luteum, Over, IVF.

ACKNOWLEDGMENTS

Even why at the front page of this thesis dissertation only my name is written, many marvelous people gave precious contribution throughout all the steps. I appreciate their endless support and academic guidance during these hard and stressful.

I have been very lucky to have an advisor like Prof. Dr. Özgür ÖKTEM who has been a great support and has guided me through every step in this journey. He inspired me to explore new avenues and to perform research as a scientist. Working with Prof. Dr. Özgür ÖKTEM has been a great fortune and the lessons taught by him will guide me throughout my research life. I also thank Prof. Dr. Kayhan Yakın for his relentless guidance, friendship and contributions to my research life. I would also like to thank Assist. Prof. Serçin Karahüseyinoğlu as one of the professors who helped me construct my academic and research background. I am thankful to Prof. Dr. Afsun Şahin, Prof. Dr. Süleyman Nezih Hekim and Assoc. Prof. Gamze Tanrıverdi for participating in the jury of my thesis defense committee.

I like to thank my friends Bürge ULUKAN-Hande SÜER twins, Selin SELVI, Idil Su CANITEZ and Eda KUŞAN for their moral and academic support. I am also thankful for the moments we had together during our studies some of which were fun some of which crazy. I would also like to thank my current labmates and also previous labmate, Gamze BILDIK for their support and collaboration. I owe a special thanks to American Hospital and Koç University Hospital IVF Units for their technical help. Research infrastructure of Koç University Translational Medicine Research Center and academic and financial support of Graduate School of Health Sciencies were precious and irreplaceable during my studies.

Very important to me has been the support of my girlfriend and best friend, Zeynep PARLAK, who has been my greatest support and motivation.

Greatest thanks go to my family which has always believed in me and motivated me to always go ahead no matter what the obstacles. I am deeply thankful and grateful to my family for everything they have given to me that has lead to this thesis and other studies during my PhD.

TABLE OF CONTENTS

LIST OF TABLES

LIST OF FIGURES

ABBREVIATIONS

ATG	Autophagy-related protein
CMA	Chaperone mediated autophagy
LAMP2A	Lysosome associated membrane protein 2a
PtdIns3P/PI3P	Phosphatidylinositol 3-phosphate
IM	Isolation Membrane
ER	Endoplasmic Reticulum
PM	Plasma Membrane
LD	Lipid Droplet
ULK1	Unc-51 like autophagy activating kinase
ATG9	Autophagy-related protein 9
ATG101	Autophagy-related protein 101
FIP200	Focal adhesion kinase family interacting protein of 200 kDa
COPII	Coat protein complex II
VAP	VAMP-associated protein
PI3KC3C1	Class III Phosphoinositide 3-kinase complex 1
WIPI 1-4 protein	WD-repeat protein interacting with Phosphoinositide
ATG 16	Autophagy-related protein 16
ATG2A	Autophagy-related protein 2A
ATG 12	Autophagy-related protein 12
ATG 5	Autophagy-related protein 5
ATG 7	Autophagy-related protein 7
ATG 10	Autophagy-related protein 10
ATG 16	Autophagy-related protein 16

ATG 4	Autophagy-related protein 4
LC3	Microtubule-associated protein 1A/1B-light chain 3
SDS-PAGE	Sodium dodecyl-sulfatepolyacrylamide gel electrophoresis
PKA	Protein kinase A
FYCO1	FYVE and coiled-coil domain autophagy adaptor 1
STK3	Serine/threonine kinase 3
RILP	Rab interacting lysosomal protein
VPS 34	Vacuolar protein sorting 34
UVRAG	UV radiation resistance-associated gene protein
INPP5E	Inositol polyphosphate-5-phosphatase E
EPG5	Ectopic p-granules autophagy protein 5
PI (3,5) P_2	Phosphatidyl-inositol (3,5) bisphosphate
mTORC1/2	Mammalian target of rapamycin complex ½
DEPTOR	DEP domain-containing mTOR-interacting protein
PRAS40	Proline-rich Akt substrate 40 kDa
RAPTOR	Regulatory-associated protein of target of rapamycin
LRS	Leucyl-tRNA synthetase
p62/SQSTM1	Sequestosome-1
TSC 1/2	Tuberous sclerosis proteins 1/2
EGF	Epidermal growth factor
STAT3	Signal transducer and activator of transcription 3
PKR	Protein kinase RNA-activated
eIF2α	Eukaryotic translation initiation factor 2A
GSK3β	Glycogen synthase kinase 3 beta

TLRs	Toll-like receptors
IFN-γ	Interferon gamma
TNF	Tumour necrosis factor
ATP	Adenosine triphosphate
AMPK	AMP-activated protein kinase
LKB1	Liver kinase B1
CaBP	Ca2+ Binding protein
ROS	Reactive oxygen species
JNK	c-Jun N-terminal kinase
TRAF	Tumor necrosis factor receptor–associated factor
PTEN	Phosphatase and TEN homolog deleted on chromosome 10
TRAF6	Tumour necrosis factor receptor associated factor 6
ATM	ATM serine/threonine kinase
SREBP	Sterol regulatory element binding protein
HMG-CoAR	Hydroxymethyl-glutaryl coenzyme A reductase
LDL	Low-density lipoprotein
LDLR	Low-density lipoprotein receptor
INSIG 1	Insulin induced gene 1
HDL	High-density lipoprotein
LDL	Low-density lipoproteins
SR-BI	Scavenger receptor class B type 1
APOE	Apolipoprotein E
APOB	Apolipoprotein B
LAL	Lysosomal acid lipase

ACAT	Acyl-CoA cholesterol acyl transferase
cAMP	Cyclic adenosine monophosphate
HSL	Hormone sensitive lipase
StAR	Steroidogenic acute regulatory protein
START	Steroidogenic acute regulatory-related lipid transfer
OMM	Outer mitochondrial membrane
IMM	Inner mitochondrial membrane
SSD	Sterol-binding domain
NPC1/2	Niemann–Pick C protein 1/2
TSPO	Translocator protein of mitochondria
CRAC	Cholesterol recognition amino acid consensus
VDAC	Voltage-dependent anion channel
ANT	Adenine nucleotide transporter
PRAX-1	TSPO-associated protein-1
MtPTP	Mitochondrial permeability transition pore
NADPH	Nicotinamide adenine dinucleotide phosphate
SF1	Steroidogenic factor 1
PGCs	Primordial germ cells
BMPs	Bone morphogenetic proteins
SMAD	Small mothers against decapentaplegic
FSH	Follicle stimulating hormone
FSHR	Follicle stimulating hormone receptor
LH	Luteinizing hormone
LHR	Luteinizing hormone receptor

GnRH	Gonadotropin-releasing hormone
PKC	Protein kinase C
MAPK	Mitogen-activated protein kinase
3β-HSD	3β-Hydroxysteroid dehydrogenase
17β-HSD	17β-Hydroxysteroid dehydrogenase
P450scc	Cholesterol side-chain cleavage enzyme
P450aro	Gonadal aromatase enzyme
CYP17A1	Steroid 17-alpha-hydroxylase/17,20 lyase
DHEA	Dehydroepiandrosterone
hCG	Human chorionic gonadotropin
CL	Corpus luteum
TAGs	Triacyclglycerols
ATGL	Adipose triglyceride lipase
CREB	Cyclic AMP-responsive element-binding protein
IRB	Institutional review board
Ph	Potential of hydrogen
FBS	Fetal bovine serum
HEPES	4-(2-hydroxyethyl)-1-piperazineethanesulfonic acid
HGrC1	Human non-luteinized granulosa cell line
BSA	Bovine serum albumin
DPBS	Dulbecco’s phosphate buffered saline
EDTA	Ethylenediaminetetraacetic acid
DAPI	4′,6-diamidino-2-phenylindole
HLGCs	Human luteal granulosa cells

IVF	*In-vitro* fertilization
RIPA buffer	Radioimmunoprecipitation assay buffer
ECL	Enhanced Chemiluminescence
OPU	Ovarian pick-up
RBC	Red blood cell
DMEM/F12	Dulbecco's modified eagle medium/nutrient mixture F-12
PSA	Penicillin-streptomycin-amphotericin B
DMSO	Dimethyl sulfoxide
SDS	Sodium dodecyl sulfate
BCA	Bicinchoninic acid
PVDF	Polyvinylidene difluoride
TBS-T	Tris buffered saline-Tween
PBS-T	Phosphate buffered saline-Tween
ECLIA	Electro-chemiluminescence immunoassay
PFA	Paraformaldehyde

Chapter 1: Introduction

1.1. Types of autophagy

The discovery of the lysosome, the digestive organelle of the cell, in 1955 by Christian de Duve opened a new horizon in cellular research[1]. This was followed by detailed studies on many different cellular functions involving lysosomes. An intriguing mechanism soon discovered was autophagy, through which the cell is "eating" itself by transporting different materials to be degraded into the lysosomes. Molecular mechanisms of the process were clarified following the identification of autophagy-related genes and proteins (ATGs) and their mammalian counterparts[2]. Implications of autophagy in physiologic and pathologic conditions earned its discoverer a Nobel Prize.

Autophagic mechanisms can be divided into three forms. Macroautophagy (will be referred to as autophagy) is the main form of autophagy used by the cell to degrade different types of cargo like protein aggregates, damaged or harmful organelles, and even invading microorganisms. A wide range of materials being targeted and degraded by autophagy are associated with different clinical conditions like neurodegenerative diseases and metabolic syndrome. In response to stress or starvation, the targeted material is selected and captured in double vesicle organelles named autophagosomes, and with the help of the cytoskeleton components, it is directed towards lysosomes to be degraded. Basic units of the degraded material are recycled back into the system to serve as a nutrient or constructive source for the cell[3].

Chaperone-mediated autophagy (CMA) is another type of autophagy that is present only in mammalian cells. CMA selectively targets damaged proteins or protein aggregates that contain a specific KFERQ motif. Targeted proteins are unfolded using different chaperones in the cytosol and translocated into the lysosomal lumen by a specific multimeric protein named Lysosome Associated Membrane Protein 2A (LAMP2A). Following degradation, basic units of proteins (amino acids) are recycled to be used as an energy source or for *de novo* protein synthesis. Due to its cargo selectivity for protein aggregates, CMA turned out to be of high interest in neurodegenerative diseases and cancer[4].

Microautophagy is the third form of autophagy that assists macroautophagy in energy-deprived conditions to generate nutrient sources using the cell's resources. The

cargo is enclosed in invaginating lysosome-derived vesicles and degraded with the help of lysosomal enzymes and hydrolases. As in other autophagic mechanisms, degraded constituents are recycled back in the system as energy source for the cell[4].

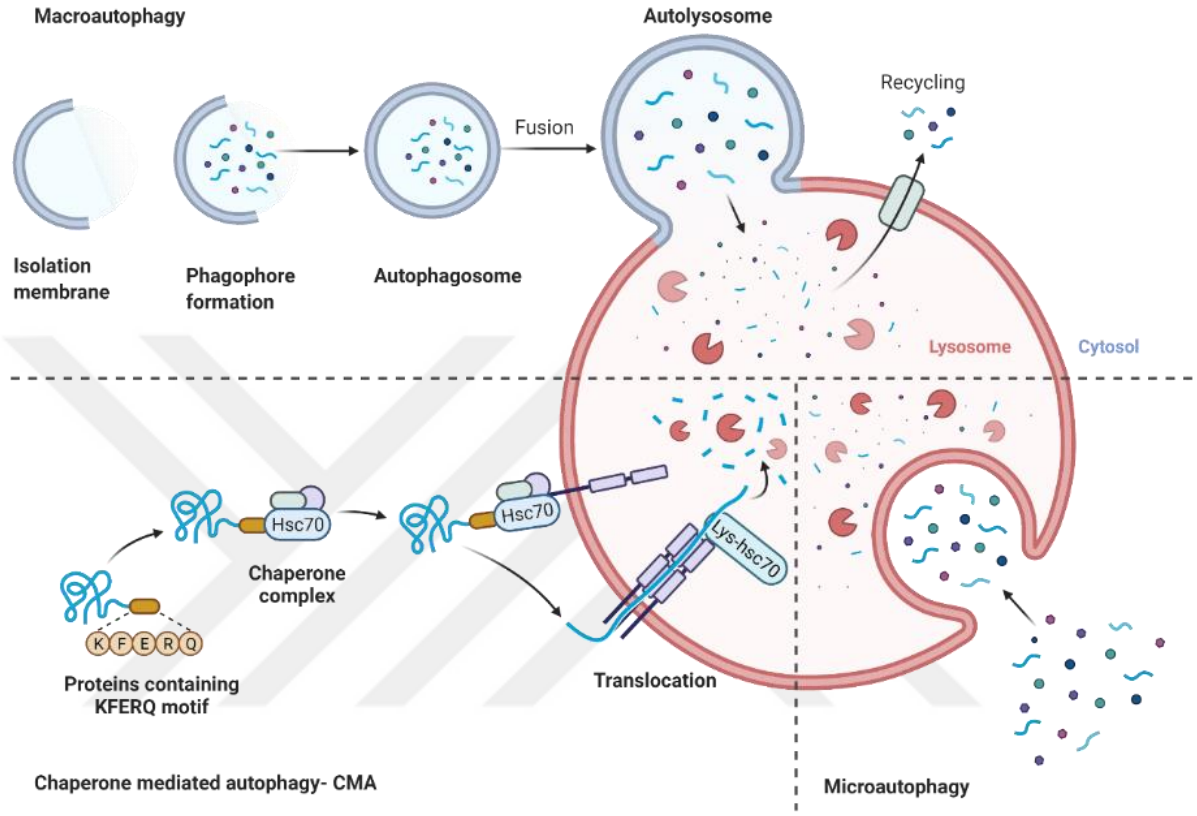

Figure 1. *Cellular autophagy mechanisms. Three common autophagy types occur in the cell. Macroautophagy sequesters different cytoplasmic cargo load into double membranous organelles, autophagosomes, and degrades it after fusing with the lysosomes. Chaperone-mediated autophagy (CMA) recognizes KFERQ motif found in different proteins and transfers them, by means of LAMP2A, into the lysosomes to be degraded. Microautophagy degrades cytosolic cargo by membranous invaginations of the lysosome.*

1.2. Molecular mechanism of autophagy

Autophagy is a dynamic process involving different steps. According to the present model in mammalian cells, autophagosomes originate from a cellular membranous source, elongate, encapsulate the cargo and then seal to form a double membranous structure, "the mature autophagosome". This structure is then targeted to the lysosome where its outer membrane fuses with it and the inner membrane is engulfed and degraded together with the cargo inside the lysosome. An array of signaling pathways takes part in this intricate and complex process.

1.3. Induction and phagophore genesis

The most common intracellular trigger for autophagy is scarcity of a specific source of energy like amino acids and/or glucose. In theory, any type of cellular stress that disturbs homeostasis may lead to activation of autophagy, as a survival mechanism to adapt to the changing conditions. When the stress signal is perceived from the cell by numerous signaling pathways, autophagic proteins are directed to a membrane-holding site in the cytoplasm containing PtdIns3P. This site is the origin of isolation membrane (IM) [5]. How this membrane is formed is still debatable, but the most plausible ones are the endoplasmic reticulum (ER) [5], plasma membrane (PM) [6], mitochondria[7], and lipid droplets (LDs) [8]. ER is likely the origin of membranes as it was shown that autophagosomes are formed by an ER membrane protrusion evolving into an omegasome[5]. This structure is rich in PI3P and is formed as a response to intracellular stress. ER has also some subdomains which act as contact sites with the other organelles serving as isolation membrane sources in the cell like PM, mitochondria, and LDs. Two very important proteins, ATG9, located in vesicles and the sole membrane protein of core autophagic apparatus, and ULK1 are found in these membrane sources[9]. ULK1 mediates the transport of ATG9 vesicles by phosphorylating ATG9 on Ser 14 position. ATG9 endows lipids and proteins to the autophagosomal membrane and together with ULK1 enables the coordination of membrane genesis and later engagement of autophagic proteins leading to autophagosome maturation. ULK1 complex in mammals is composed of four different proteins- ULK1/2, ATG13, FIP200 and ATG101. This complex is first engaged to the isolation membrane and then its presence is stabilized by PI3P[9]. ULK1 complex also interacts with a specific type of vesicle, COPII, which makes possible ER-

to-Golgi transfer[10]. COPII vesicles are synthesized from ER exit sites and their assembly is partially mediated by SEC12 protein[10]. At the same time, VAP proteins are ER proteins which tether ER with other membranes at contact sites. FIP200 and ULK1 can interact with SEC12 and VAP proteins to smoothen engagement of ULK complex at the initiation site starting on the ER[11]. The second complex with a crucial role in autophagosome genesis is the class III PI3K complex 1 (PI3KC3-C1) which is composed of VPS34, BECN1, p150 and ATG14L[12]. PI3P is synthesized by the interaction of this complex with the substrate lipid on the membranes, phosphatidylinositol (PI). PI3P interacts with WIPI1-4 proteins which have different binding substrates and mediate different functions in isolation membrane genesis. WIPI2 serves as a scaffold protein and brings ATG16 to IM, WIPI3 interacts with ULK1 complex through binding to FIP200 and WIPI4 binds to ATG2A to further mediate IM synthesis[13-14]. IM synthesis and development depends on the exact coordination of both ULK1 and PI3KC3 complex and ATG9 vesicles. This coordination leads to the birth of an omegasome from the ER and later to its evolution into the IM.

1.4. Phagophore elongation

The next step in autophagosome development is the extension or elongation of the synthesized IM. This phase comprises a class of ubiquitin-like ATG8 homologs LC3 proteins which are present in the cell as uncleaved proteins. They are cleaved by the protease ATG4 in a cascade reaction to be activated for PE conjugation. Two different reactions take place to control autophagosome elongation[15]. The first reaction is triggered by covalently conjugating ATG12 to ATG5 mediated by two ubiquitin like enzymes, E1 (ATG7) and E2 (ATG10). ATG5 can also bind to ATG16 creating a heterohexamer complex composed of ATG5, ATG12 and ATG16. This complex has a role in determining the location of autophagosome by behaving as an ubiquitin-like ligating enzyme (E3). LC3 protein is cleaved by ATG4 to uncover the glycine amino acid at the C-terminus. Then the consecutive reactions of E1 (ATG7), E2 (ATG10) and E3 (ATG5-12-16) lead to the conjugation of phosphatidylethanolamine (PE) to glycine position of LC3[16]. This reaction mediates the conversion of the proteins from a dispersed from into a lipidated, membrane-associated form. In the case of LC3, it is converted from LC3-I to LC3-II, respectively. Lipidated LC3 has regulatory roles in different steps of autophagy

like autophagosome maturation[17], movement[18], autolysosome formation[18] and inner membrane degradation of autophagosomes[19]. At the same time, it serves as a scaffold for binding of adaptor proteins during the process. From the experimental point of view, LC3 is crucial since it is located in the IM and remains in the autophagosome even when it is being degraded by the lysosome. Consequentially, LC3 is also degraded by autophagy and since in SDS-PAGE and immunofluorescence LC3-I can be easily discerned from LC3-II, this makes it a perfect marker for studies on autophagic flux and activity[20].

1.5. Membrane curvature

A structural feature that affects the action of ATG5-12-16 complex in the phagophore elongation is membrane curvature[21]. As the membrane lengthens, both elongation sides show high curvature, with the base being less curved. Its stabilization is achieved by the ATG5-12-16 complex[22]. The exact process of phagophore elongation is still debatable. One hypothesis states that the two sides of the boundaries of the membrane lengthen until they join ends together to form autophagosomes or they form by fusion of different vesicles[23]. The second hypothesis states that IM synthesis is started simultaneously at several sites and several ligation events take place to form the autophagosome. Regulation of elongation step is done at different steps starting with the dual activity of ATG4 which can also deconjugate LC3 from the membrane to control phagophore elongation[24]. At the same time, PKA phosphorylation of LC3 can negatively control its activity[25].

1.6. Autophagosome maturation

Isolation membrane elongation goes forward to phagophore sealing to form the autophagosome. This double membrane vesicle needs to go through maturation to be able to fuse with the lysosome. Maturation process starts with clearing of the ATG proteins from the outer membrane, a step in which only LC3 remains. A group of proteins (SNARE proteins) composed of syntaxin 17 and synaptosomal-associated protein 29 (vesicle-SNAREs) and vesicle-associated membrane protein 8 (VAMP8, target-SNAREs) are recruited to assist fusion of autophagosomes[26]. The kinesin motor proteins which mediate transport of the vesicle at the plus end direction to the lysosome, are also

recruited. Kinesins are associated to autophagosome by specific adaptors like FYCO1, a process mediated by LC3 binding[27]. LC3 is also a target of post-translational modifications like the one at threonine 50 by Hippo kinase STK3, which is crucial for a successful fusion event[28].

1.7. Fusion: Autolysosome formation

Since lysosomes are located at the perinuclear region and autophagosomes are synthesized at different parts of the cytosol, they need to move towards the organelle. This movement is made possible by autophagosome binding to dynactin-dynein motors mediated by Rab7 and RILP, moving in a minus end direction[29]. The purpose of this processes is to bring the lysosome and the autophagosome in close proximity. Priorly recruited SNAREs assist in tethering both organelles to form autolysosomes. Fusion step is controlled by BECN1-VPS34-UVRAG complex acting as a PI3K complex. This complex is regulated by binding to a protein named Rubicon, a negative controller of the complex and regulated by different inducement factors and autophagic proteins[30]. Forming of autolysosomes is also regulated by two other proteins, EPG5 and INPP5E. EPG5 assists SNAREs assembly in both autophagosomes and lysosomes[31]. INPP5E converts PI (3, 5) P_2 to PI3P and is a positive regulator of the fusion step since the converted PI3P helps stabilize the cytoskeleton supporting the fusion step[32].

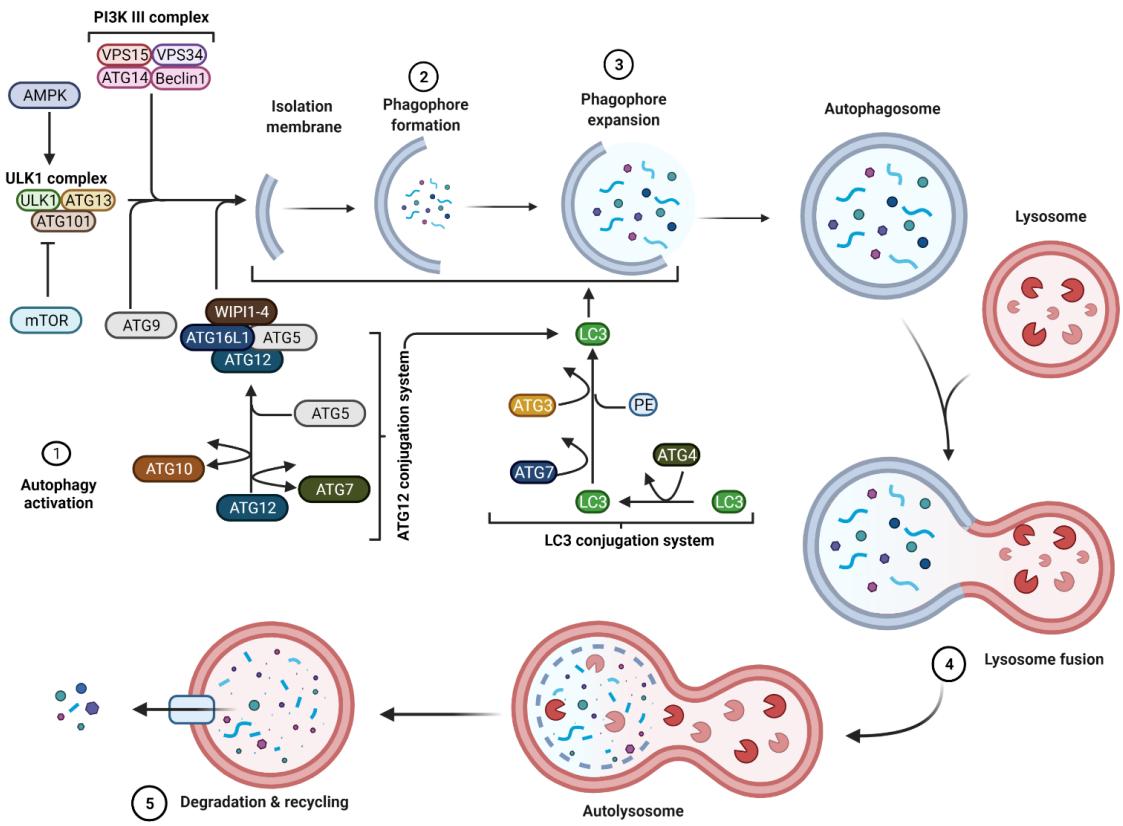

Figure 2. *Overview of autophagy process. 1) Induction of autophagy by different cellular cues leads to triggering of the activation mechanisms with a strong emphasis on ULK1, PI3K III complexes and ATG9 containing vesicles. 2 and 3) Isolation membrane turns into a phagophore which starts to elongate and encapsulate the cargo inside it. In this step E1-E2-E3 ubiquitination conjugation system (ATG12 and LC3 systems) play a vital role. 4) Phagophore maturation and closure forms the autophagosome which fuses with the lysosome to degrade the cargo and forming the autolysosome. 5) Action of different lysosomal hydrolases and enzymes degrades the cargo into its constituent elements and returns them back into cytosol.*

1.8. Regulation of autophagy

Sensitive signaling mechanisms have evolved in eukaryotes to preserve homeostasis. In times of scarcity, cells must sustain ongoing crucial cellular processes. Among several responses to intracellular and intercellular stress conditions, autophagy is of utmost importance. Autophagy itself is highly regulated by an array of signaling and metabolic factors. Autophagy is basically controlled by Serine Threonine kinase mTOR

(mammalian target of rapamycin), a key regulator protein of cell proliferation and homeostasis[33]. mTOR is a serine threonine kinase, part the phosphoinositide 3-kinase (PI3K)-related kinase family and by interacting with different proteins it forms 2 different complexes: mTOR complex 1 (mTORC1) and mTOR complex 2 (mTORC2)[34]. mTORC1 is composed of six protein components, four of which are shared with mTORC2[34]. One of the shared components is the mammalian lethal withsec-13 protein 8 (mLST8 or GβL) which binds to the kinase domain of mTOR to stabilize raptor-mTOR interaction and plays a role in regulation of cell size signaling[35]. The other shared protein is the DEP domain containing mTOR-interacting protein (DEPTOR) which is an mTOR binding factor with versatile effects[36]. Tti1 is the next factor which interacts with mTOR after forming a complex with Tel2, which stabilizes mTOR but also has a role in guiding the assembly of mTORC1 and mTORC2[37]. Proline-rich Akt substrate 40 kDa (PRAS40) is one of the subunits specific to mTORC1. PRAS40 is part of the mTORC1 complex and inhibits substrate binding to this complex[38]. Regulatory-associated protein of mammalian target of rapamycin or raptor serves as a scaffold protein for the mTOR complexes and mediates mTOR action in cells[39]. Although both complexes have an active role in metabolism, cell cycle progression, proliferation, and other important processes for the cell, only mTORC1 has an active role in regulating autophagy.

1.8.1. Amino acid shortage

Amino acid starvation is the most known and effective inducer of autophagy. Lack of specific amino acids like leucine and glutamine has the highest impact on autophagy. Both leucine and glutamine have different regulatory mechanisms on mTOR. mTOR activity is controlled by means of leucyl-tRNA synthetase (LRS) which senses rising levels of leucine and stimulates mTORC1 activation through EGO complex[40]. In terms of signaling, low amino acid levels are first sensed extracellularly through G-protein coupled receptors T1R1/T1R3, leading to a decreased mTOR activity and autophagy activation[41]. Intracellular amino acid availability is sensed by means of Rag GTPases located on lysosomal membranes, which in turn forms heterodimers of RagA/RagB with RagC/RagD and binds raptor to mediate signaling to mTORC1[42]. In conditions of low amino acid availability, Rag heterodimer uncouples from raptor and causes separation of mTOR and Rheb from lysosome membrane leading to autophagy activation[43]. At the

same time, mTOR has a role on Ulk-Atg13-FIP200 complex by binding to and phosphorylating Atg13 and Ulk1 in the genesis of autophagosome formation[44]. Another important protein playing a part in amino acid availability control is p62/SQSTM1, an autophagic cargo receptor, which can also bind to the Rag complex leading to mTORC1 activation[45]. While under normal conditions p62 inhibits mTORC1 activation, in stressful conditions it triggers sequestration of to-be-degraded autophagic cargo.

1.8.2. Insulin, glucose and EGF signaling

A high glucose level in the cellular environment causes inhibition of autophagy due to the excess of energy and abundance of nutrients. Insulin in the cell, binds to its receptors leading to PI3KC1 activation, producing PtdIns3P at the cell membrane[46]. This produces Akt which inhibits TSC1/2 (mTOR inhibitor) leading to autophagy inhibition[46]. In cardiomyocytes though, autophagy is directly regulated by glucose levels in the cell. Glycolysis enzyme hexokinase II, in low glucose conditions, directly binds to and inhibits mTOR leading to autophagy activation. In conditions where glucose is increased and the amount of the substrate of hexokinase II, glucose 6-phosphate, starts to increase in the cell, autophagy will be gradually inhibited[47].

Since autophagy plays a crucial role in different vital intracellular processes, it is also highly associated with growth factors. Among them, EGF exerts the most prominent action on the process, either directly or indirectly. It inhibits autophagy by phosphorylating Beclin1 which leads to inducement of Beclin1 dimerization, inactivating the protein[48]. EGF can also inhibit autophagy through GRB2 and GAB2 and their downstream signaling mechanisms affecting mTOR. On the other hand, EGF can phosphorylate and trigger STAT3 dimerization causing it to release PKR, the eIF2α domain. This leads to an increase in expression of autophagic markers LC3 and Atg5, implying an increase in autophagic flux[49]. Another interesting regulator of autophagy *in-vitro* is serum availability in the media. Lack of serum activates GSK3, and through secondary signaling mechanisms, causes Ulk1 activation and augments the rate of autophagosome formation[50].

1.8.3. TLR and cytokines

Immune system can regulate autophagy with its effectors as also autophagy affects immune system differently both in health and disease. The main immune system regulators of autophagy are toll-like receptors (TLRs) and cytokines. TLRs are part of the innate immune system while cytokines are a class of signaling molecules. Both TLRs and cytokines play roles in a wide array of processes like cell growth, proliferation, and differentiation. Different cytokines have different actions on autophagy, mediated by different signaling pathways. IL-6, through regulating STAT3, decreases expression of autophagic proteins and leads to autophagy inhibition while IL-10 uses Akt signaling mechanism to inhibit autophagy. On the other hand, TNF and IFN-γ induce autophagy to mediate protection of macrophages from bacterial infections[51]. TLRs generally regulate Beclin1 protein causing its polyubiquitination and uncoupling from Bcl2. This uncoupling enables Beclin1 to form PI3KC3 complex which is vital to the autophagosome formation. Crucial to this regulation by TLRs are two adaptor proteins, MyD88 and TRIF[52].

1.8.4. Energy level and Ca^{2+} ions

ATP molecule is the energy currency of the metabolism, and its level defines the energy status of the cell. ATP is converted to AMP when energy is being spent for different purposes in the cell. When the energy of the cell is low, it leads to a low ATP/AMP ratio leading to AMP binding to AMPK. This binding phosphorylates and activates LKB1 which may further activate autophagy mediated by two different pathways in which mTOR is the main subject of action to be inhibited. LKB1 may signal mTOR by TSC1/2 complex or may phosphorylate raptor subunit of the mTOR complex both leading to inhibition of mTOR and thus autophagy activation[53-54]. AMPK protein may also activate autophagy at the step of autophagosome formation by phosphorylating Ulk1 and stabilizing PI3KC3 complex[55].

Ca^{2+} ion is a critical signaling factor included in many cellular and metabolic pathways in the cell. Its concentration is deliberately controlled, and many different pathologic disabilities arise from problems in this fine-tuned ion balance. The main storage sites for Ca^{2+} in the cell are mitochondria, ER and Golgi. This ion can regulate autophagy through IP3R, a Ca^{2+} channel activated by IP3 and it also interplays with

Beclin1. In a condition when energetics in the cell is optimal, Beclin1 is not bound to IP3R, and Ca-BP (Ca^{2+} Binding protein) is under-expressed in the cell leading to an inhibition of autophagy. In case of scarcity, Beclin1 binds to IP3R and there is an increase in Ca-BP proteins in the ER lumen leading to autophagy activation. In the mitochondria, changes in Ca^{2+} levels depending on energy status of the cell may lead to a diminished ATP synthesis and decreased ATP/AMP ratio. This results in activation of autophagy mediated by AMPK[56].

1.8.5. Oxidative stress and Nitric oxide

Reactive oxygen species or free radicals are synthesized as by-products of many cellular reactions in the cell. While they have signaling functions, when they accumulate in high concentrations, they can be detrimental to homeostasis and cell physiology. In terms of autophagy regulation, H_2O_2 and O_2^- are the most important ROS molecules. ROS regulates autophagy by using different mechanisms in different sites in the cell. In shortage conditions, ROS quantity increases in mitochondria and oxidizes and inactivates Atg4, stabilizing Atg8[57]. Also, the production of free radicals by the mitochondria might turn the organelle into a target for degradation by mitophagy, a different type of autophagic process[58]. ROS may also activate autophagy by activating JNK, mediated by Atg9-TRAF6 interplay, leading to an increase in expression of important autophagic proteins. Lastly, H_2O_2 acts at the plasma membrane to inhibit PTEN leading to PI3KC1 downregulation, consequentially activating mTOR and inhibiting autophagy[59].

Nitric oxide is a gas, which is the product of the reaction carried out by nitric oxide synthase (NOS) in the body. Similar to ROS, NO plays a signaling role in immune and cardiovascular systems but in higher levels it causes nitrosative stress in the cell. In terms of autophagy, it has different roles in different cell lines. For instance, it activates autophagy in MCF-7 cell line mediated by ATM-mTOR pathway leading to an increase in autophagic proteins whilst in HeLa cells it inhibits autophagy by different mechanisms with a special focus on autophagosome synthesis mediated primarily by AMPK-TSC1/2 leading to mTOR activation[60-61]. This context-dependent regulation of autophagy by NO seems to raise more questions and further complicates our understanding about NO signaling and autophagy.

There are also other regulators of autophagy which either use the same mechanisms as the ones stated above or different specific ones. This shows a specific picture of how intertwined and redundant the control mechanisms of autophagy are, a process which is responsible for maintaining vital functions in the cell like homeostasis and energy production in times of shortage. Also, despite the clear definitions of autophagic processes there is still a redundancy in terms of cargo selectivity and degradation. At the same time, upstream signaling, controlling and mechanisms of all three autophagic processes intertwine in different steps. All these factors complicate the calculation and control of all the variables involved when planning and conducting specific experiments on autophagy.

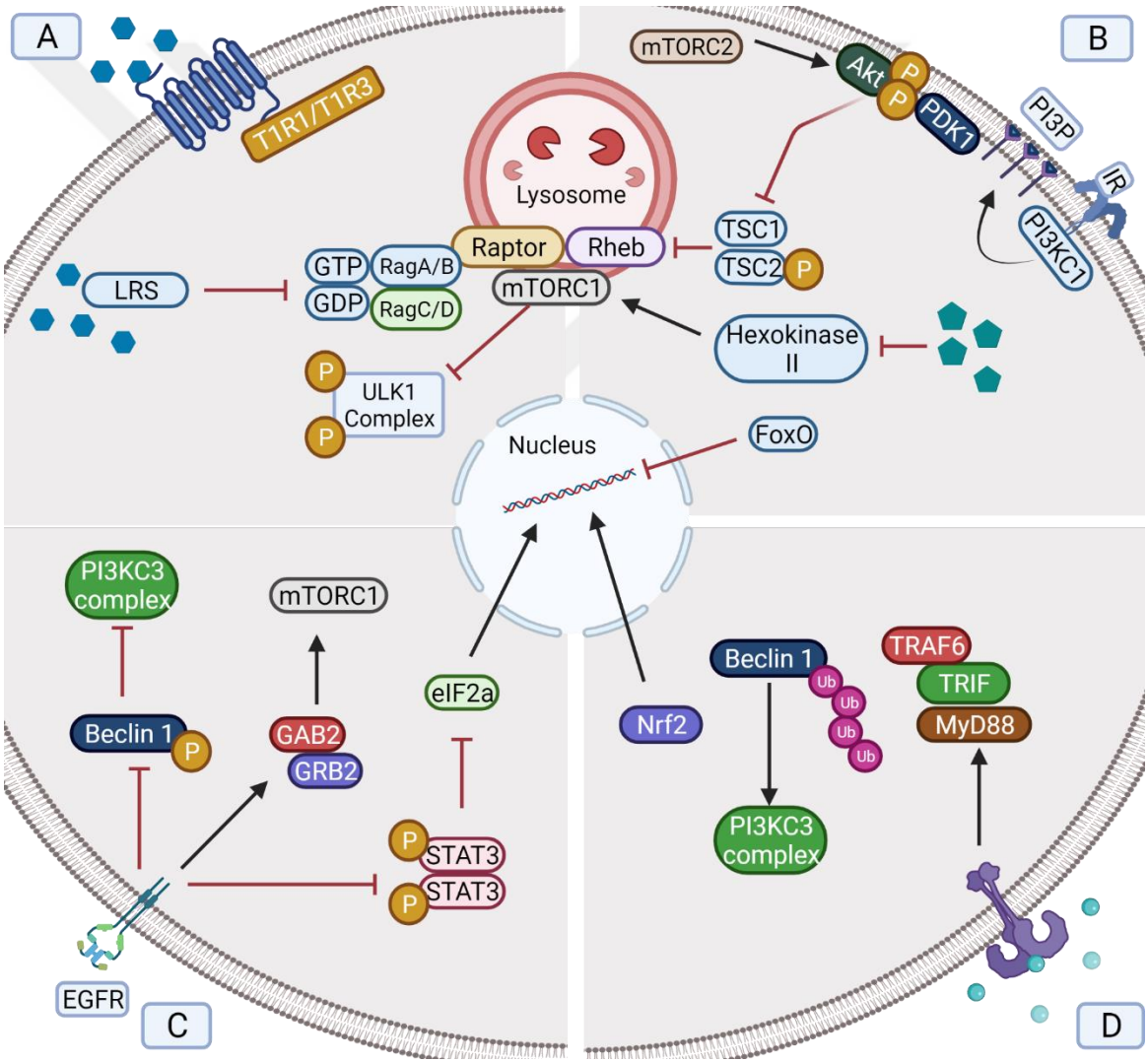

Figure 3. *Regulation of autophagy. A) Extracellular amino acid availability is sensed by T1R1/T1R3 while the intracellular level is sensed by LRS activating autophagy through*

mTOR. Rag complexes also may sense amino acid availability and in scarcity conditions their deactivation leads to separation of Rag from raptor leading to autophagy activation through mTOR. B) Insulin binding to its receptor activates PI3KC1 synthesizing PI3P activating PDK1-Akt-TSC1/2 which inhibits autophagy through mTOR or inhibits gene transcription of autophagy related proteins through FoxO. Glucose-6-phosphate, substrate of hexokinase II, meaning a fed state in the cell, inhibits autophagy through mTOR. C) Binding of EGF to its receptor phosphorylates Beclin 1 or activates GAB2/GRB2 inhibiting autophagy or phosphorylates STAT3 activating autophagy. D) LPS binding to TLR4 recruits MyD88-TRIF-TRAF6 complex which ubiquitinates Beclin1 activating PI3KC3 leading to autophagy induction.

1.9. Steroidogenesis

Steroidogenesis is a multistep process which synthesizes steroid compounds from their precursor, cholesterol occurring mostly in adrenal gland and gonads. The process starts with cholesterol being transported from circulation into the cytosol and later into mitochondria, in which, with the help of different enzymatic reactions, yields different steroid hormones with a broad spectrum of activity. Except its role as a precursor for steroid hormones, cholesterol exhibits a constructional role in different cellular membranes. Due to its insolubility most of the cholesterol is found in complexes with polar lipids on the plasma membrane mostly, giving it fluidity and flexibility. These complexes are tightly regulated by the size of the hydrophilic head and the number of double bonds present in the phospholipids of the plasma membrane (PM) [62]. When binding capacity of membrane lipids is exceeded, remaining cholesterol is transported into different cellular membranes, comprising what is defined as the "free" cholesterol[63]. Free cholesterol is a pool of cholesterol molecules which is not grounded in the plasma membrane but is accessible and it serves as the basic unit for steroidogenesis[63]. Another cholesterol-enriched membrane system is the endosomal trafficking system with an emphasis on *trans*-Golgi part[64]. ER is a crucial cholesterol synthesis and homeostasis organelle but contains only 1-2 percent of cellular cholesterol. Sterol regulatory element binding protein (SREBP) is a transcription factor residing in an inactive form on ER membrane, which under suboptimal cholesterol conditions in the cell, is transported to Golgi and activated by cleavage. Activated SREBP enters the nucleus leading to an

increase in transcription of cholesterol related genes like hydroxymethyl-glutaryl coenzyme A reductase (HMG-CoAR) and low-density lipoprotein receptor (LDLR) [65]. These genes will code for an increase in cholesterol synthesis and import from different cellular sources. When the cholesterol level is adjusted in the cell, HMG-CoAR degradation is mediated by INSIG and stimulated by increasing levels of a cholesterol intermediate[66].

Cholesterol can be synthesized *de novo* in the cell using the mevalonate pathway, starting from acetyl CoA as a substrate. The cholesterol synthesis starts with conversion of squalene to lanosterol and a sequence of approximately 20 reactions converts lanosterol to cholesterol. The rate limiting step in this pathway is the one mediated by HMG-CoAR, ER membrane protein, yielding mevalonate[67]. The synthesized cholesterol can be hydroxylated to oxysterols, fatty acylated to cholesteryl esters in all types of cells or oxidized to steroid hormones only in steroidogenic cells by means of different enzymatic reactions. Approximately 30 percent of the cholesterol in human is food-mediated and is primarily absorbed by the small intestine. With the help of apolipoproteins and fine packaging coat, this cholesterol is further transported into the liver, which will be later processed and/or secreted to be delivered in different body tissues[68].

1.10. Cholesterol synthesis and trafficking

After cholesterol is *de novo* synthesized or taken through diet, it needs to be transported to its target tissues and cell types. Steroidogenic cells possess different cholesterol transport systems, adjusted by different regulatory triggers. Currently, there are four known pathways cholesterol is being used for steroidogenesis: uptake of LDL via receptor-mediated endocytosis; uptake of HDL via SR-BI; cholesterol from LDs; ER-synthesized cholesterol committed to steroidogenesis[69].

Non-selective or LDL-mediated cholesterol pathway starts with recognition of lipoproteins like APOE and APOB by LDLR, which is present in most of the cells. Then, with the help of a transporting vesicle and a specific coat protein like clathrin, these cholesterol containing particles are endocytosed and taken up into the cytoplasm[70]. Endocytosed vesicles fuse with endosomes and get rid of their coat proteins. At the late endosome stage, pH is decreased at 5.5 to make ready for the fusion step with lysosome. The endosomal trafficking of LDL is tightly regulated by Rab5 and Rab7 proteins[71]. Late

endosomes containing LDL and lipoproteins are fused with lysosome, where lipoproteins are degraded into amino acids by means of different proteases while LDL is converted into free or active cholesterol by lysosomal acid lipase (LAL) [72]. This cholesterol can either be a substrate for steroidogenesis or esterified by acyl-CoA cholesterol acyl transferase (ACAT) and stored in LDs[73].

Selective absorption of cholesterol is achieved by means of another receptor, scavenger receptor SR-BI. This receptor is ubiquitously expressed in cells and directly translocates cholesterol from HDL into the cell by creating a hydrophilic gate-like structure in which cholesterol freely embeds into PM[74]. The uptaken cholesterol can be active cholesterol, which translocates easily in the cell, or can be esterified. The esterified cholesterol needs to be liberated before being committed to steroidogenesis. When cholesterol concentrations are low, cAMP signaling pathway leads to phosphorylation and activation of hormone sensitive lipase (HSL) which hydrolyzes cholesterol esters into free cholesterol, increases HMG-CoAR, LDLR and inhibits ACAT, leading to an increase in active cholesterol pool in the cell to be used as a substrate for steroidogenesis[75].

Lipid droplets are cellular organelles where cholesterol esters are stored. These cholesterol esters are synthesized from active cholesterol mediated by action of ACAT, in conditions of high cellular cholesterol levels. Accumulation of cholesterol esters leads to protrusion of LDs from ER into the cytosol. Size and density are two important factors related to LD biology. In steroidogenic cells, LDs are high in numbers but small in size in order to maintain a high surface area for further lipid extraction from LDs[76]. In conditions of intracellular cholesterol scarcity, cholesterol esters are extracted from LDs and converted to free cholesterol by means of HSL action. As an alternative pathway, LDs interacting with endosomes enable translocation of cholesterol esters into endosomes which will consequentially fuse with lysosomes and liberate cholesterol. This interaction is regulated by different Rab proteins[77].

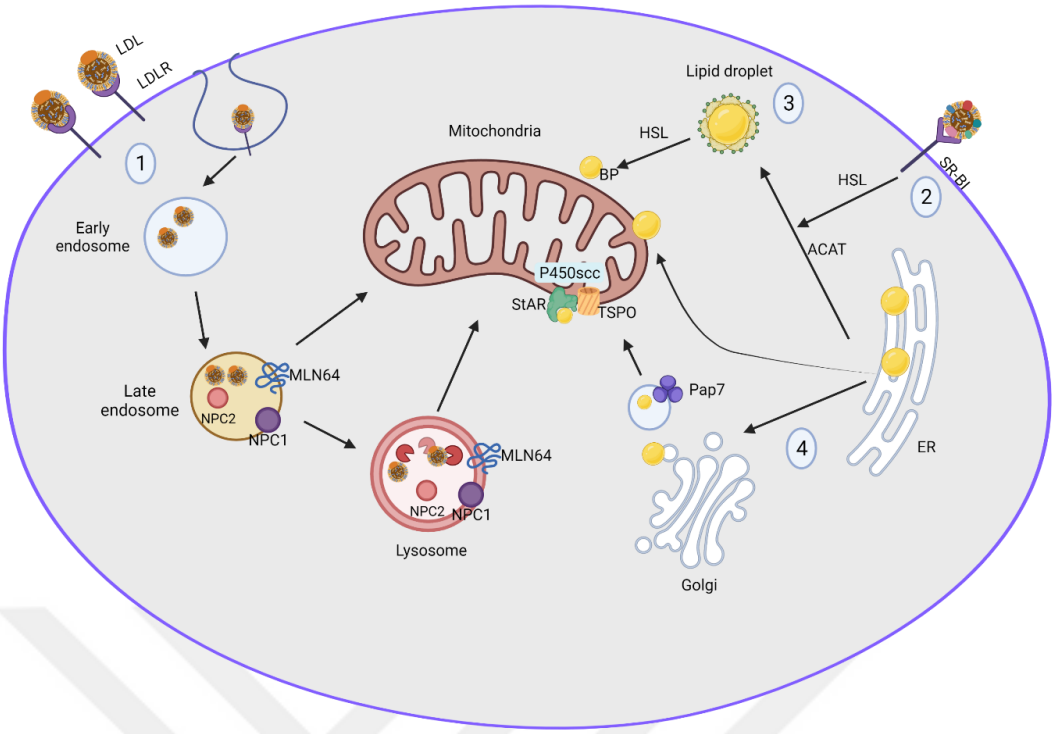

Figure 4. *Cholesterol uptake and cellular trafficking. 1) LDL loaded with cholesterol binds to LDLR and is taken inside the cell by receptor mediated endocytosis. It enters endosomal route and aided by MLN64 and NPC2-NPC1 system it is either directly transferred to mitochondria or degraded in lysosomes and then transferred to mitochondria. 2) HDL loaded with cholesterol binds to SR-BI receptor and is loaded to PM. HSL converts it to active cholesterol which can be transferred to mitochondria or through ACAT can be stored in LDs. 3) HSL can convert cholesterol esters present in LDs into free cholesterol which can bind to transporting proteins and transferred to mitochondria. 4) Cholesterol synthesized de novo in ER can either diffuse from ER to mitochondria based on a gradient or transported to Golgi network and mediated by PAP7 transferred to mitochondria. All 4 pathways converge in the mechanism of cholesterol transport into OMM by StAR, OMM to IMM by TSPO-scaffolded complex and conversion to pregnenolone by P450scc.*

1.10.1. Cholesterol binding proteins-StAR

In steroidogenic cells, the purpose of all these mechanisms is to uptake cholesterol, convert it into free cholesterol to be used for steroid hormone synthesis.

Another class of proteins which help mediate this action are the cholesterol binding proteins. Most of these proteins contain a steroidogenic acute regulatory-related lipid transfer (START) domain which plays a role in cholesterol binding and intracellular trafficking[78]. This domain is composed of 210 amino acids and forms a hydrophobic passage which stabilizes after binding of one cholesterol particle[79]. This motif was first discovered in steroidogenic acute regulatory (StAR) protein which has a crucial role in transportation of cholesterol to mitochondria. StAR contains a mitochondrial-targeting sequence at the N-terminus which directs it to outer mitochondrial membrane (OMM) even after this motif is degraded[80]. Degree of steroidogenesis activation also depends on the duration that StAR is located at OMM, with increasing transporting capacities at larger times. At the C-terminus, StAR contains another important functional motif, the sterol-binding domain (SSD). Cholesterol is thought to bind to SSD and after surface residues of this domain at the OMM become protonated, the ensuing conformational change enables the release of the bound cholesterol molecule into the mitochondria[81]. Cholesterol binding and release from StAR are necessary but not adequate to stimulate steroidogenesis in the cells.

1.10.2. MLN64-NPC2-NPC1 pathway

MLN64 also contains a START domain in the C-terminus which makes MLN64 a cholesterol binding protein enablıng transfer of active cholesterol in the cytosol. The domain located at the amine terminus helps addressing of MLN64 to late endosomes, with an emphasis on LDL particles intracellular trafficking[82-83]. MLN64 is colocalized with two very important proteins for cholesterol metabolism in the cell, NPC 1 and 2 proteins, and is thought to act downstream of NPC1[84]. Terminology was derived from the mutation-related pathology named as the Niemann-Pick type C disease, a very serious disorder leading to accumulation of cellular cholesterol in endosomes and lysosomes by impairing its trafficking[85]. NPC1 is located in late endosomes and lysosome membranes while NPC2 is located in the lumens of late endosomes, lysosomes and also in the cytosol. NPC1 and NPC2 both bind cholesterol at opposite conformations based on the position of the polar group, 3β hydroxyl[86]. NPC2 mediates transfer of cholesterol in liposomes faster than NPC1 but when NPC2 is part of the trafficking system, the rate is increased by more than 100-fold[86]. These two molecules work as part of a system in which

cholesterol uptaken by LDL particles is hydrolyzed by means of LAL and converted to active cholesterol to bind to NPC2. Then free cholesterol is transferred to NPC1 which embeds this cholesterol in lysosomal membrane and cholesterol is unidirectionally transported to ER[86]. NPC2-NPC1-lysosome/late endosome-ER pathway is used mostly for cholesterol uptaken from LDL and used in the synthesis of steroid hormones[87].

1.10.3. TSPO complex

There are some other important proteins acting downstream of StAR with an important emphasis on cholesterol transport and steroidogenesis. Mitochondrial transporter protein (TSPO) is confined in OMM and contains cholesterol recognition amino acid consensus domain (CRAC) located in C-terminus. When this protein is activated by ligand binding, it leads to steroidogenesis activation and by means of CRAC, cholesterol transport from OMM to inner mitochondrial membrane (IMM) is facilitated[88]. Hormonal stimulation activating cAMP signaling pathway leads TSPO to interact with different proteins to form a complex and increase the rate of cholesterol transport from OMM to IMM. Proteins composing this complex are voltage-dependent anion channel (VDAC), adenine nucleotide transporter (ANT), TSPO-associated protein-1 (PRAX-1), and the TSPO and protein kinase A (PKA) regulatory subunit RIα-associated protein 7 (PAP7) [89]. Formation of this complex leads to higher cholesterol transport into IMM, higher steroid synthesis and an increase in the number of contact sites between mitochondria and other organelles in the cell. VDAC itself interacts with ANT protein and together they form mitochondrial permeability transition pore (mtPTP) which may affect the cell's steroid synthesis[90]. PAP7, on the other hand, binds to PKA-RIα and targets it close to TSPO and other important proteins in steroidogenesis to regulate them through cAMP-mediated phosphorylation and through this localization to maximize the signaling. Of the phosphorylated proteins, StAR is the most important one, approximately doubling its activity mediated by PAP7 activity. Hormone treatment of different steroidogenic cells leads to PAP7 and StAR transport to mitochondria leading to a PKA-RIα, PAP7, TSPO and StAR complex formation at the OMM which modulates cholesterol transport to IMM and consequentially steroidogenesis rate[91]. StAR has a critical role in cholesterol transfer to OMM while TSPO modulates its further transport to IMM.

1.10.4. P450 class of proteins

When cholesterol enters the IMM, it can be committed to steroidogenesis by becoming the substrate of the reactions catalyzed by cytochrome P450 enzymes. These are a class of oxidative enzymes containing a heme group in their structure and activate oxygen using this group and electrons donated from NADPH[92]. Different P450 enzymes take part in steroidogenesis but P450 side chain cleavage (SCC) is the crucial, rate limiting enzyme that bestows a cell its steroidogenic capacity. Transcription of P450scc is tightly regulated through PKA and PKC signaling mechanisms, which act on different promoters of this gene[93]. Steroidogenic factor 1 (SF1), an orphan transcription factor that recognizes regulatory motifs in the gene sequences of P450scc, and other steroidogenic enzymes modulating the level of steroidogenicity in the cell[94]. Level of transcription determines the level of expression of P450scc, consequentially the steroidogenic ability of the cell. So, a cell is referred as steroidogenic if it expresses P450scc and is able to convert, through three consequential reactions, cholesterol to pregnenolone, the substrate for all steroid hormones. Pregnenolone then with the action of another non P450 enzyme, 3β-hydroxysteroid dehydrogenase and help of a mitochondrial translocase, can be converted to progesterone, a crucial sex steroid hormone[95]. Another P450 class enzyme with a role in sex steroidogenesis is P450aro which converts androgens to oestrogens.

1.11. Folliculogenesis

Reproduction is a highly regulated and coordinated process in humans where different organs and signaling pathways participate. Ovary in females is the gonad and also the source of sex steroid synthesis serving as a reproductive endocrine gland. Embryonic development of gonads in humans starts with the formation, proliferation, and migration of primordial germ cells (PGCs) to the indifferent gonad ridge. The triggers of these processes are several, but a great emphasis is put on BMP-SMAD signaling pathway and different chemoattractant gradients secreted from the ridge. Female germ cells enter meiosis until diplotene of meiosis I, which resumes later on during active reproductive life. Following germ cell cluster breakdown oocytes get surrounded by a flat one layer of epithelial cells, pre-granulosa cells, giving rise to primordial follicles. Conversion of this flat layer of cells into cuboidal marks the transition of primordial to primary follicles.

Proliferation of the cuboidal layer of granulosa cells, oocyte growth and development of another layer of somatic cells, theca cells, next to granulosa cells are characteristics of secondary follicles[96]. During the pre-antral stage cellular development is mainly gonadotropin independent while at the end of the pre antral stage, follicles start to gain responsivity towards FSH[97]. The impact that the development of theca cells and proliferation of granulosa cells and their interaction have in the follicles also increases, but the main determinant of follicular growth and maturation is the oocyte itself[98]. Theca cells are formed from ovarian stroma mesenchymal cells in response to different signaling factors secreted by the growing follicles, in a gonadotropin independent process[97]. These cells will later differentiate into theca interna layer with a crucial function on androgen synthesis and theca externa which provides support to the follicle and plays a role during ovulation[99]. Development of the antral follicles start with formation of an antrum cavity inside the follicles leading to functional differentiation of two granulosa cell populations[96]. The cell layer surrounding the oocyte is termed cumulus granulosa cells which supports its development and growth. The layer bordering the follicle is named mural granulosa cells and plays a role in steroid hormone synthesis[100]. At this stage follicles become totally gonadotropin responsive and hypothalamus-hypophysis-ovary axis starts to act. FSH induces steroidogenesis and further proliferation and growth of granulosa cells by also inhibiting their cell death[101]. Coordination of gonadotropin action and cellular context in the follicles leads to restarting of meiosis in the oocyte, cumulus expansion and finally ovulation, in which the oocyte is ejected from the follicle into the uterine tract. The remaining theca and granulosa cells develop into luteinized forms and consequentially corpus luteum[96]. As a conclusion, follicles are formed due to the interaction between the oocytes, granulosa, theca, stromal cells, and their development is modulated by two gonadotropins, luteinizing hormone (LH) and follicle stimulating hormone (FSH).

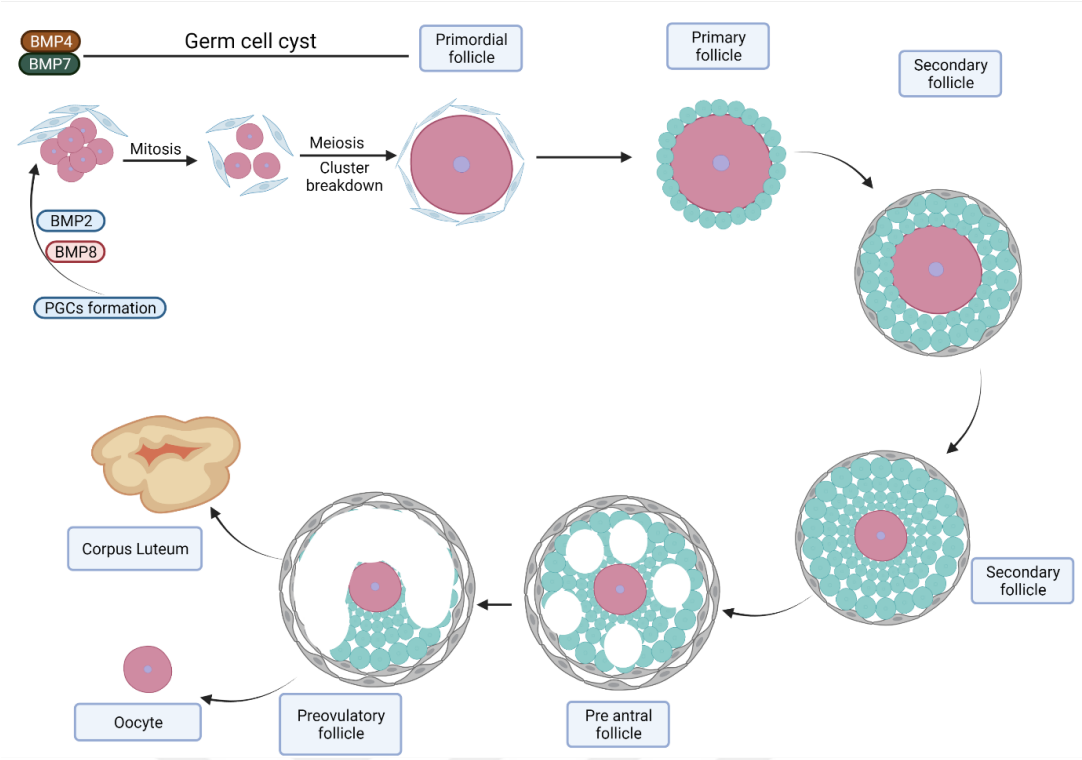

Figure 5. *Folliculogenesis in humans. This process starts with formation of PGCs, and after a tightly regulated signaling cascade (BMP signaling mainly), PGCs migrate to the genital ridge leading to germ cell cluster breakdown. Primordial follicle is formed with a pre-granulosa cell layer. Formation of a real granulosa cell layer marks the conversion to primary follicle and proliferation of it is a signature of a secondary follicle. Theca cells also form at this stage. At the end of secondary follicle phase this process starts to be dependent on gonadotropins. Creating of small cavities and fusion of these cavities to form a single one, are markers of antral and preovulatory follicles respectively. Ovulation delivers the oocyte to the uterine tract while the remaining granulosa, theca and stromal cells luteinize and form corpus luteum.*

1.12. Ovarian steroidogenesis

Sex steroid synthesis in females is triggered by two gonadotropin hormones, FSH and LH. These two hormones are regulated by the pulsatile secretion of gonadotropin-releasing hormone (GnRH) synthesized in the hypothalamus. At the beginning of the menstrual cycle, GnRH is secreted in a low frequency leading to an increase in FSH synthesis. FSH binds to its receptor (FSHR), which is a G-protein coupled receptor,

activating different secondary signaling mechanism like PKC, cAMP, and mitogen-activated protein kinase (MAPK) [102]. Pre-ovulatory granulosa cells express only FSHR, but mature granulosa cells are sensitive to both FSH and LH. Therefore, FSH is responsible from the maturation of granulosa cells by rendering these cells them responsive to LH[102]. Presence of both LHR and FSHR in granulosa cells induces expression of two P450 class enzymes crucial for steroidogenesis, P450scc and aromatase[103]. Theca cells through LHR are responsive even to small amounts of LH in circulation. LH binds to its receptor in theca cells and through mainly activating cAMP secondary messenger signaling system upregulates different proteins needed in sex steroid synthesis like P450scc, 3β-HSD, StAR and CYP17A1. Granulosa cells triggered by FSH binding upregulate 17β-HSD and CYP19A1. This consequently leads to an increase in uptake of cholesterol into theca cells, by means of StAR translocated into IMM, and its conversion to pregnenolone by P450scc. CYP17A1 converts this substrate into dehydroepiandrosterone (DHEA) and the last reaction in theca cells is catalyzed by 3β-HSD converting DHEA to androstenedione. This is the route androgens follow in theca cells. Androstenedione is transferred into granulosa cells which convert it firstly to estrone and lastly to estradiol, catalyzed by CYP19A1 and 17β-HSD, respectively[96, 99,104]. This conversion forms the basis of two-cell, two-gonadotropin theory in ovarian steroidogenesis in which androgens are provided from theca cells and converted to estrogens by granulosa cells[104]. Increase in levels of estradiol synthesized by the pre-ovulatory follicle leads to an LH surge ejecting the oocyte into the uterine tract. This surge also causes luteinization of remaining granulosa and theca cells in the ovary, genesis of corpus luteum (CL) and progesterone synthesis[105]. Progesterone is also synthesized from pregnenolone through the action of 3β-HSD. This is the second ovary-synthesized sex steroid hormone preparing endometrium for the upcoming pregnancy and also maintaining that pregnancy. In case of successful fertilization and implantation of the embryo, another hormone is produced by the syncytiotrophoblast cells. Human chorionic gonadotropin (hCG) hormone has a wide array of functions like promoting progesterone synthesis from CL and inducing angiogenesis of the uterine tract to fulfil fetal support[106].

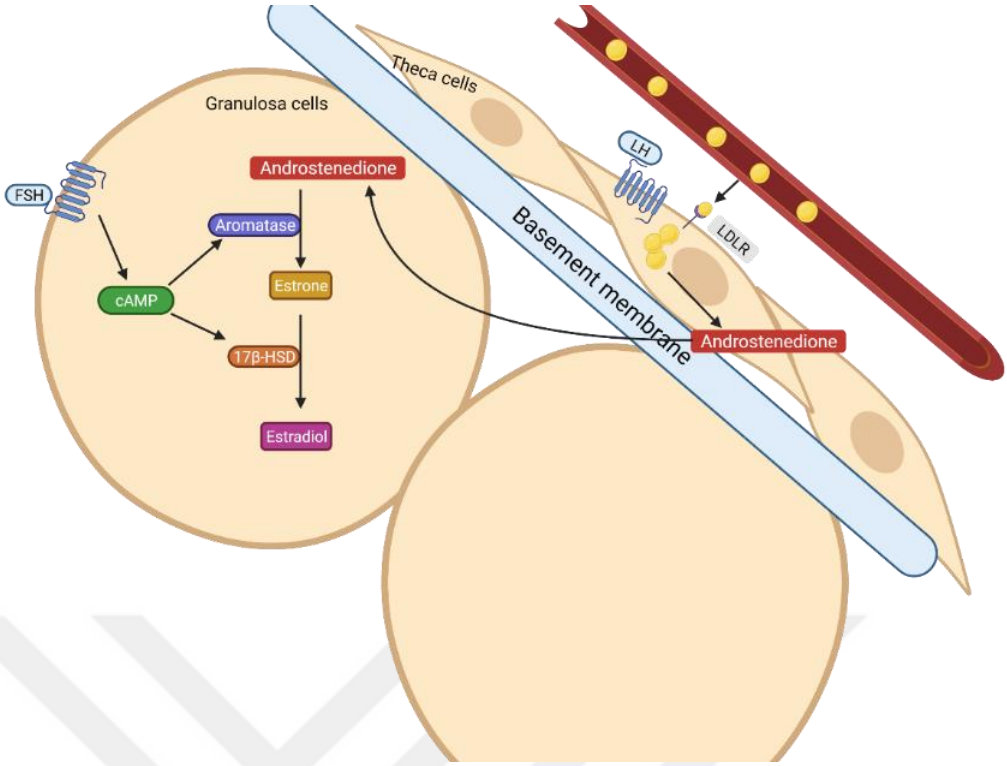

Figure 6. *Schematic image of two-cell, two-gonadotropin theory. This is the basis of estradiol synthesis in granulosa cells from androgens produced in theca cells. Responsivity of theca cells to LH causes upregulation of expression of specific steroidogenic enzymes. Cholesterol is taken up into the theca cells by means of LDL-mediated endocytosis it is converted firstly to pregnenolone mediated by P450scc and then by different enzymes to androstenedione. By diffusion androstenedione passes through basement membrane to granulosa cells. Granulosa cells are responsive to FSH, which after binding to FSHR activates cAMP secondary signaling molecule and upregulates expression of aromatase and 17β-HSD. Androstenedione is converted by means of aromatase to estrone and 17β-HSD converts it to estradiol.*

1.13. Lipophagy

Lipid droplets are single layered, cytosolic organelles used to store lipids as triacyclglycerols (TAGs) and cholesterol esters. Phospholipid monolayer contains a class of proteins, perilipins, which regulate important aspects like packaging, droplet size and availability of the LDs to degrading pathways. Lipids stored in LDs can be used as sources of energy, membrane constituents, and signaling molecules like steroid hormones[107].

Contents present in LDs can be degraded through two different pathways. Lipolysis mediates degradation of TAGs and cholesterol esters by the action of two important cytoplasmic lipases, adipose triglyceride lipase (ATGL) and HSL[108]. LDs can also be degraded by a special autophagic process named as macrolipophagy (lipophagy) in which LDs are encapsulated as a cargo and are degraded through the autophagic mechanism[109]. Degradation of LDs is synchronized between two pathways[110]. LDs, based on their size, can be sequestered as whole or in small parts, in case of a small or large LD, respectively[109]. Availability and accessibility of LDs for degradation are dependent on clearance of the overlaying proteins, perilipins. In other words, perilipin proteins degradation is a prerequisite of LD degradation. These proteins contain KFERQ motif and are degraded by CMA[111]. Lipophagy is under control by master key regulators of the cell like mTOR, AMPK and CREB[112-114].

Lipophagy is a process which consists of an interplay between autophagy, LD degradation, cholesterol availability and sex steroid synthesis. To the best of our knowledge, no human data is present on the effect of this process on ovary sex steroid synthesis. Similar studies show the effect of autophagy on lipid metabolism in hepatocytes[109] and cholesterol trafficking and testosterone synthesis on Leydig cells[115]. In this translational research study, we aimed to observe the role of autophagy in cholesterol synthesis, trafficking and accessibility as well as in steroid hormone synthesis and utilization by inducing and activating autophagy in isolated primary human granulosa luteinized cells, human non-luteinized granulosa cell line and corpus luteum tissue, with a specific emphasis on basal and induced steroidogenesis.

Chapter 2: Materials and Methods

2.1. Study plan and length

This is a translational research study performed at Koç University Research Center for Translational Medicine (KUTTAM) located in Koç University Hospital between 2018-2021. Materials researched in this study are primary human luteal granulosa cell, human non-luteinized granulosa cell line and human corpus luteum tissues.

2.2. Patients

Human luteal granulosa cells were collected from the aspirated follicular fluid of the patients undergoing oocyte pick-up (OPU) procedure in the *in-vitro* fertilization (IVF) centers of Koç University Hospital and American Hospital. 80 patients were recruited for this study (mean age ± SD: 32.3 ± 4.4) based on the sample size calculation and power analysis.

Ovarian stimulation in these patients was undertaken with a gonadotrophin releasing hormone antagonist (250 mg/d, Cetrotide, Merck-Serono, Istanbul, Turkey) combined with recombinant human follicle stimulating hormone (rhFSH, 225-275 IU/day Gonal-F, Merck-Serono, Istanbul, Turkey). Final maturation of the oocytes was induced with 250 μg recombinant hCG (Ovitrelle; Merck-Serono, Istanbul, Turkey) when a leading follicle of ≥ 19 mm and two or more trailing follicles of ≥ 17 mm were recorded. Follicular aspiration was performed 36 hours after ovulation trigger. Women below 40 years of age with male factor infertility were included in the study. Those who had been diagnosed as unexplained infertility, polycystic ovary syndrome or endometriosis were excluded.

Corpus luteum tissues were collected from five patients (mean age ± SD: 25.3 ± 5.2) who had undergone laparoscopic ovarian tissue sampling for fertility preservation (n=5) during the luteal phase of the menstrual cycle. Corpus luteum was gently removed from the tissue and used for the assays.

This study was approved by the institutional review board of Koç University (IRB#2019. 299. IRB2.092). Informed constent was taken from all the recruited patients

and sensitive health and personal data was preserved according to the rules and regulations regarding data privacy and protection.

2.3. Chemicals and reagent

2.3.1. Chemicals

Chloroquine diphosphate salt, which stalls autophagosome lysosome fusion step by decreasing lysosomal pH inhibiting autophagy, was obtained from Fisher Scientific (CAS#: 50-63-5, Thermo Fisher Scientific Inc., MA, USA). Vinblastine sulphate salt, a chemotherapeutic agent which inhibits autophagy, was purchased from Merck (CAS#: 143-67-9, Sigma-Aldrich Company GmbH Germany). InSolution rapamycin, which inhibits mTOR and activates autophagy, was purchased from Calbiochem (CAS#: 553211-1MG, Sigma-Aldrich Company GmbH Germany). Ovitrelle (250 μg/0.5 mL) and Gonal-f (75 IU), both stimulators of ovarian steroidogenesis, were purchased from Merck (Sigma-Aldrich Company GmbH Germany). All the reagents were applied at their physiological range of action to the primary cells, cell lines and tissues.

Oil Red O, a dye of neutral lipids in the cells, was purchased from Merck (CAS#: 1320-06-5, Sigma-Aldrich Company GmbH Germany). Lysotracker (CAS#: L7526), a dye lively staining lysosome and Mitotracker green and red (CAS#: 7514 and 7513), a dye lively staining mitochondrion, were purchased from Invitrogen (Thermo Fisher Scientific Inc., MA, USA). All Alexa probes, used as secondary antibodies in the immunofluorescence procedure, were purchased from Life Technologies (Thermo Fisher Scientific Inc., MA, USA). Super Block reagent (CAS#: AAA125) was obtained from Biotech Life Science (ScyTek Laboratories, Inc USA). YO-PRO®-1 Iodide was obtained from Life Technologies (CAS#: Y3603, Thermo Fisher Scientific Inc., MA, USA).

Signal Silence® Beclin-1 siRNA I (CAS#: 6222), Signal Silence® Atg5 siRNA I (CAS#: 6345) and Signal Silence® Control siRNA (CAS#: 6568, Unconjugated) were obtained from Cell Signaling Technology Inc. (MA, USA). Lipofectamine® 3000 (CAS#: L3000-075), transfection reagent, was obtained from Invitrogen (Thermo Fisher Scientific Inc., MA, USA).

2.3.2. Cell culture media and supplements

Dulbecco's Modified Eagle Medium: F12 (1:1 mixture) with HEPES (15mM), L-Glutamine and 3.151 g/L glucose was purchased from Lonza Bioscience (CAS#: BE12-719F, Switzerland). Fetal Bovine Serum (FBS) (CAS#: 16140071) heat inactivated (HI), cell culture tested, Opti-MEM™ I Reduced Serum Medium (CAS#: 31985070) and Penicillin-Streptomycin (5,000 U/mL) (CAS#: 15070063) were obtained from Gibco (Thermo Fisher Scientific Inc., MA, USA). Amphotericin B solution (CAS#: A2942) was obtained from Merck (Sigma-Aldrich Company GmbH Germany). TransIT-X2® Dynamic Delivery System (CAS#: MIR 6006) was purchased from Mirus (Madison Wisconsin, USA).

2.3.3. Cell line

Human non-luteinized granulosa cell line (HGrC1) was donated by Akira Iwase (Nagoya University, Japan).

2.3.4. Primary antibodies

Anti-LC3A/B XP® Rabbit (CAS#: 12741), Anti-SQSTM1/p62 Mouse (CAS#: 88588), Anti-Atg5 Rabbit (CAS#: 12994) and Anti-Beclin-1 Rabbit (CAS#: 3495) primary antibodies were obtained from Cell Signaling Technology Inc. (MA, USA). Anti-Vinculin primary antibody was purchased from Sigma-Aldrich Company (CAS#: V4139, GmbH Germany). Anti-StAR (CAS#: sc-166821), Anti-3β-HSD (CAS#: sc-515120) and Anti-Aromatase (CAS#: sc-374176) were obtained from Santa Cruz Biotechnology, Inc (CA, USA). Anti-Perilipin 3/TIP47 (CAS#: ab47638), Anti-LAMP2 (CAS#: ab25631), Anti-PARP (CAS#: ab191217) and Anti-Actin-Phalloidin (CAS#: ab179467) were purchased from Abcam (USA).

2.3.5. Secondary antibodies

Anti-rabbit IgG (CAS#: 7074P2) and anti-mouse IgG (CAS#: 7076P2) HRP-linked Antibodies were purchased from Cell Signaling Technologies Inc. (MA, USA).

Goat anti-Mouse IgG (H+L) Alexa Fluor 488 (CAS#: A32723), Goat anti-Rabbit IgG (H+L) Alexa Fluor 488 (CAS#: A32731), Goat anti-Mouse IgG (H+L) Alexa Fluor 594 (CAS#: A32742) and Goat anti-Rabbit IgG (H+L) Alexa Fluor 594 (CAS#: A32740) were purchased from Invitrogen (Thermo Fisher Scientific Inc., MA, USA).

2.3.6. Different reagents

Bovine serum albumin (BSA) (CAS#: 9048-46-8), Dimethyl sulfoxide (CAS#: 67-68-5), 100 percent methanol (CAS#: 67-56-1), Trypan Blue (CAS#: 72-57-1), Triton™ X-100 (CAS#: 9036-19-5), Tween-20 (CAS#: P9416), Dulbecco's Phosphate Buffered Saline (DPBS) (CAS#: 56064C), 10X Phosphate Buffered Saline (PBS) (CAS#: P5493), 0.25 percent Trypsin-EDTA Solution 1X (CAS#: 59428C), Tris-base (CAS#: 77-86-1), Hoechst 33342 (CAS#: 875756-97-1), Tris-HCl (CAS#: 1185-53-1), Sodium Chloride (CAS#: 7647-14-5), Paraformaldehyde (CAS#: 30525-89-4) and glycine (CAS#: G8898) were obtained from Merck (Sigma-Aldrich Company GmbH Germany). cOmplete™ EDTA-free Protease Inhibitor Cocktail (CAS#: 4693132001) and Phosphatase Inhibitor Cocktail (CAS#: P2850-5ML) were purchased from Roche (Sigma-Aldrich Company GmbH Germany). 4′,6-diamidino-2-phenylindole or DAPI was obtained from Abcam, UK. Superblock solution was purchased from ScyTek, USA.

2.3.7. Instruments

Micropipettes (10 µl, 20 µl, 200 µl and 1000 µl, Eppendorf, Germany), Serological pipettes (5 ml, 10 ml, 25 ml and 50 ml, Greiner Bio-One, Austria), Cell culture flasks (T-25 and T-75, Sarstedt, Inc. Germany), Eppendorf tubes (0.5 ml, 1.5 ml and 2 ml, Sarstedt, Inc. Germany), Falcons (15 ml, 50 ml, Sarstedt, Inc. Germany), Filters (250 ml, 500 ml, 1000 ml, Sarstedt, Inc. Germany), Cell culture plates (6-, 12-, 24-, 48- and 96-well, Sarstedt, Inc. Germany), Coverslip (12 mm and 13 mm, Sarstedt, Inc. Germany), Cryovials (1.8 ml, Stellar Scientific, USA), Haematocytometer (Neubauer, Isolab), PVDF membrane 0.45 µm (Sigma-Aldrich Company GmbH Germany), Whatman paper (Sigma-Aldrich Company GmbH Germany), Glass bottomed plates (Sarstedt, Inc. Germany), 0.22 µm filter sets (Sarstedt, Inc. Germany), Dual-colour protein marker (Bio-Rad, USA), Centrifuges (Eppendorf, Germany), CO_2 incubator (Heraeus, Germany),

Inverted microscope (), -20°C and -80°C freezers (Beko, Turkey and Thermo Fisher Scientific Inc., MA, USA), Magnetic Stirrer and Heater (Sartorius AG, Germany), BioChem Vacuum (BVC professionals, England), Vortex (Heidolph, Germany), Laminar flow cabinet (Thermo Fisher Scientific Inc., MA, USA), Homogenizator (IKA T10 standard, IKA), Balance (Uni Bloc, Shimadzu), Waterbath (VWR, USA), pH meter (Mettler, Toledo), Mini-PROTEAN Tetra Cell Electrophoresis System, Mini Trans-Blot Cell Blotting System, ChemiDoc Gel Imaging System (Bio-Rad, USA), Real-Time PCR (Roche, Switzerland).

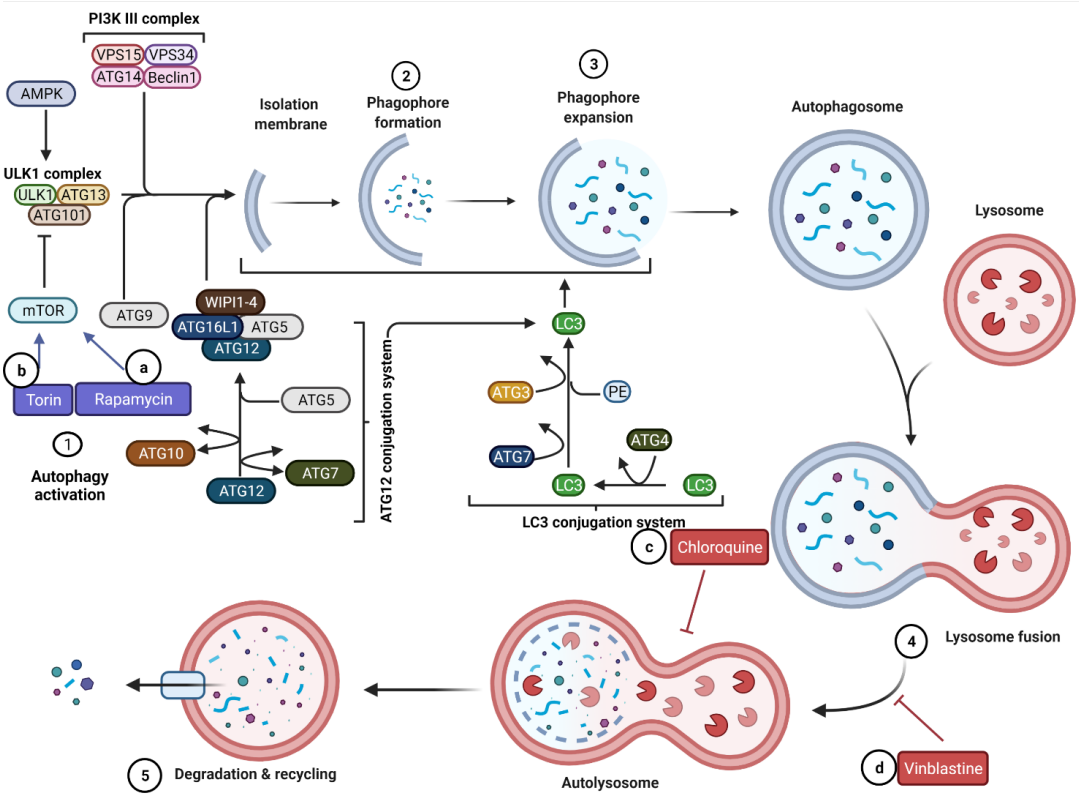

Figure 7. *Action mechanisms of autophagy pharmacological activators and inhibitors. a) Rapamycin is a specific inhibitor of mTORC1 complex, key master switch complex activating autophagy. b) Torin uses the same mechanism as rapamycin, the only difference being that torin inhibits both mTOR complexes, both leading to autophagy activation. c) Chloroquine is a weak base which upon entering the lysosome changes lumen pH, inhibiting degradation causing an accumulation of autophagic cargo in lysosome. d) Vinblastine, also a chemotherapeutic agent inhibits fusion of mature autophagosome with lysosome stalling autophagy at that stage*[116].

2.4. Primary human luteal granulosa cells

2.4.1. Isolation of HLGCs

When a dominant follicle(s) was observed in the patient receiving an IVF treatment, ovulation was triggered with hCG. After 24-36 hours these follicles were collected in order to be fertilized *in-vitro*. During the oocyte pick up procedure, a guiding needle is inserted through the vagina passing through the ovaries and entering into each follicle larger than 10 mm by emptying the follicle liquid. The foolicular aspirate contains the the oocyte to be used in the IVF laboratory as well as luteinized granulosa cells, epithelial cells, fibroblasts and red blood cells (RBCs). All these cells that accompany the oocyte, are discarded by the end of a routine follicular aspiration procedure. RBCs are the highest in number in this fluid and since they are denser than HLGCs, they may attach and coat the cell culture vessel surface causing HLGCs to float in the medium and not be able to attach. Clearing RBCs from the follicular fluid will yield a HLGC-rich culture. At the same time, blood clots and different tissue fragments resembling HLGCs should be cleared before culturing since they damage HLGCs.

80 IVF patients who underwent OPU procedure were recruited to this study and HLGCs were isolated from their follicular fluids. A procedure similar to that employed by Lobb et. Al[117] was changed and optimized to the needs of our cells and this modified procedure used to isolate human luteal GCs during this study. Collected follicular fluids in IVF laboratory were transfered into 50 ml centrifuge tubes with conical bottoms. This tubes were balanced and centrifuged at 500 g for 5 minutes with a soft acceleration and decceleration. Supernatant was aspirated through a vacuum pipe while the pellet was kept undisturbed. The size of the pellet and the amount of erythrocytes in it determines the amount of solutions to be added later. In a normal sized pellet, 18 ml of double distilled water (ddH_2O) and 2 ml of concentrated 10X phosphate buffer saline (10X PBS, pH=7.4) is added. Antibacterial and antifungal antibiotics were added to both the ddH_2O and 10X PBS to minimize the risk of contamination since being a primary cell culture and since female reproductive tract has a rich flora it imposes a high risk for contamination in our culture of HLGCs. After adding the ddH2O, the pellet is resuspended gently for approximately 20-30 seconds and then 10X PBS is added. Centrifugation at 500 g for 5 minutes with a soft acceleration and decceleration follows and the supernatant is discarded since it now contains swelled RBCs. Another washing step is repeated if the

red blood cells are still present in the pellet. Normally 2 washing steps are performed in order not to damage and put under stress human luteinized granulosa cells. After the third centrifugation again at at 500 g for 5 minutes with a soft acceleration and decceleration, supernatant is discarded and the pellet now contains mostly HLGCs. This pellet is resuspended using DMEM/F12 cell culture media supplemented with 10percent (v/v) FBS and 1percent (v/v) Penicillin-Streptomycin-Amphotericin B Solutions. After the resuspension HLGCs are counted.

2.4.2. Counting of HLGCs

After the washing steps the pellet is resuspended with cell culture media. At this step, small tissue particles, if present, are discarded and the mixture is made homogenous by gentle, constant pipeting. In order to have an equal seeding and cell density in the cell culture vessels, HLGCs are counted using Trypan Blue method. This method discerns the dead cells from the live ones by their ability to not uptake trypan blue due to the plasma membrane selectivity and integrity of a live cell. Firstly, 10 μl of trypan blue solution is transferred onto a paraffin paper and after the cell mixture containing human luteinized granulosa cells is well resuspended, the same volume is taken from the cell homogenate and mixed with the trypan blue on the paraffin. The resultant 1:1 mixture is then transferred into a haematocytometer, mediated by the capillary effect of the coverslip on it. Four corner squares are counted for the live cells and the average is calculated. This value is multiplied by the volume of the media used to resuspend the pellet and the factor of the haematocytometer which in our case is 10^4. Based on the number of viable cells counted by this method an equal number of live human luteinized granulosa cells is seeded at different cell culture dishes.

2.4.3. Culture of HLGCs

HLGCs were cultured in DMEM/F12 supplemented with 10 percent (v/v) FBS and 1 percent (v/v) penicillin-streptomycin-amphotericin B (PSA) solution at an incubator with 37°C with 5 percent CO_2 values. Due to their primary origin, these cells do not proliferate even when promoted with a proliferation stimulus. For this reason, handling of the isolated HLGCs is vital to their attachment and continuation for a short

period in culture. These cells are cultured in different cell culture dishes based on their terminal experimental purpose. In case of conventional immunofluorescence procedure HLGCs are seeded in a 24-well or 12-well plate with the wells being added a suitable coverslip prior to seeding procedure. In case of live immunofluorescence procedure these cells are seeded on small glass bottom plates to minimize the side effects arising from the refraction index. In case of western blot procedure human luteinized granulosa cells are seeded into 6-well plates to increase the number of cells yielding a high protein concentration. Lastly in case of real time polymerase chain reaction (RT-PCR) experiment cells are seeded into 12-well plates. Density and number of cells varies depending on the dimensions of the cell culture dish.

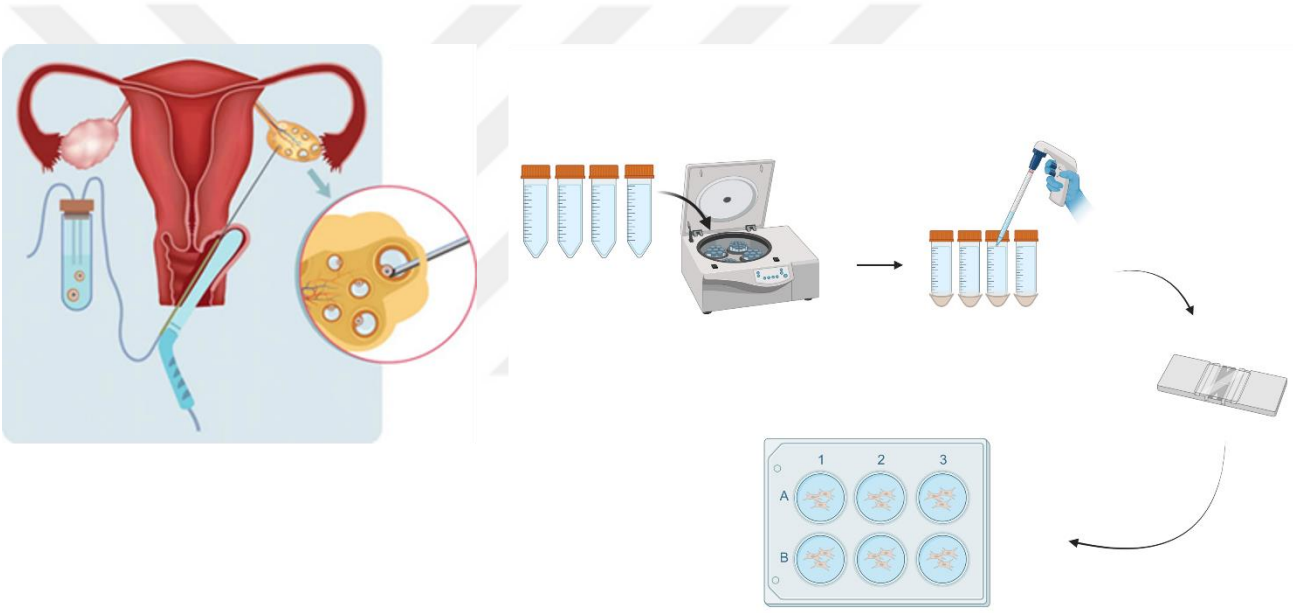

Figure 8. *Illustrative drawing of the OPU procedure carried out in the IVF laboratory and human luteal granulosa cell isolation and culture.*

2.4.4. Characterization of HLGCs

In this study human luteinized granulosa cells are characterized in a two-step procedure. HLGCs synthesize both sex steroid hormones estrogen and progesterone, in vitro, and respond to outside stimulus and change their hormone synthesis pattern (118). In our isolated and cultured cells, the only type of cells that can synthesize both these hormones are the HLGCs leading to characterization that the isolated cells are indeed

human luteal granulosa cells. For these sex steroid hormones to be synthesized a great amount of lipids should be present inside the cells or should be synthesized *de novo*. To be able to observe the presence of the lipids which serve as a source for sex steroid hormones we stain the cells with Oil Red O which is a dye staining neutral lipids in the cells. So, the cells designated by their characteristic shape, excessive lipid content which serve as a substrate for sex steroid hormones synthesis determines that the isolated and cultured cells are indeed human luteinized granulosa cells.

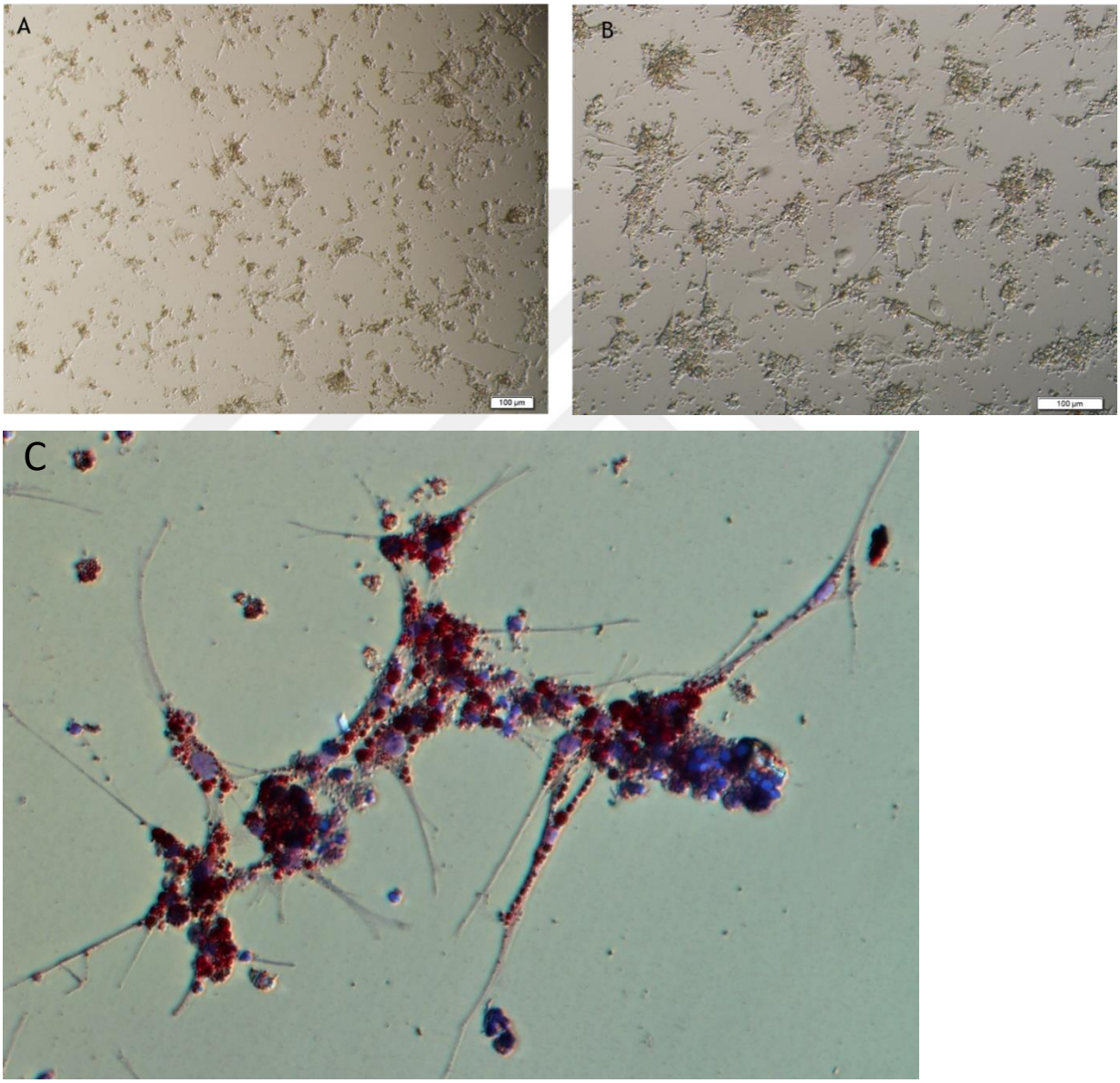

Figure 9. *Characterization of human luteal GCs. Image representation of the characteristic shape of the isolated human luteinized granulosa cells observed in light*

microscope at A) 4X and B) 10X. C) Lipid content of HLGCs shown by the Oil Red O dye further characterizing our isolated cells as HLGCs.

2.5. Treatment of HLGCs

Following counting and equal seeding human luteal GCs will be kept in culture for 24 hours and then their attachment rate and development will be observed. Plates showing a high density, high attachment rate, homogenous culture and well-developed shapes of the cells will be selected to be treated. All treatment concentrations were applied in their physiological ranges and/or previously tested concentrations.

2.5.1. Inducing steroidogenesis

Human luteal granulosa cells are cells which synthesize sex steroid hormones and have a very active steroidogenic activity. For this reason, different steroidogenic proteins and enzymes are present and are highly expressed in these cells. Examples of these proteins are StAR, 3β-HSD, 17β-HSD, and aromatase. To further prove this fact and to observe how induced steroidogenesis will affect autophagy and cholesterol uptake and trafficking we treated human luteal GCs with different, increasing concentrations of hCG. The layout of the experiment was as follows:

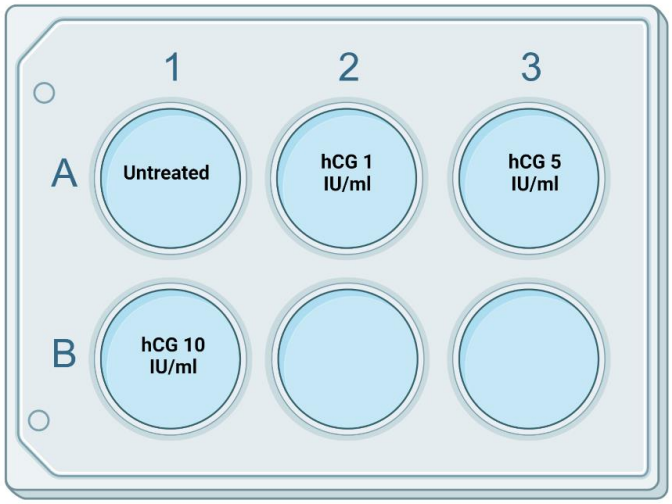

Figure 10. *Image representation of promoting steroidogenesis experiment by using hCG. Untreated stands for culture media only.*

2.5.2. Inducing autophagy

To pharmaceutically induce autophagy we used rapamycin inhibiting formation of mTORC1 complex and leading to inducing of autophagy. This activator was used in previously proven and optimized ranges of concentrations.

2.5.3. Inhibiting autophagy

We pharmaceutically inhibited autophagy at two different steps, at fusion step using vinblastin and at hydrolysis step using chloroquine. Both inhibitors of autophagy were used at previously proven and optimized ranges of concentrations. The layout of the experiment was as follows:

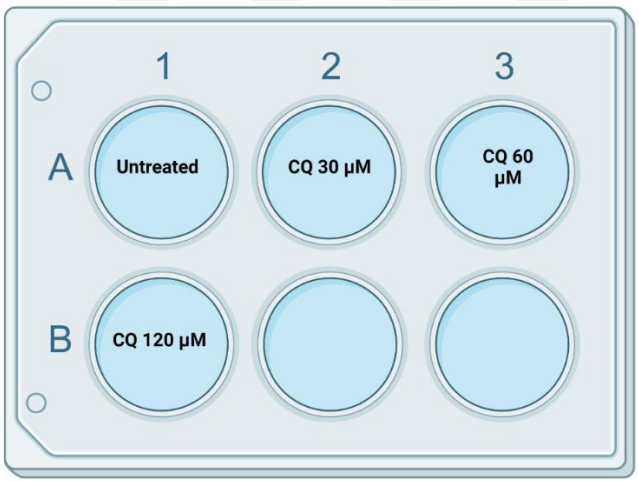

Figure 11. *Image representation of pharmacologically inhibiting autophagy. This experiment is exemplified by using only chloroquine. Untreated stands for culture media only.*

2.5.4. Stimulating steroidogenesis and inhibiting autophagy

To observe the effect(s) of stimulated steroidogenesis in basal autophagy and to observe the changes occuring when autophagy is gradually inhibited/activated we performed an experiment in which dual treatments regarding steroidogenesis and autophagy were included. The layout of the experiment was as follows:

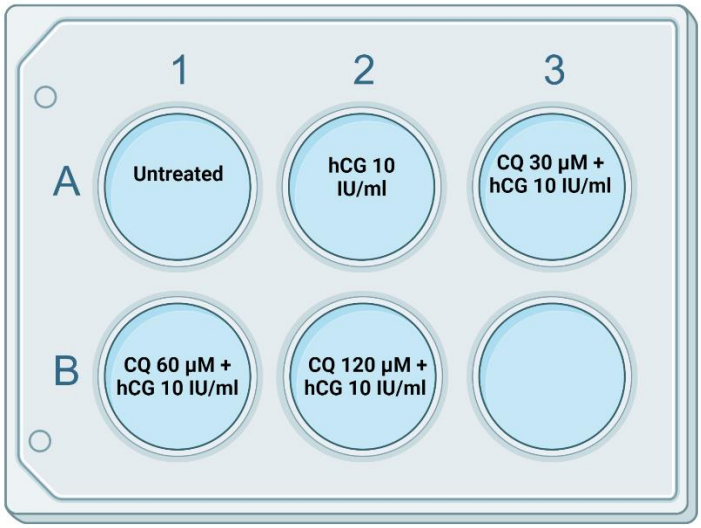

Figure 12. *Image representation of simultaneously pharmacologically inhibiting autophagy and stimulating steroidogenenesis. This experiment carried out in HLGCs is exemplified by using chloroquine and hCG. Similar setup is applied for inhibiting autophagy. Untreated stands for culture media only.*

2.6. Human Ovarian Tissue

2.6.1. Preparation and culture of ovarian tissues

Ovarian cortical tissues and corpus luteum tissues were obtained under aseptical techniques. After being transferred to the laboratory the tissues were firstly washed into a glass petri dish with 1X PBS and then were cut into equal pieces with dimensions of 0.4 cm x 0.4 cm x 0.4 cm and lastly were cultured *in-vitro* in 6-well plates with 3 ml of DMEM/F12 culture media supplemented with the respective treating reagent.

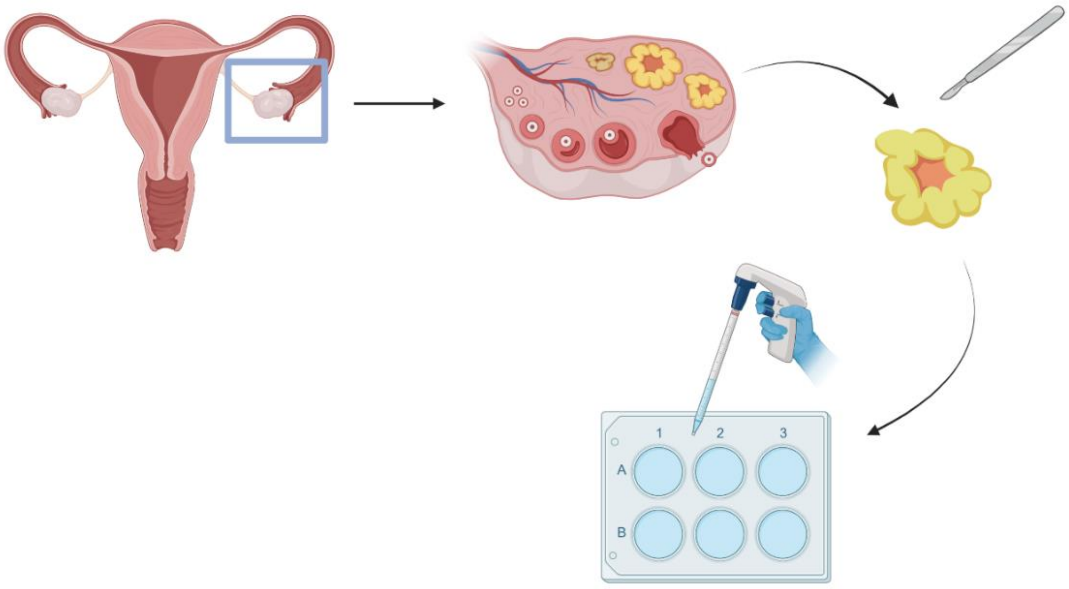

Figure 13. *Image representation of obtaining, preparing, and culturing ovarian cortical tissues (not shown) and corpus luteum tissues.*

2.6.2. Treatment of ovarian tissues

Except using human luteal GCs which are steroidogenic cells, we wanted to observe the effect(s) of inhibiting autophagy on basal and stimulated steroidogenesis in a different tissue. For this reason we used ovarian cortical tissue and corpus luteum tissue, both of which steroid synthesizing tissues and with an important role in maintaining ovary steroidogenesis and reproduction in general. In this experiment we used a single concentration of chloroquine (50 μM) and hCG (10 IU/ml) to inhibit autophagy and stimulate steroidogenesis respectively. All concentrations were optimized and used in physiological ranges. Treatment groups were as follows:

a) Untreated- Culture media only.
b) hCG (10 IU/ml).
c) Chloroquine (50 μM).
d) Chloroquine (50 μM + hCG 10 IU/ml).

Duration of the treatments was 24 hours, and the tissues were treated directly after being cut into small pieces and cultured.

2.7. Mitotic granulosa cell line

This cell line is developed from primary granulosa cells of a 35-year-old female and then immortalized by lentiviral transfer of some key steroidogenic genes like StAR, aromatase, gonadotropin receptors and P450scc. This cell line shares characteristics with primary granulosa cells in the follicles at the early stages of development. For this reason, it may be used to study the molecular and transcriptional factors defining the transition from the gonadotropin-irresponsive to gonadotropin-responsive stage in folliculogenesis[119].

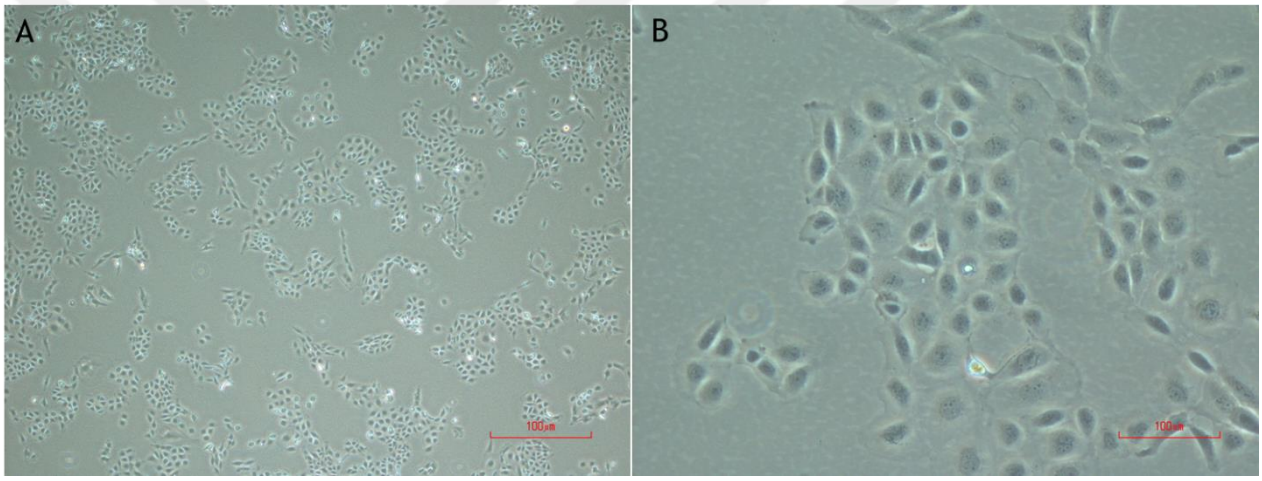

Figure 14. *HGrC1 cell line observed under the light microscope. A) 4X and B) 20X magnification.*

2.7.1. Thawing of cells

Previously cryopreserved cells were taken out of the nitrogen tank and quickly warmed to 37°C. The molten cell mixture was transferred into a 15 ml falcon tube. Afterwards pre-warmed cell culture media was slowly and drop by drop added to the mixture and with mild mixing action not to cause harm to the thawed cells from the rise in the osmotic pressure directly. To discard DMSO used in the cryopreservation of cells, which is toxic and harmful to them, the cell mixture was centrifuged at 500 g for 5

minutes. Supernatant was discarded while the pellet is resuspended in cell culture media. This cell mixture was seeded into a cell culture dish and the next day medium was changed to remove non attaching cells and remaining DMSO. To be able to get the best results from the experiments that will be carried, the cell line is at least once subcultured and then used for that specific experiment.

2.7.2. Culturing and subculturing conditions

HGrC1 cell line was cultured on DMEM/F12 cell culture media supplemented with 10 percent (v/v) FBS and 1 percent (v/v) Penicillin-Streptomycin-Amphotericin B Solutions. It was incubated at 37°C, 5 percent (v/v) CO_2 and 95 percent (v/v) air conditions.

Subculturing the cells was decided when the cells achieved 75-85 percent confluency. The cells in the cell dishes were firstly washed with 1X DPBS (pH=7.4) then treated with 0.25 percent Trypsin-EDTA and incubated for 5 minutes at 37°C. To inactivate trypsin activity FBS-supplemented cell culture media was added and cells were collected. Cell mixture was centrifuged at 500 g for 5 minutes and the supernatant was discarded. Remaining pellet was resuspended in the cell culture media.

2.7.3. Cell counting

After the cell subculturing step, when the cells were resuspended with the cell culture media as explained in section 6.1. 10 µl of the cell mixture was mixed with 10 µl of trypan blue solution on a paraffin paper and leaded in one side of the haematocytometer. 4 different squares were counted for viable cells and after taking the average the number was multiplied with the volume of the media used to resuspend the pellet and the factor of the haematocytometer which in our case is 10^4. Cell seeding is performed in an equal number and based on the number of the cells counted.

2.7.4. Cell freezing

When the cells achieved confluency (75-85 percent) and are ready to be subcultured, they are treated with trypsin as explained in section 6.2. After the cells are detached from

the culture dish, they are transferred in a 15 ml falcon and centrifuged at 500 g for 5 minutes. Meanwhile a freezing mix composed of 10 percent (v/v) dimethyl sulfoxide and 90 percent of cell culture media (DMEM/F12) supplemented with 20 percent (v/v) FBS. The centrifuged cells supernatant was discarded while the pellet was resuspended in the freezing solution. Density at of the cells was calculated to be at 1.2×10^6 cells per cryovial. Cryovials were firstly preserved at -80°C within a freezing container for 12-24 hours then transferred into a liquid nitrogen tank for long term storage.

2.8. siRNA Treatment

After the cells were isolated and cultured at 6-well plate for Western Blot (500.000 cell/well) and at 24-well plate (100.000 cell/well) for immunofluorescence. siRNA treatment was performed after 24 hours in culture of the human luteal GCs. We picked two vital genes playing a role in autophagy to silence in human luteal GCs, Beclin1 and Atg5 to silence using siRNA technology. TransIT-X2 was used as a transfection reagent and was previously warmed in room temperature and gently mixed to create a homogenous mixture. The method explained here was applied for Western Blot technique in 6-well plate. 250 µl of Opti-MEM I Reduced Serum was warmed in room temperature and transferred in a new 1.5 ml Eppendorf tube. Based on the siRNA stock concentration we calculate that the final, working solution of each siRNA/well to be 50 nm and the required quantity was transferred in the Opti-MEM I Reduced Serum solution and was gently mixed. 7.5 µl of TransIT- X2 was added to the solution and after gentle mixing it was incubated at room temperature for 30 minutes. Following incubation, siRNA solution was dropwise transferred to each well and the plate was gently moved for the dropwise to be homogenously distributed in the whole well. siRNA treatment duration was optimized and we used two different timelines 24- and 48-hours. Opti-MEM I Reduced Serum, TransIT-X2 and siRNA quantities were adjusted for 24-well plate. Spent media was collected for hormone synthesis measurements while cells were either collected for Western Blot technique or were fixed to proceed with conventional immunofluorescence.

2.9. shRNA Treatment

Since gene silencing using siRNA is not stable and transfecting non-viral material to primary cells is challenging and the result is not very efficient we choose another gene silencing technology to inhibit one important autophagy gene, Beclin1, in a mitotic human granulosa cell line, HGrC1. shRNA technology offered us a stable transfection enabling silencing of Beclin1 gene through generations with a high efficiency in HGrC1 cell line. After sub-culturing 300.000 cells/well were seeded and shRNA treatment was performed after 24 hours. For every shRNA transfection reaction two different mixtures were prepared. In Solution A, shRNA plasmid DNA was diluted in shRNA plasmid transfection medium while in Solution B, shRNA plasmid transfection reagent was diluted again in shRNA plasmid transfection medium. Solution A was gently mixed with Solution B and were incubated at room temperature for 40 minutes. While the solutions were in incubation, cells were washed twice with shRNA transfection medium and shRNA plasmid transfection medium was added together with mixed solution (A+B). Solutions were added in a dropwise manner and the plate was gently moved to lead to homogenous distribution of the added reagents. The cells were cultured for 6-10 hours with these reagents at 37 °C, 5 percent CO_2 conditions and then cell culture media was replaced with 10 percent added DMEM/F12 cell culture media. Then cells were treated with an increasing FSH concentration (25-50 mIU/ml) while control shRNA and Beclin1 shRNA were in a constant concentration. Spent media was collected for hormone synthesis measurements while cells were collected for further protein isolation and Western Blot.

2.10. Protein expression

2.10.1. Cell lysate preparation

Human luteal GCs and HGrC1 cells were seeded in 6 well plates with a density of 500.000 cells/well and 300.000 cells/well respectively. The reason for the difference in cell number is due to the proliferation of HGrC1 cell line while HLGCs are a non-proliferating cell line. After application of the treatment(s) 24 hours after seeding, collecting of the cells is done based on the duration of the respective treatment(s). The spent media is discarded by vacuum and cells are washed once with 1X DPBS. Later cells are treated with 0.25 percent Trypsin-EDTA and incubated for 5 minutes at 37 °C. Culture

media is added to the wells to inactivate trypsin and the mixture is transferred into a 1.5 ml eppendorf tube and centrifuged at 1000 g for 8 minutes. Supernatant is discarded, pellet resuspended with 1X DPBS and centrifuged at 1000 g for 8 minutes. Supernatant is discarded while pellet containing cells is resuspended with RIPA buffer mixture (150 mM NaCl, 1.0 percent Nonidet P-40, 0.5 percent sodium deoxycholate, 0.1 percent sodium dodecyl sulfate (SDS), 50 mM Tris,1 µl of 100X proteinase inhibitor cocktail/100µl RIPA and 5 µl of 20X phosphatase inhibitor/100µl RIPA). RIPA buffer quantity depends on the size of pellet, with 100 µl RIPA buffer mixture being the standard one. After resuspending the pellet with RIPA buffer mixture, eppendorf tubes are kept on ice and vortexed for 30 seconds every 5 minutes in a total of 30 minutes. Later tubes are centrifuged at 14000 rpm for 15 minutes at 4°C and supernatant containing proteins are transferred into new 1.5 ml eppendorf tubes while the pellet containing cell debris is discarded. Proteins are transferred into an -80 °C freezer for further storage.

2.10.2. Lysate preparation from tissues

After corpus luteum tissues are cultured in 6-well plates and treated with the respective chemicals tissue pieces are collected into a flat bottom 2 ml eppendorf tubes. Collected tissues are firstly washed with 1X DPBS and then later RIPA buffer mixture is added, and the tubes are put into ice for the latter procedures. Standard volume for average tissue volume is 180-200 µl of RIPA buffer mixture. Tissues are now homogenized with help of a homogenizer in two steps firstly 45 seconds and then after 30 seconds pause another 45 seconds more. Homogenized tissues are left on ice for 30-45 minutes in order for the lysate to settle down and centrifugation at 14000 rpm for 15 minutes at 4°C. Last steps were done as explained in section 2.10.1.

2.10.3. Protein concentration quantification

Protein concentration was calculated using Pierce™ BCA Protein Assay Kit. This kit measures protein concentration in samples by detecting cuprous cation, Cu^{1+}, by BCA. For this purpose, BSA is used as a standard in 8 different concentrations (2000-1500-1000-750-500-250-125-25 µg/ml) and lastly a blank sample containing ultrapure water. 10 µl of all these standards were loaded in duplicates in a transparent, flat bottom 96-well

plate. 10 µl of the samples were loaded in duplicates in the same plate. Working reagent is prepared from reagent A and reagent B in a ratio of 50:1. From this working reagent solution 200 µl is added to each well in the 96-well plate, both standards and samples. Then the solution is gently mixed, and the plate is incubated for 30 minutes at 37°C. Afterwards the plate is read at 592 nm in a spectrophotometer. The data are imported, and protein concentrations are calculated accordingly.

2.10.4. SDS-PAGE

To be able to run the proteins through SDS-PAGE a mastermix of 4x Laemmli buffer and β-mercaptoethanol in the ratio of 10:1 is prepared, and it is added to the protein samples based on their volume on a ratio of 3:1 (protein volume: mastermix). Then cells are heated at 95°C for 5 minutes, put on ice and then spawn down. Gel-casting apparatus was adjusted, and the ready-made gels were put, and the apparatus was closed and put in the tank. After removing the comb, 1X running buffer (192 mM glycine, 25 mM Tris and 0.1 percent (w/v) SDS, pH=8.3) was added to the tank. Dual colour protein molecular weight marker was loaded at the first well and then on turn the prepared samples. Electrophoresis was started at 80 V until the proteins pass through the stacking part of the gel and then the voltage was increased at 100 V until the proteins run through the separating gel, which is followed by the bromophenol blue part of the prepared protein samples. The most common used ready-made gel was Mini-PROTEAN® TGX™ Precast Protein Gel, 10-well, 50 µl volume/well and 4-20 percent, suitable for separation of polypeptides >10 kDa.

2.10.5. Immunoblotting

Following electrophoresis procedure, the gels were taken out of the gel casting apparatus and left in the tank while transfer set up was being arranged. Semi-dry transfer method was employed and the type of PVDF membrane used was the one with 0.45 µm pore size. Firstly, the PVDF membrane was activated with 100 percent methanol and then transferred into the 1X transfer buffer. Whatman papers were also soaked in 1X transfer buffer. The cassette was adjusted according to the sandwich setup, starting with the Whatman paper then the PVDF membrane, the gel and lastly again Whatman paper. The

transfer parameters were 30 minutes in 1.0 A and 25 V. After transfer process is finished, its efficiency is checked by applying Ponceau S solution (0.1 percent (w/v) in 5 percent acetic acid) on the membranes for 1 minute on shaker which binds to the positively charged amino groups and non-covalently to non-polar regions in the proteins. Following determination that transfer was achieved successfully the membrane was washed twice with 1X TBS-T (20 mM Tris-HCl, pH 7.8, 150 mM NaCl, 0.1 percent, Tween 20 (v/v) pH 7.4) on shaker. Afterwards membranes were blocked on five percent (w/v) non-fat dry powder milk prepared in TBS-T for 1 hour at room temperature. Later the membranes were washed on shaker 3 times 5 minutes each and then primary antibodies were applied on the membrane. Duration of primary antibodies was ~16 hours (overnight) at +4°C on shaker. Primary antibodies were diluted, at 0.2 percent Sodium Azide (v/v) in 0.3 percent BSA prepared in 1X TBS-T, according to the manufacturer's directions and optimization results. Following incubation primary antibodies were collected for reusage while the membrane was washed on shaker 3 times 5 minutes each. Secondary antibodies were prepared on five percent (w/v) non-fat dry powder milk prepared in TBS-T according to the manufacturer's directions and optimization results and incubated for 1 hour at room temperature on shaker. Lastly the membrane was washed on shaker 3 times 5 minutes each while Clarity™ Western ECL Substrate was prepared. This kit contains Clarity Western Peroxide Reagent and Clarity Western Luminol/Enhancer Reagent which are mixed in a ratio of 1:1 with the membrane incubated for 2 minutes in the master mix preparation. The membrane was then transferred into ChemiDoc Gel Imaging System for imaging under the chemiluminescence mode. Exposure time depends on the expression of proteins and quality of the primary-secondary antibody complex formation.

2.11. Gene expression

2.11.1. Total RNA isolation

Human luteal GCs were seeded in a 6-well plate at 500.000 cells/well and the treatments were applied 24 hours after seeding. After the duration of the treatments is fulfilled, cells were detached by adding 300 µl of Trizol reagent and after collection, were transferred into 1.5 ml eppendorf tubes. 50 µl of chloroform is added on the top of the samples and after being inverted several times were incubated at room temperature for 15

minutes. Later samples were centrifuged for 15 minutes at 12000 g at 4°C. After this step, phases were observed in the tubes and the clear phase containing RNA was collected and transferred into new 1.5 ml eppendorf tubes. 150 µl of isopropanol was added and the samples were incubated on ice for 15 minutes. Samples were centrifuged for 15 minutes at 12000 g at 4°C and the pellet is cleared by adding 75 percent (v/v) ethanol and centrifuged at 5000 g for 10 minutes at room temperature. Supernatant was discarded while the pellet was dried out in room temperature and resuspended by RNase-DNase free water. Concentration of the isolated total RNA is read spectrophotometrically at 260 nm by using a Nanodrop (Thermo Fisher Scientific, MA, USA) device firstly calibrating it with a blank sample then measuring the samples. After measurement of the RNA concentrations samples were stored at -80 °C for further usage.

2.11.2. Reverse Transcriptase Polymerase Chain Reaction

1000 ng cDNA was synthesized from the isolated RNA samples using Sensiscript Reverse Transcriptase kit. According to producer's guidance the duration of the process was 1 hour, and the components of the reaction were as follows in the following table. Synthesized cDNA samples concentrations were measured by using a Nanodrop (Thermo Fisher Scientific, MA, USA) device.

Components	**Volume/reaction**
10x Buffer	2 µl
dNTP (5mM)	2 µl
Oligo-dT primer (10 µM)	2 µl
Sensiscript Reverse transcriptase enzyme	1 µl
RNase-DNase free water	Dependent
Template	Dependent
Total reaction volume	20 µl

Table 1. *cDNA reaction synthesis mix using Sensiscript Reverse Transcriptase kit.*

2.11.3. Quantitative Real-Time Polymerase Chain Reaction

After cDNA synthesis, quantitative real-time PCR expressions of different genes were studied using SYBR® Green Quantitative RT-qPCR Kit. Samples were checked on triplicates and relative quantification analysis was normalized using a housekeeping gene, GAPDH, which is ubiquitously expressed and is not affected by the treatments applied to our cells. Standard curves were obtained and compared when performing the analysis. Primers used in this study are listed in the following table.

Gene		**3'-Sequence-5'**
GAPDH	F:	ATGGAAATCCCATCACCATCTT
	R:	CGCCCCACTTGATTTTGG
StAR	F:	AAACTTACGTGGCTACTCAGCATC
	R:	GACCTGGTTGATGATGCTCTTG
SCC	F:	CAGGAGGGGTGGACACGAC
	R:	AGGTTGCGTGCCATCTCATAC
3β-HSD	F:	GCCTTCAGACCAGAATTGAGAGA
	R:	TCCTTCAAGTACAGTCAGCTTGGT
17β-HSD	F:	TGGGGTCCACTTGAGCCTGAT
	R:	TGCTGTGGGCGAGGTATTGG
Aromatase	F:	GGTCACCACGTTTCTCTGCT
	R:	GCAAGCTCTCCTCATCAAACCA
17α-OH	F:	GTTTCAGCCGCACACCAACT
	R:	ACTCACCGATGCTGGAGTCA
Beclin1	F:	TCCCGAGGTGAAGAGCATCG
	R:	TCGCCTGGGCTGTGGTAAGT
Ambra 1	F:	CGGGTTGTCGCCCTTTTCTAC
	R:	GACAGGGACATCAGTCGCTTCAG

Table 2. *Primers for the genes and their forward and reverse specific sequences.*

Cycle	Temperature	Time	Stage
1	95 °C	5 minutes	Initial Denaturation
2 (40 repeats)	95 °C	10 seconds	Denaturation
	62 °C**	30 seconds	Annealing
	72 °C	30 seconds	Extension
3	95 °C	5 seconds	Melting curve
	65 °C	1 minute	
	97 °C	Continuous	
4	40 °C	30 seconds	Cooling

Table 3. *Parameters of the qRT-PCR reaction. ** Temperature at this stage depends on the working temperature of the specific primer used in the reaction.*

2.12. Viability analysis

To observe the effects of different treatments on the viability of human luteal GCs we used an apoptosis detecting dye, YO-PRO™-1. This carbocyanine nucleic acid stain dye has an absorbance at 491 nm and emission at 509 nm and gives a green, fluorescent signal to the apoptotic cells. During apoptosis cells are unable to maintain a selectively permeable plasma membrane leading to a loss of integrity, stability and eventually cell death. YO-PRO™-1 uses this property by staining cells that are experiencing apoptosis by entering inside the cells and fluorescently staining them. Being very large in size and since live cells have a selectively permeable membrane it's not possible for this dye to enter inside viable cells. A very important advantage of this dye is that it only stains apoptotic/dead cells and not the live ones, making them useful for subsequent experiments on remaining viable cells.

After the cells were treated with the respective treatments, spent media was aspirated and fresh media supplemented with YO-PRO™-1 (0, 1 μM), to stain apoptotic cells, and Hoechst 33342 (1 μg/ml), to stain cell nucleus. After 30 minutes of incubation at 37 °C at 5 percent CO_2, fluorescent imaging of the cells was achieved using suitable channels in a fluorescent-sensitive microscope. Three hundred cells were counted in five different highly magnified areas in the treated cells and the percentage of the cells permeant to YO-

PRO™-1 was calculated. From this percentage the ratio of viable to apoptotic/dead cells was obtained.

2.13. Estradiol, Testosterone and Progesterone hormone level measurements

Since human luteal GCs are a steroidogenic type of cell, they synthesize sex steroid hormones estrogen and progesterone even in their basal activity. Following different treatments HLGCs synthesize these hormones at different rates in the culture media. Before cells are collected or fixed, 1 ml of the spent media is collected to perform the measurement. A highly sensitive and specific assay, Electro-chemiluminescence immunoassay (ECLIA), is used to measure the levels of estradiol, testosterone and progesterone in the culture media. Specific kits to progesterone (Elecsys Progesterone II, Cobas), estradiol (Elecsys Estradiol II, Cobas) and testosterone (Elecsys Testosterone II, Cobas) were performed according to the manufacturer's instructions and also optimized accordingly. All kits were employed on the Cobas®-6000 (Roche, Switzerland) analyzer series device. Lowest detection limit of E_2 was 5.00 pg/ml (18.4 pmol/ml), for P_4 was 0.05 ng/ml (0.159 nmol/ml) while for T was 0.025 ng/ml (0.087 nmol/L). The variance between the data in the assay in percentage (Intra-assay CV) was 2.4 percent for E_2, 2.3 percent for P_4 and 2.3 percent for T. Consistency between the mean values for the high and low controls on each measurement in percentage (Inter-assay CV) was 3.8 percent for E_2, 3.2 percent for P_4 and 3.5 percent for T.

2.14. Cell Imaging

2.14.1. Conventional Immunofluorescence Imaging

Before the cells are going to be seeded into 12-well or 24-well plates, 12-mm or 15-mm coverslip was put in the wells. Following seeding, different treatments were applied and after the cell culture media was aspirated cells were washed with 1X DPBS and then fixed in 4 percent paraformaldehyde (PFA) for 20 minutes at room temperature, washed twice with PBS and permeabilized (unless stated otherwise) with 0.2 percent Triton-X 100 in 1X DPBS for 15 minutes. Blocking was performed with Superblock (ScyTek,

USA) for 20 minutes at room temperature. After washing with 0.2 percent Tween-20 in Phosphate Buffer Saline (PBS-T), incubation with primary antibody was performed at 4 °C overnight, protected from light and in a suitable vessel. Primary antibody dilutions were done firstly according to the manufacturer's instructions and then in specific cases were optimized. Following overnight incubation coverslips were washed with PBS-T and secondary antibody solutions were applied on the coverslips. Secondary antibody incubation was performed for 90 minutes at 37 °C and then coverslips were gently washed and dried for them to be enclosed into slides by using fluoroshield mounting medium with DAPI, a dye staining nucleus in the cells. Slides were collected and protected at 4°C until the imaging was performed. The images are going to be taken under appropriate channels using a confocal microscope (Leica, DMI8).

Oil Red O is a fat-soluble dye which is used for staining of neutral lipids in the cells. Since HLGCs are sex steroid synthesizing cells they contain lipids which are used as a source for hormone synthesis. Oil Red O working solution (0.5 percent) was prepared by boiling 0.5 g Oil Red O in 100 ml, 100 percent isopropanol. Cells were washed with 1X DPBS and fixed with 4 percent PFA for 20 minutes at room temperature. Following washing with DPBS, cells were rinsed with 60 percent isopropanol and stained with Oil Red O for 20 minutes at room temperature. Later, cells were washed with 60 percent isopropanol and running tap water sequentially and prepared for immunofluorescence staining steps. Permeabilization was performed (when necessary) with 0.2 percent Triton X-100 containing DPBS for 20 minutes at room temperature. Blocking of nonspecific epitopes was achieved by incubating the samples in Super Block solution for 20 minutes at room temperature. Thereafter, the cells were incubated with primary antibodies overnight at 4 °C. Afterwards cells were washed three times with DPBS-Tween, then incubated with secondary antibodies for 90 minutes at 37 °C. Lastly cells were washed three times, then covered with a fluoroshield mounting medium with DAPI and slides were collected and protected at 4°C until the imaging was applied. Images were taken using a confocal microscope (Leica, DMI8).

2.14.2. Confocal Live Cell Imaging

To be able to stain and track organelles we used two different dyes. The first was mitotracker, a green (when needed red)-fluorescent stain that can confine to mitochondria

no matter what the mitochondrial potential be while lysotracker is a red-fluorescent stain used to label acidic organelles in the cell. Both these dyes easily permeate cell membranes staining live cells and both of them do not require a secondary antibody to give signal. After the respective treatments the spent culture media was aspirated and a new replenished media with the dyes were added to the cells. Formulations were as follows:

i. Mitotracker (1 μM) is added to the fresh media and the cells are incubated for 1 hour at 37 °C, 5 percent CO_2.
ii. Lysotracker (1 μM) is added to the fresh media and the cells are incubated for 1 hour at 37 °C, 5 percent CO_2.

Following incubation images were taken in a confocal microscope (Leica, DMI8) complemented with a DMI8 S platform which supplements the cells with CO_2, heat and maintains a suitable environment to make possible the live imaging of the cells.

2.15. Statistical analysis

The obtained values in the results section were calculated as the mean ± standard deviation (SD) from minimum triplicate experiments. Sample size required for statistical significance and proper interpretation of the results was calculated based on the qRT-PCR assays and immunoblot assays. In this study the ΔΔCt method for relative quantitation of target gene mRNAs was used[120]. The mean and SD values were calculated from three different readouts taken for each target gene in the RT-PCR assay. mRNA levels of the target genes used in the qRT-PCR assay and hormone levels are continuous variables therefore, they were expressed as mean ± SD. ANOVA and Bonferroni were used to perform the statistical analysis if the data were parametric and Kruskal-Wallis test or Dunn post-hoc test were used for nonparametric data. Paired t-test was applied to compare the signal intensity of the steroidogenic enzymes and hormone levels before and after different treatments. Analysis regarding presentation of nominal data in this study were performed by using Chi-square tests. Statistical significance was set at 5 percent ($*p < 0.05$), GraphPad Prism was used to analyse the data and create the graphs while figures were created using BioRender.

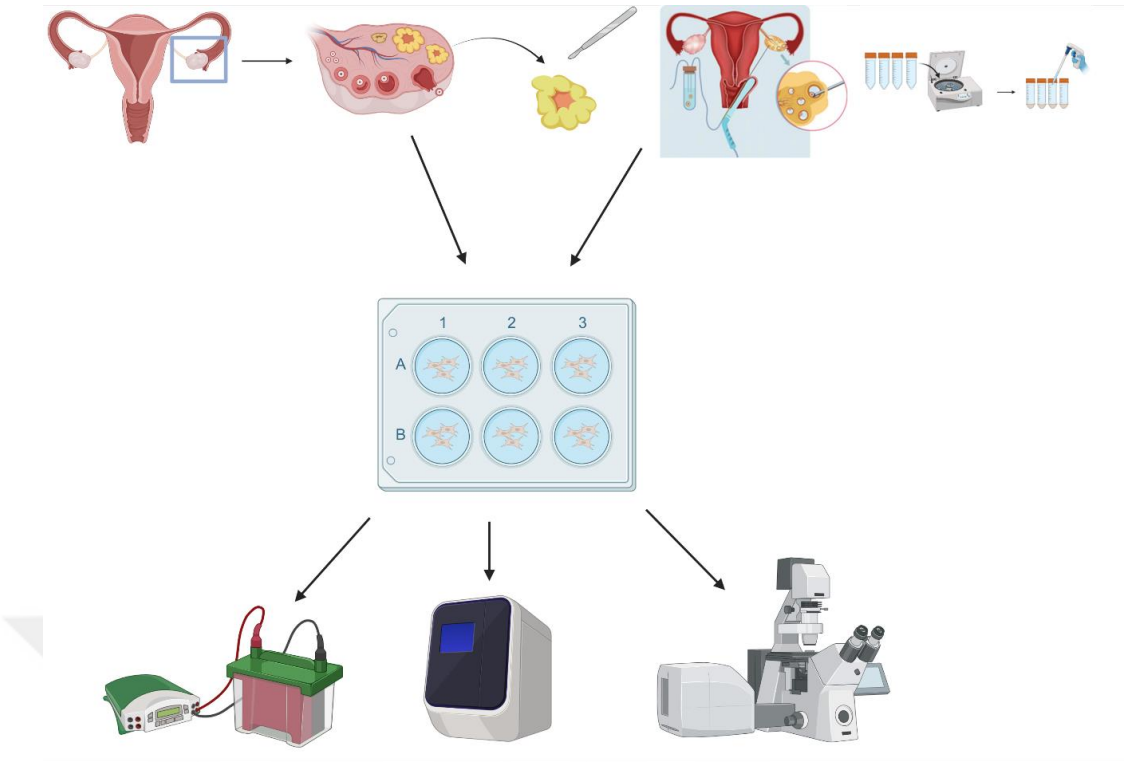

Figure 15. *Outline of the main experimental setup used in this study.*

Chapter 3: Results

3.1. Luteotropic hormones hCG/LH increase steroidogenesis through activating autophagic process

Primary human luteal GCs obtained from IVF patients are capable of maintaining their viability and steroidogenic activity and producing detectable amounts of E2 and P4 in culture for several days. They also respond to exogenously administered luteotropic hormones hCG/LH by increasing their steroidogenic activity and P4 output over basal state as previously shown by our lab and the others (Ref to be added). In agreement, hCG treatment significantly up-regulated the expression of StAR and 3β-HSD in immunoblot analysis (Fig. 16A) and the confocal images (Fig. 17, Fig. 18), and resulted in a significant increase in P4 production in these cells (Fig. 16C). Interestingly, we observed that the expression of microtubule-associated protein 1A/1B light chain 3B-II (LC3B-II) decreased in immunoblotting after hCG treatment (Fig. 16A).

3.2. Stimulation of steroidogenesis by luteotropic hormones hCG/LH is associated with increased autophagic activity in human luteal granulosa cells

Since LC3B-II itself is an autophagy substrate degraded following the fusion of autophagosome with lysosome this observation led us to hypothesize that hCG might induce autophagic flux and therefore, there might be link between autophagy and steroidogenesis in these cells.

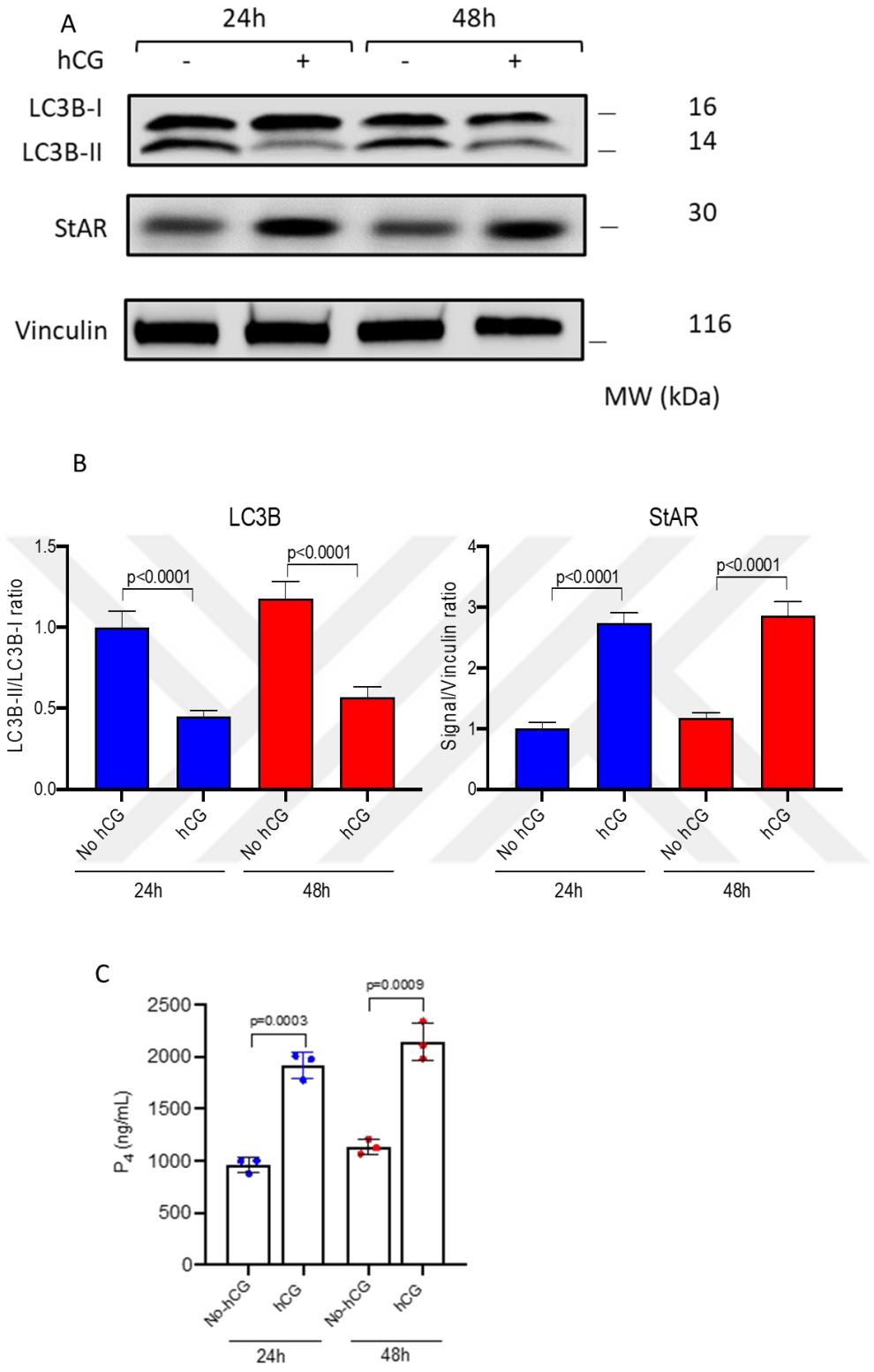

Figure 16. Treatment of human luteal GCs with hCG at different time points. A) Western Blot analysis of huma luteal granulosa cells treated with hCG (10 IU/ml) at 24- and 48 hours. B) Quantification of StAR expression and LC3-II/LC3-I ratio of the Western Blot analysis at A. C) Graphical representation of the hCG-mediated progesterone synthesis in HLGCs.

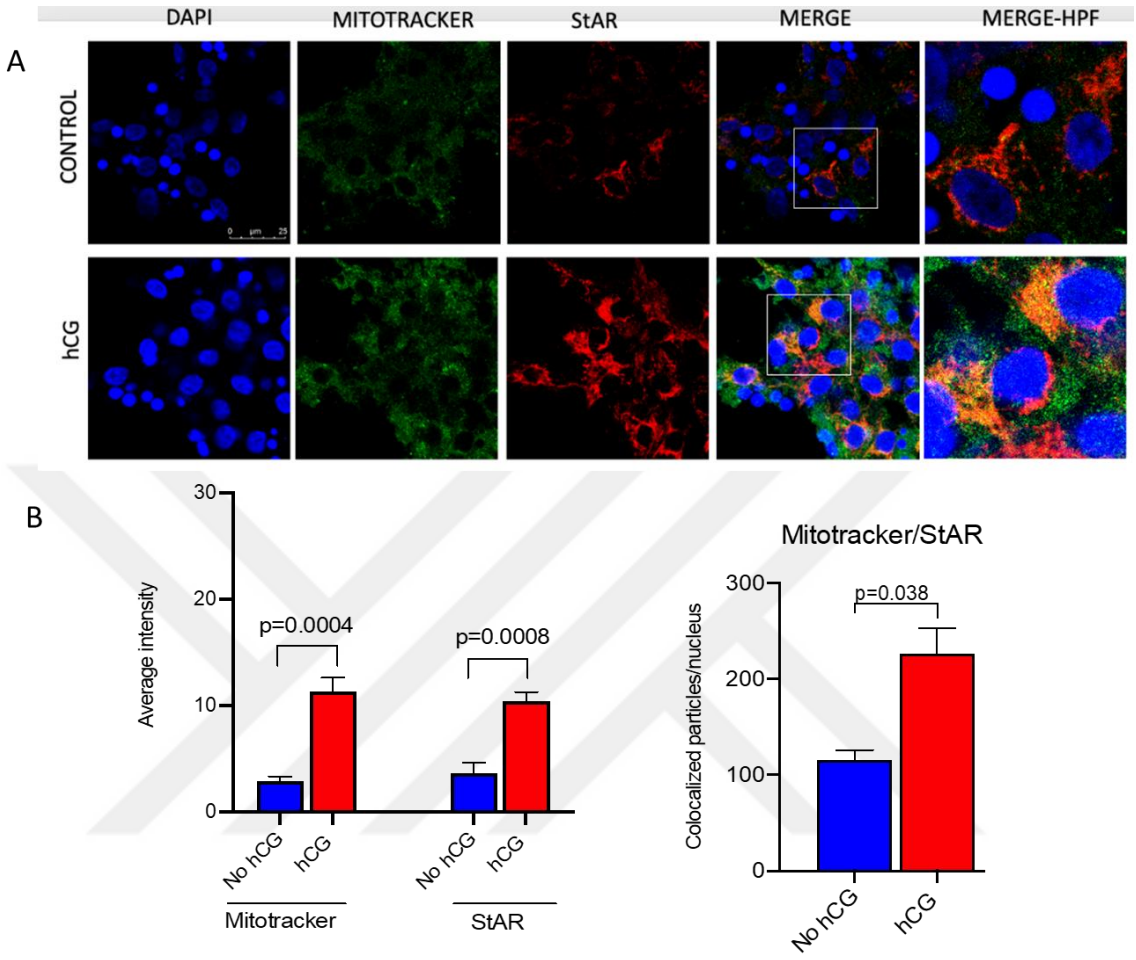

Figure 17. Confocal images after hCG treatment of StAR-Mitotracker. A) An increase in StAR expression, mitochondrial mass and their colocalization after the hCG treatment of luteal GCs is observed. B) Intensity of both StAR expression, Mitotracker signal and their colocalization is graphically shown.

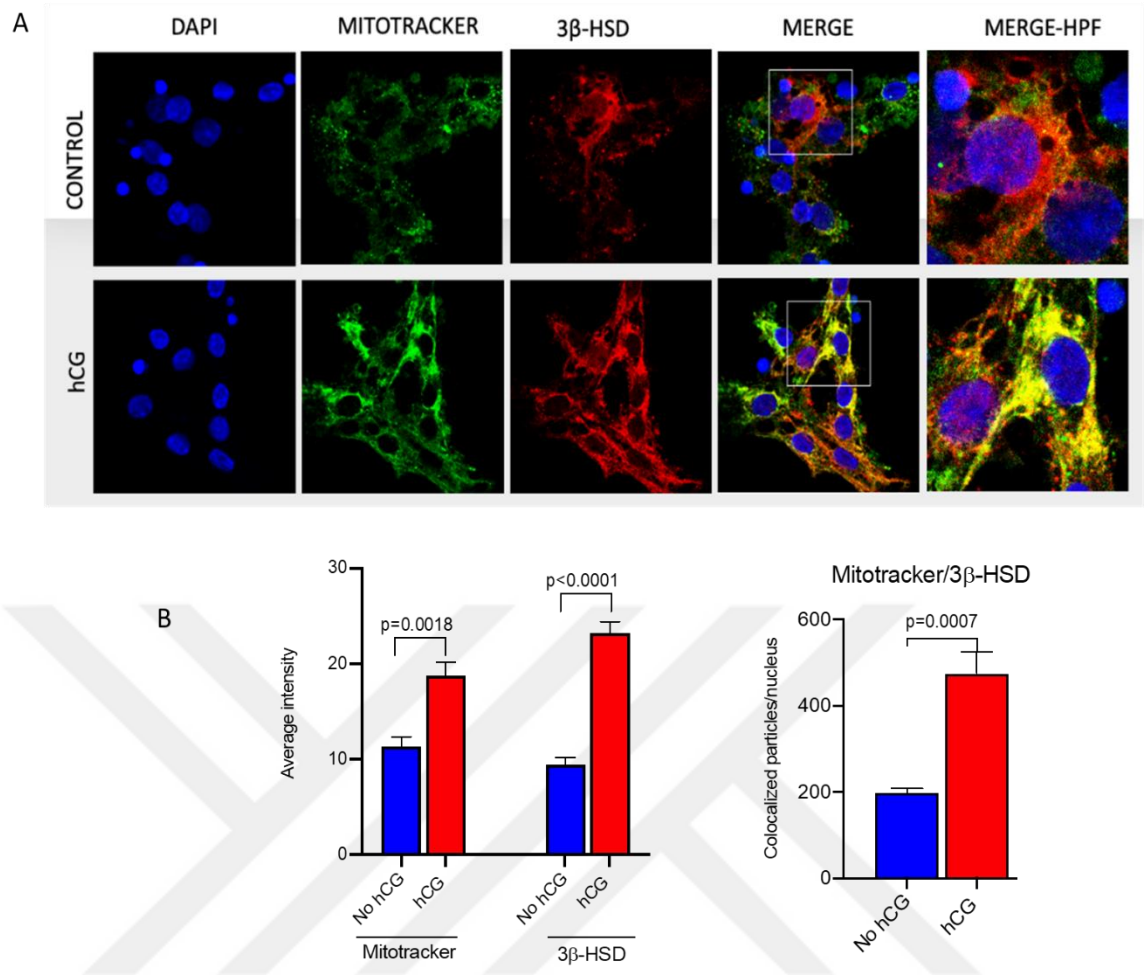

Figure 18. Confocal images after hCG treatment of 3β-HSD-Mitotracker. A) An increase in 3β-HSD expression, mitochondrial mass and their colocalization after the hCG treatment of luteal GCs is observed. B) Intensity of both 3β-HSD expression, Mitotracker signal and their colocalization is graphically shown.

To investigate this hypothesis, we treated the cells with hCG combined with increasing concentrations of pharmacological autophagy inhibitor chloroquine and observed that P4 production of the cells exposed to chloroquine began to drop gradually LC3B-II and the autophagic cargo adaptor protein SQSTM1/p62 accumulated in immunoblot analysis (Fig. 19A) and P4 production of the cells exposed to chloroquine (Fig. 19C) began to drop gradually in comparison to those cells treated with hCG alone.

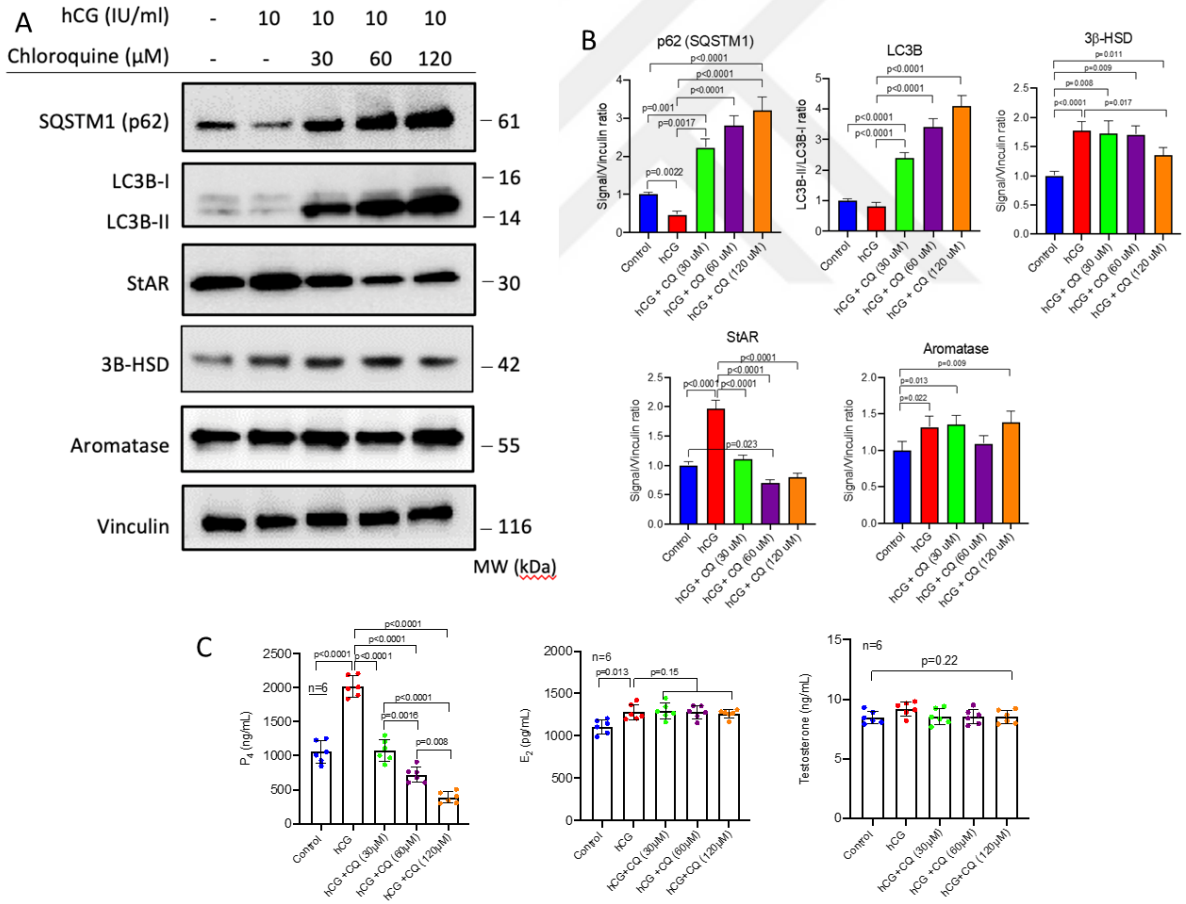

Figure 19. Incremental inhibition of autophagy and steroidogenesis stimulation. A) Western blot analysis of hCG (10IU/ml) and increasing dose dependent chloroquine (30-60-120μM) treatment of HLGCs. B) Quantification of protein expression with respect to vinculin and LC3-II/LC3-I ratio of the Western Blot analysis at A. C) Graphical representation of hormone synthesis after hCG ± dose dependent chloroquine treatment.

Double immunofluorescence staining showed that the signal intensity of LC3 and LC3/lysotracker co-localization gradually increased in the cells following the same treatment protocol, indicative of blockage of autophagy (Fig. 20).

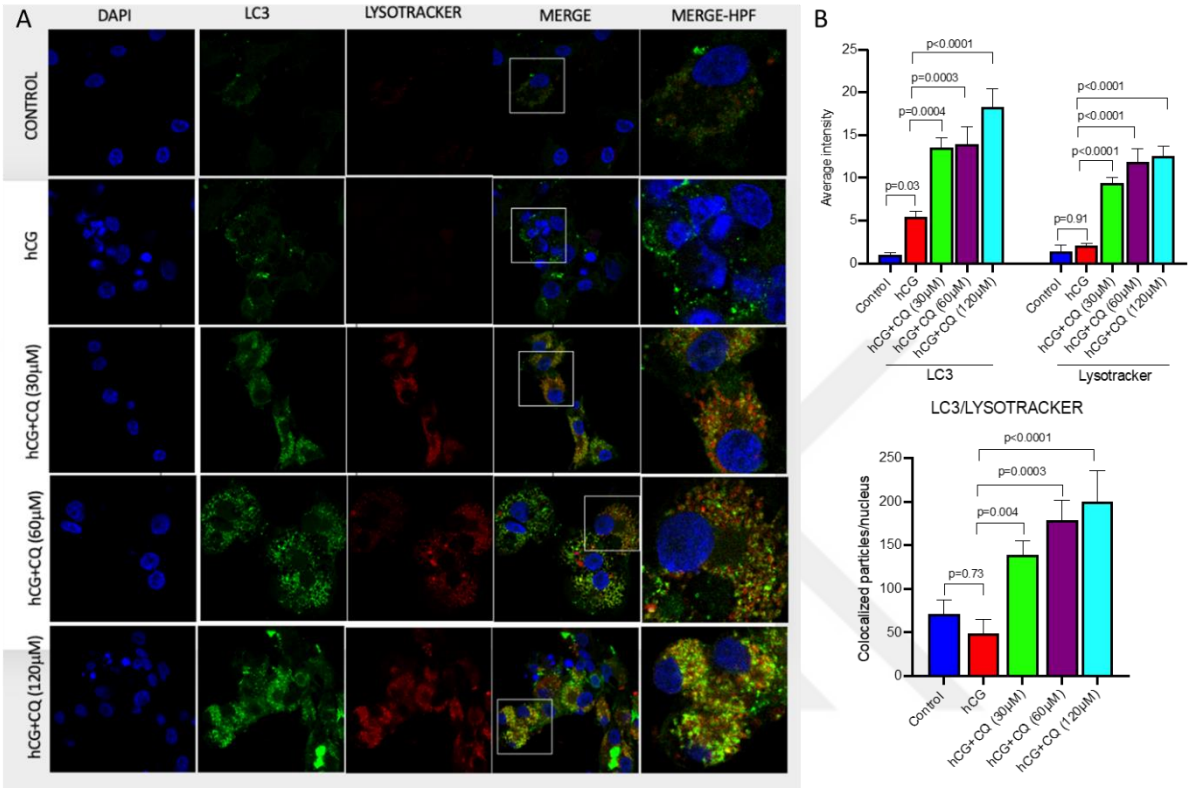

Figure 20. Confocal images of incremental inhibition of autophagy and steroidogenesis stimulation. A) hCG (10 IU/ml) and increasing dose dependent chloroquine (30-60-120 μM) treatment of luteal GCs. B) Intensity of LC3 expression and Lysotracker signal and their colocalization is graphically shown.

3.3. Inhibition of autophagy and the effect in steroidogenesis

In another set of experiments, we analyzed the impact of inhibition of autophagy on basal P4 production by treating the cells with chloroquine alone without hCG and obtained similar results. There was a gradual accumulation of LC3B-II and SQSTM1/p62 in immunoblotting (Fig. 21) together with an increase in LC3/lysotracker co-localization

in confocal microscopy (Fig. 22); and a dose-dependent progressive decline P4 output (Fig. 23) after chloroquine treatment.

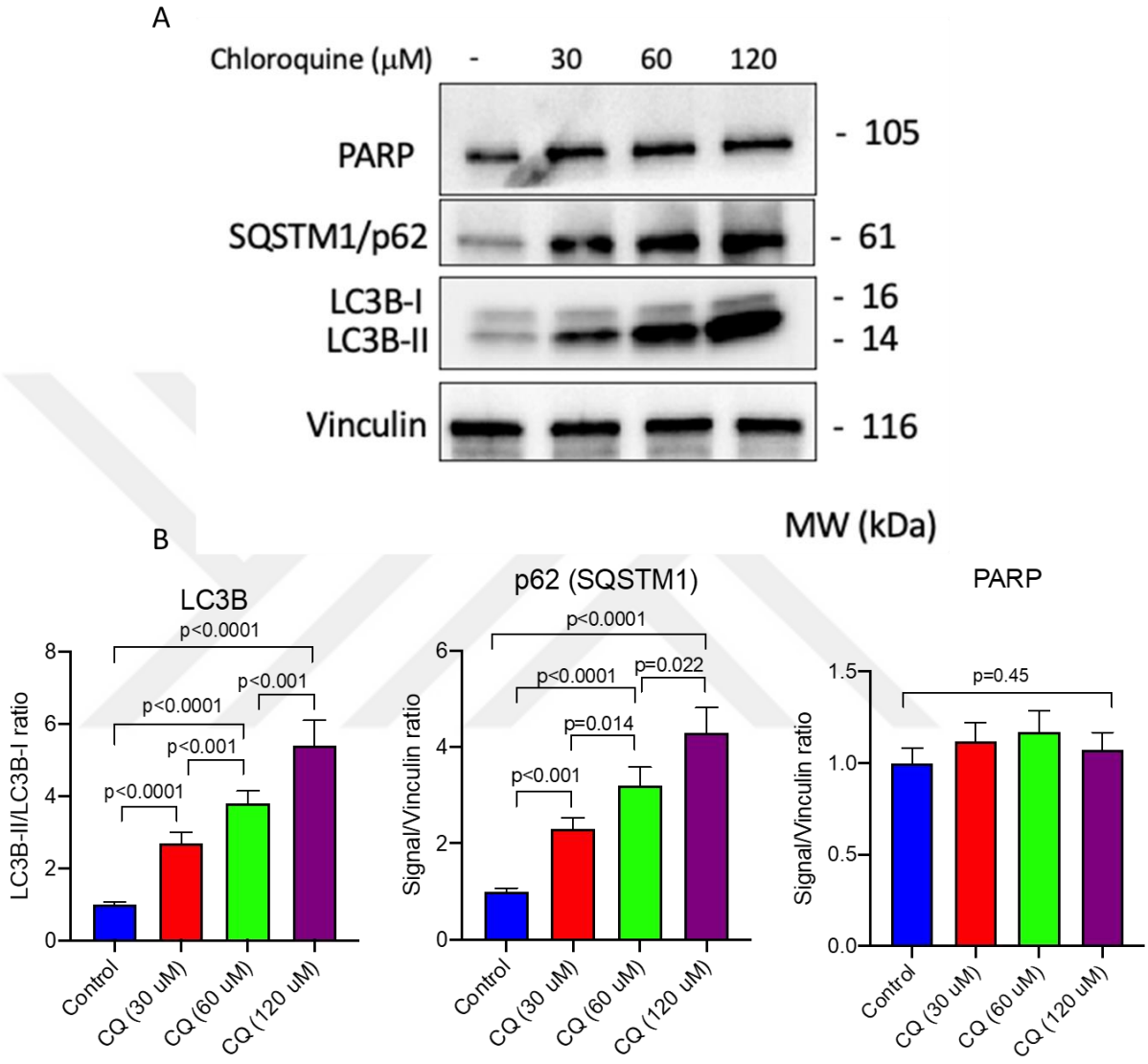

Figure 21. Incremental inhibition of autophagy in human luteal GCs. A) Western Blot analysis of chloroquine dose dependent treatment on luteal GCs. B) Quantification of protein expression with respect to vinculin and LC3-II/LC3-I ratio of the Western Blot analysis at A.

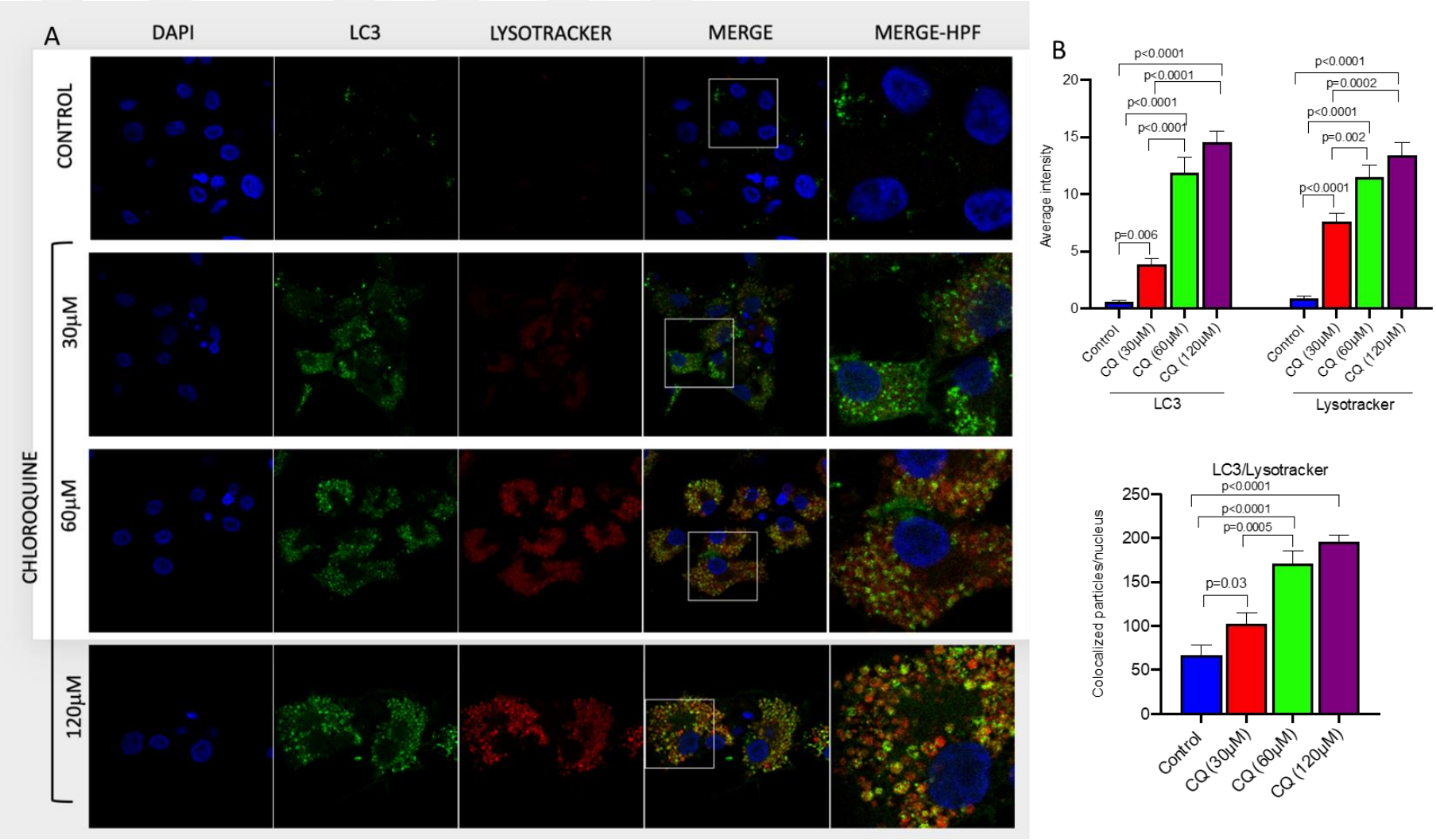

Figure 22. A) Confocal images of dose dependent chloroquine treatment on luteal GCs in which an increase in expression of LC3 and its colocalization with lysosome is observed. B) Quantification of LC3 expression, Lysotracker signal and their colocalization.

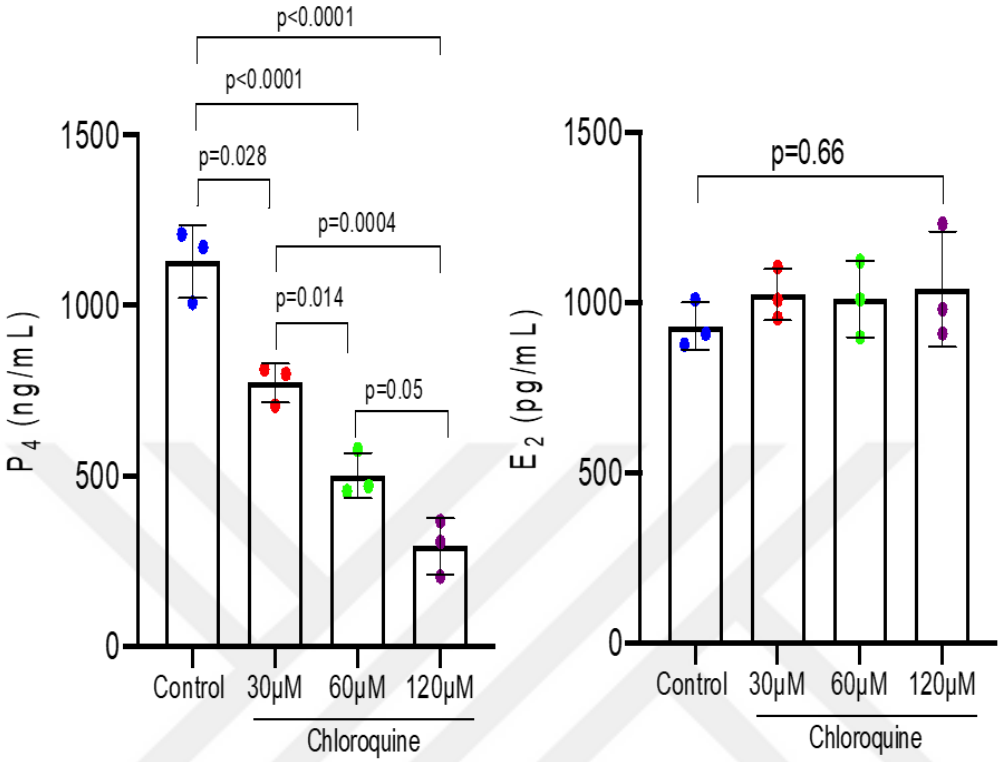

Figure 23. Quantification of estrogen and progesterone synthesis from luteal GCs in response to chloroquine dose dependent treatment.

3.4. Viability assay after chloroquine treatment

We also carried out cell dead/viability and apoptosis assays in the cells exposed to chloroquine at the same concentrations and found no difference between control and chloroquine treated cells in terms of Yo-Pro-1 uptake in immunofluorescence microscopy (Fig. 24) and PARP expression in immunoblotting (Fig. 21).

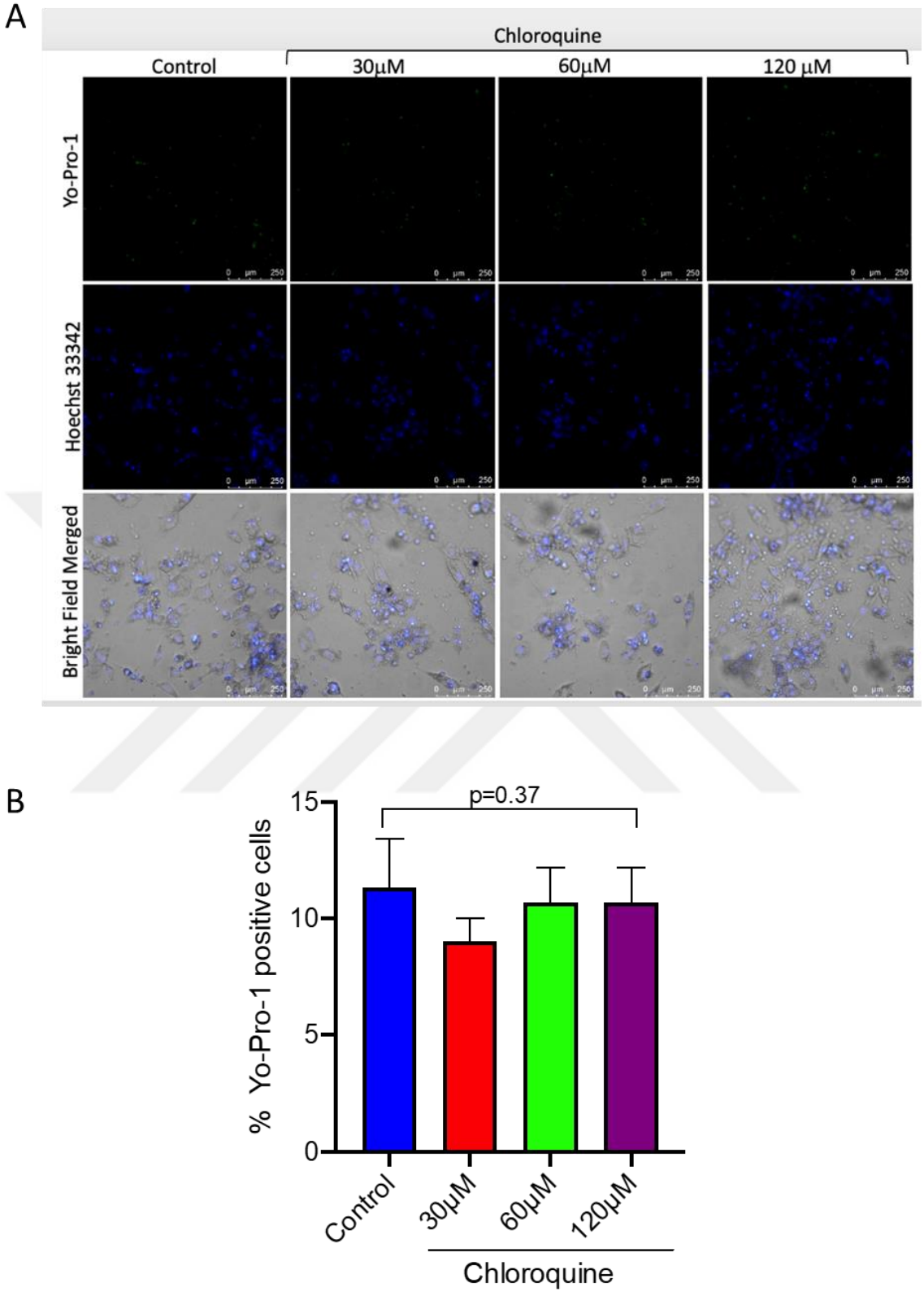

Figure 24. Cell viability assay in response to autophagy inhibition. A) Images of the Yo-Pro-1 uptake assay after the chloroquine dose dependent treatment of luteal GCs. B) Quantification of the percentage of Yo-Pro-1 positive cells analysed from the images on part A.

3.5. Inhibiting autophagy and inducing steroidogenis in Corpus Luteum with chloroquine and hCG

Treatment of the corpus luteum (CL) tissue samples with hCG ± chloroquine (Fig. 26 A) as an *ex-vivo* explant culture model yielded similar findings. Chloroquine treatment alone and in combination with hCG significantly impaired basal and hCG-induced P4 steroidogenesis respectively, in the CL tissue samples (Fig. 20 B and 20 C).

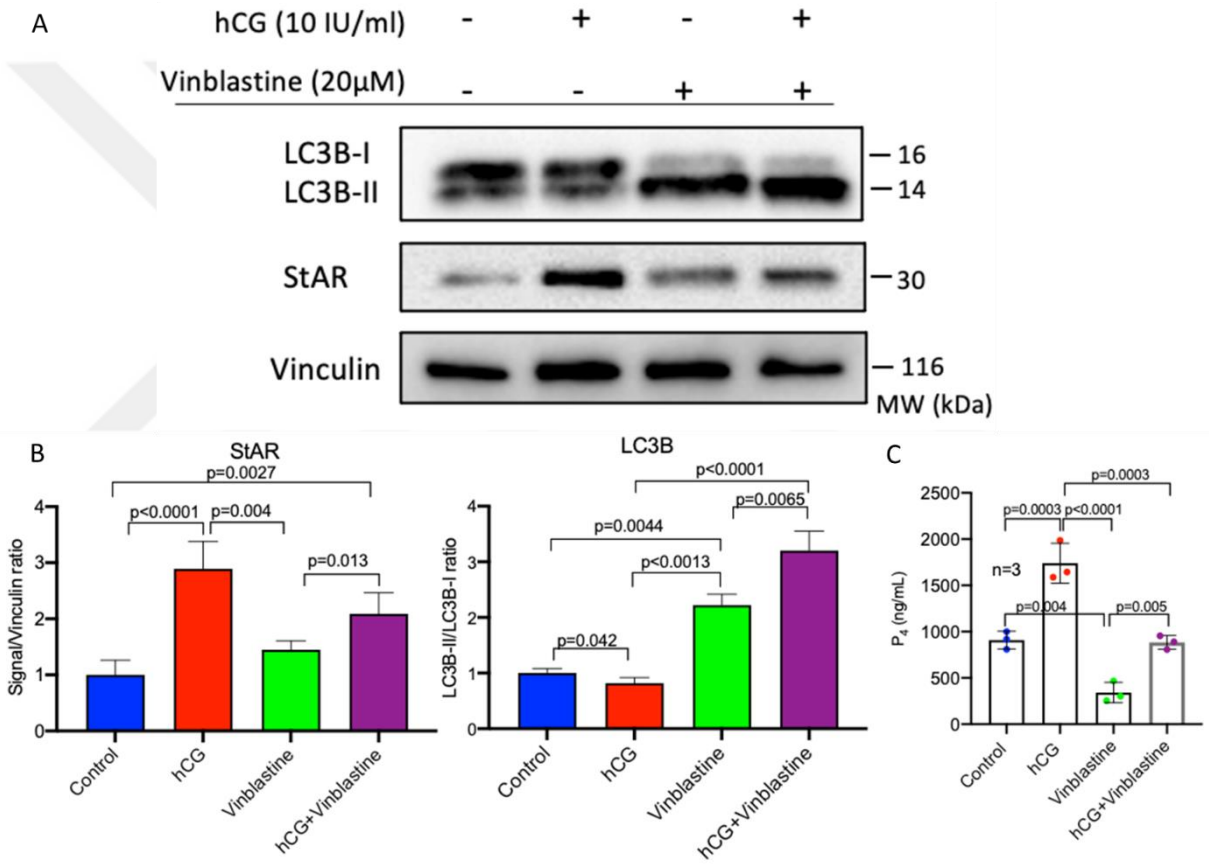

Figure 25. Autophagy inhibition by using combined vinblastine ± hCG treatment. A) Western Blot image of luteal GCs treated with hCG ± vinblastine. B) Quantification of StAR expression with respect to vinculin and LC3-II/LC3-I ratio of the Western Blot analysis at A. C) Graphical representation showing progesterone synthesis after hCG ± vinblastine treatment.

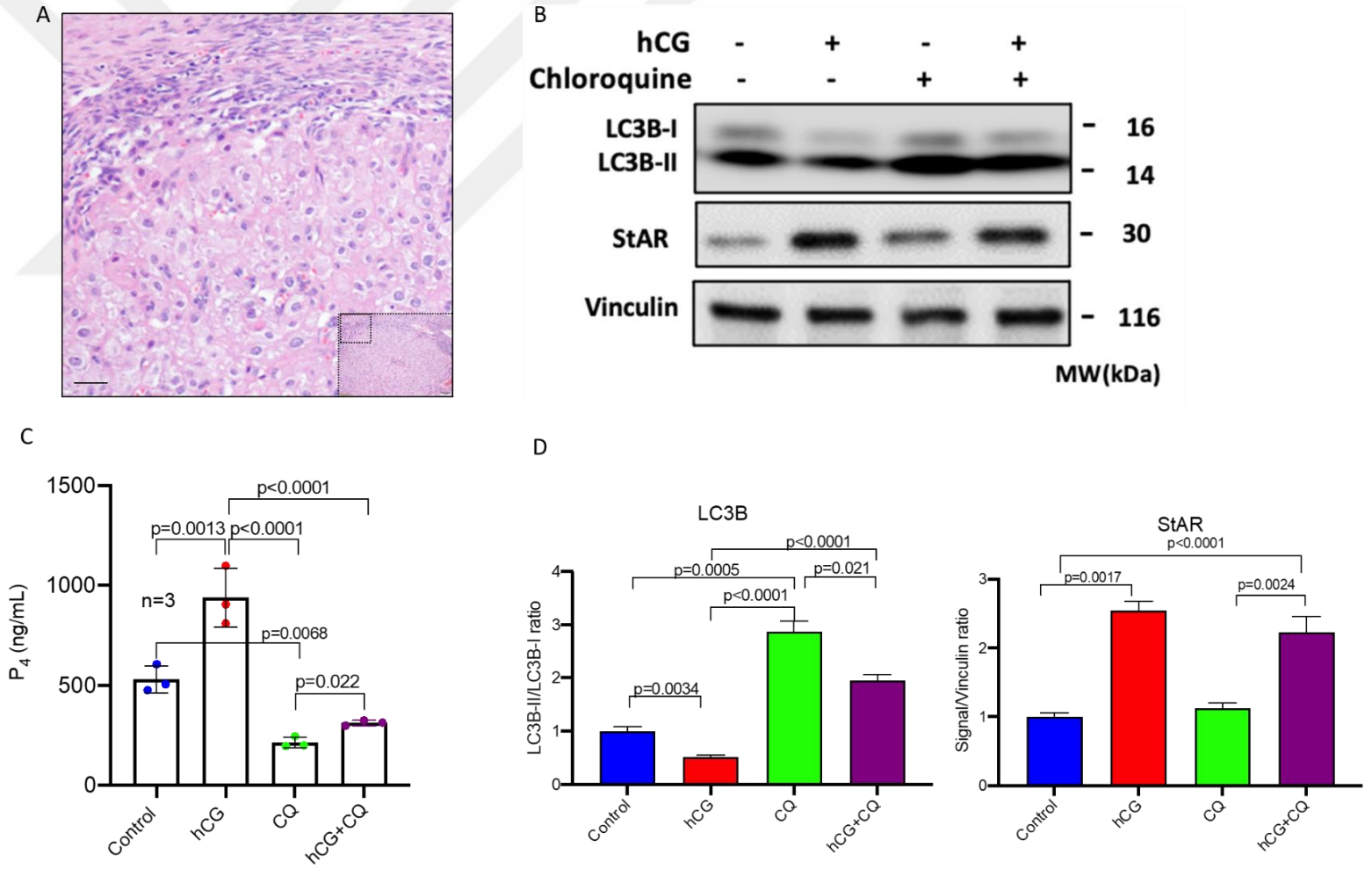

Figure 26. Autophagy inhibition by using combined chloroquine ± hCG treatment in corpus luteum tissues. A-B) Image of a section of the ovarian tissue and Western Blot image of the corpus luteum treated with hCG ± chloroquine. C-D) Progesterone synthesis and quantification of StAR expression with respect to vinculin and LC3-II/LC3-I ratio of the Western Blot analysis at B.

To substantiate our findings we treated the cells with another pharmacological autophagy inhibitor vinblastine, which inhibits the fusion of autophagosome with lysosome and obtained similar results (Fig. 25). Vinblastine impaired basal and hCG-induced P4 steroidogenesis in the luteal GCs.

Taken together, these findings suggest that hCG accelerates the autophagic flux, and pharmacological inhibition of autophagy impairs both basal (unstimulated) and hCG-stimulated P4 steroidogenesis in human luteal GCs and corpus luteum.

3.6. Hormone synthesis difference after autophagy inhibition

Interestingly, we did not observe any notable reduction in E2 output after inhibition of autophagy with pharmacological inhibitors, chloroquine, and vinblastine (Fig. 19, Fig. 23). A plausible explanation of this observation might be that 21-carbon pregnanes that continue to be produced at nanogram level after blockage of autophagy might provide sufficient amount of precursor hormones to be converted successively into 19-carbon androgens and finally 18-carbon oestrogens at picogram level. In support of this we measured testosterone (T) production simultaneously with P4 and E2 in the spent culture media of the cultured GCs and found that T production was comparable between control and chloroquine-treated cells (Fig. 19). Further, we measured the concentrations of P4, E2 and T in the cell lysates to see how accurately their levels measured in the spent culture media (output) reflect their intracellular levels (synthesis) and found no significant differences in the levels of these hormones between these two compartments (Fig. 27).

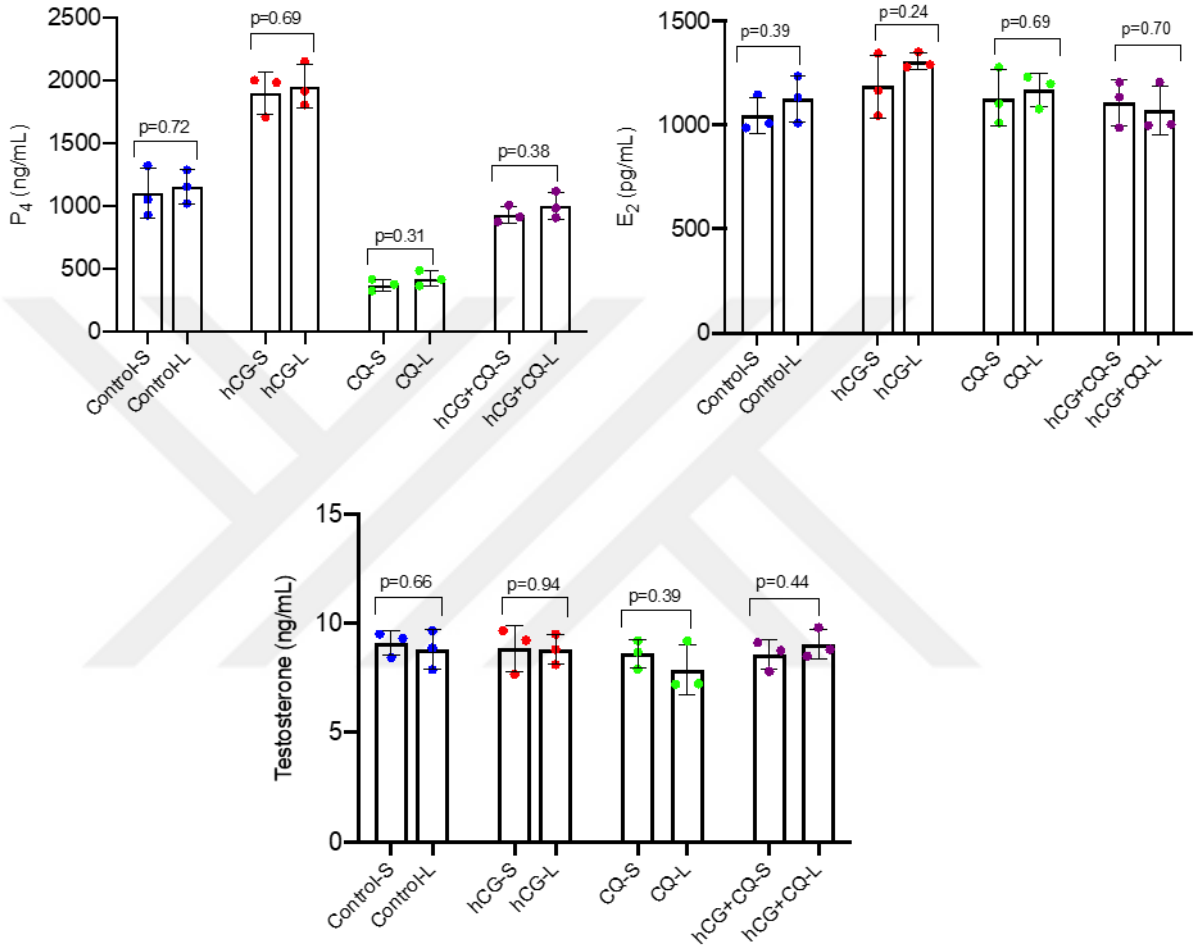

Figure 27. Comparison of hormone synthesis measured in spent culture media and in cell lysates.

3.7. Activation of autophagy and its role in steroidogenesis

In another set of experiments, we analysed the effect of autophagy induction with mTOR inhibitor rapamycin on steroidogenic function of the luteal GCs. Rapamycin treatment was associated with a marked decrease in the signal intensity of LC3 and SQSTM1 and their co-localizations with lysosome in the confocal microscopy (Fig. 28 and Fig. 29) compared to control and chloroquine treated cells. P4 production markedly improved after rapamycin treatment compared to control cells (Fig. 29). When rapamycin was combined with hCG a synergistical effect occurred and P4 output further increased compared to those treated with rapamycin or hCG alone. When rapamycin was combined with chloroquine P4 output drastically declined compared to those treated with rapamycin alone (Fig. 30). E2 production did not show meaningful changes after autophagy induction with rapamycin alone or in combination with chloroquine (Fig. 29).

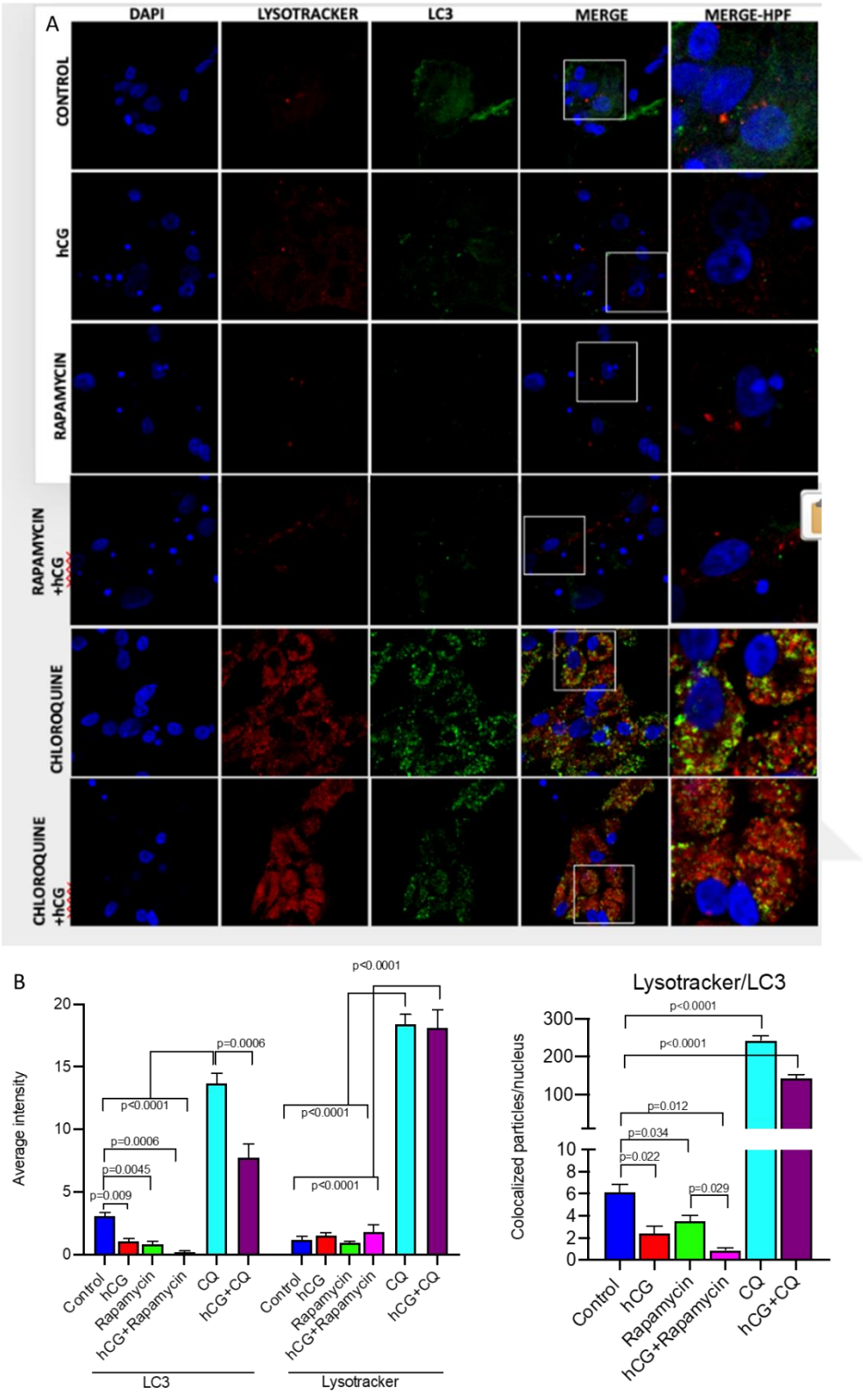

Figure 28. A) Confocal images of hCG ± chloroquine and hCG ± rapamycin treatments on luteal GCs in which changes in expression of LC3, lysosome signal and their

colocalization is observed. B) Quantification of LC3 expression and lysosome number and their colocalization.

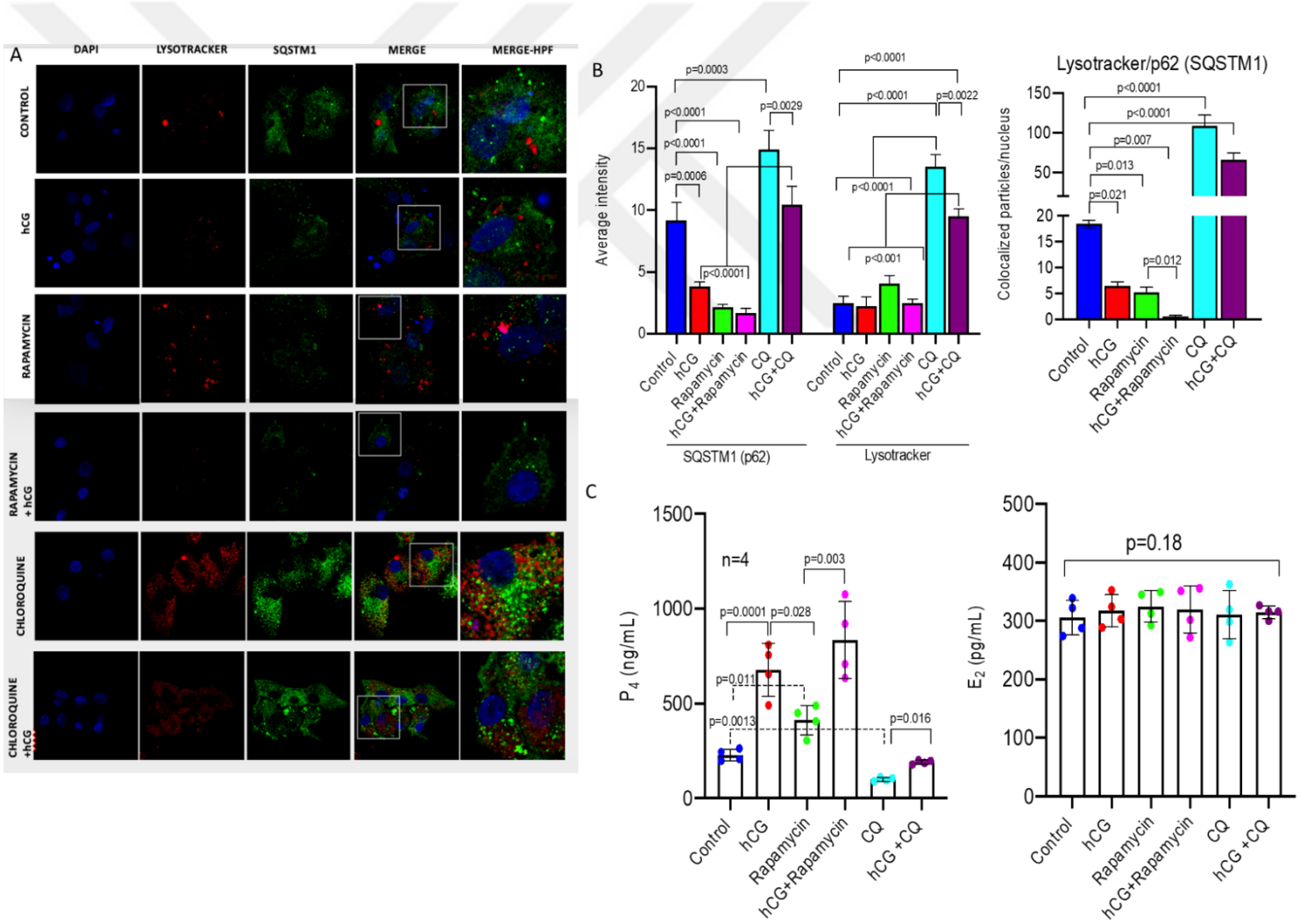

Figure 29. A) Confocal images of hCG ± chloroquine and hCG ± rapamycin treatments on luteal GCs in which changes in expression of p62 and its colocalization with lysosome is observed. B) Quantification of LC3 expression and lysosome number and their colocalization. C) E2 and P4 hormone synthesis after hCG ± chloroquine and hCG ± rapamycin treatme

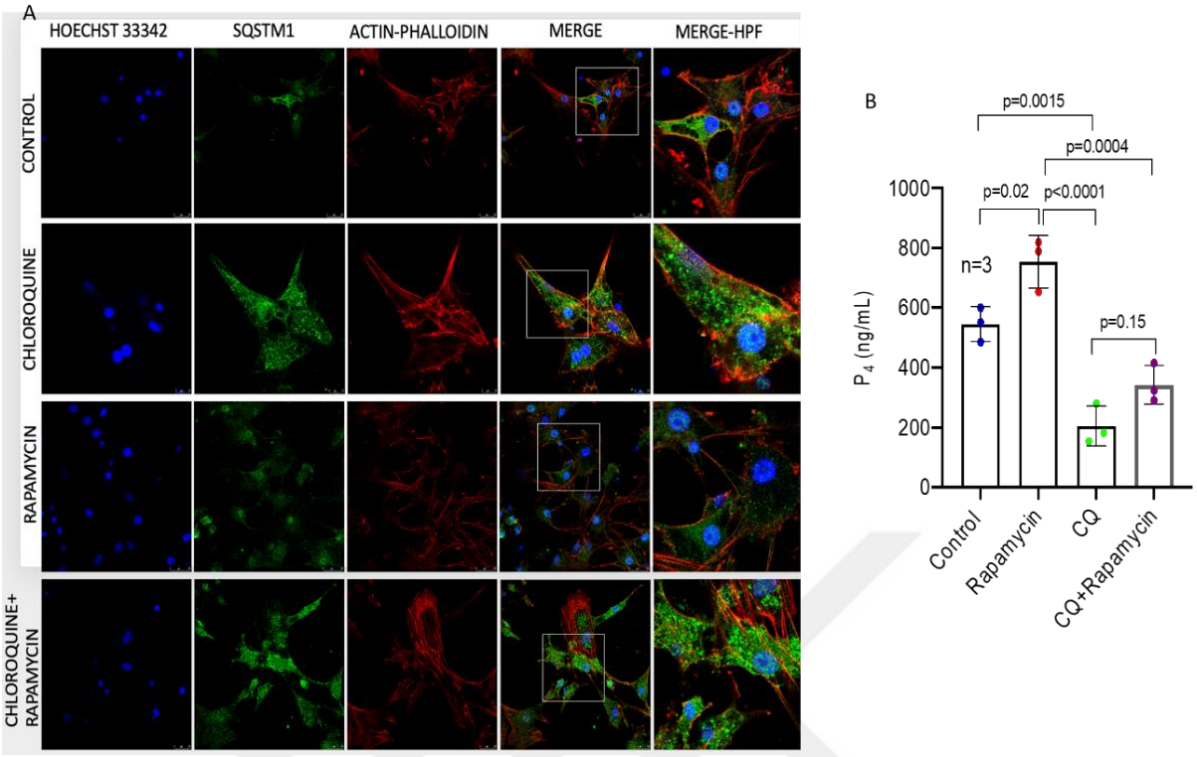

Figure 30. Confocal images of inhibiting and activating autophagy using chloroquine and rapamycin respectively. A) Cells were treated in combination to observe the effect of inhibiting and activating at the same time. B) P4 synthesis after the treatments performed at A.

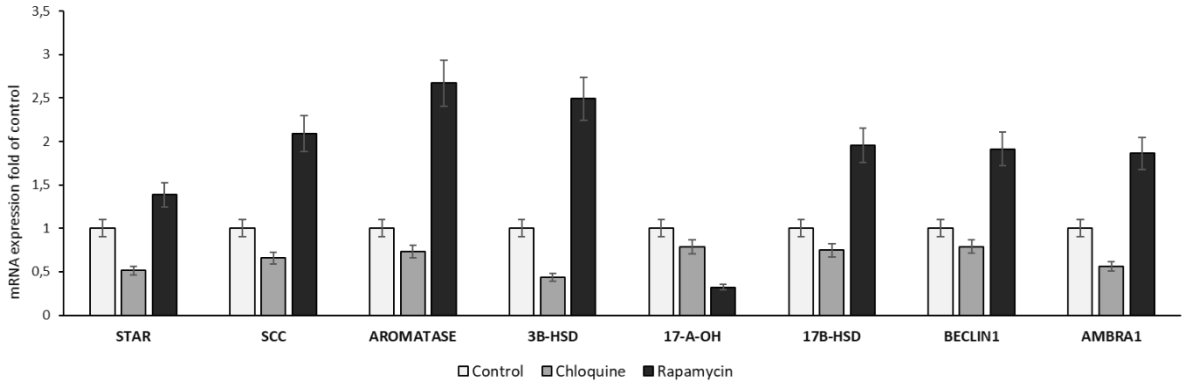

Figure 31. qRT-PCR results of inhibiting and activating autophagy in luteal GCs.

Taken collectively, these findings provide evidence that degradation of the autophagy-selective substrates, LC3-II and SQSTM1, and therefore autophagic flux are accelerated by luteotropic hormone hCG and that pharmacological inhibition and activation of autophagic process impairs and improves respectively, basal and hCG-stimulated P4 steroidogenesis in human luteal granulosa cells and corpus luteum tissue samples in-vitro.

3.8. Silencing of the autophagy gene Atg5 and Beclin1 with siRNA and shRNA technologies impairs steroidogenesis

Next, we analyzed the effect of genetic interruption of autophagy on steroidogenesis in the luteal granulosa cells. Knocking down of Beclin1 gene via siRNA significantly impaired P4 steroidogenesis. Both basal and hCG-stimulated P4 output gradually declined with increasing concentrations of Beclin1 siRNA in comparison to those cells transfected with scramble siRNA ± hCG (Fig. 32 A and 32 C). While hCG was able to up-regulate the expression of StAR and 3β-HSD in Beclin-1 silenced cells, it failed to increase their P4 production. Similar results were obtained when another autophagy gene Atg5 was knocked-down with siRNA (Fig. 33 A and 33 C). Again, as in the case of pharmacological inhibition of autophagy, E2 production was not affected by the silencing autophagy genes Beclin1 and Atg5 (Fig.32 C and Fig. 33 C).

In order to investigate the role of autophagy in estrogen synthesis arm of steroidogenesis we decided to use the mitotic non-luteinizing granulosa cells HGrC1, which only produce E2 but not P4 due to their inability to undergo luteinization. Beclin1 knockdown with shRNA resulted in a marked accumulation of SQSTM1 and LC3B-II in immunoblot analysis and caused a significant reduction in basal and FSH-stimulated E2 output. Despite FSH-induced up-regulation in aromatase expression in immunoblot analysis such a notable increase was not observed in E2 production in these cells in comparison to control cells transduced with FF, which responded to FSH by up-regulating aromatase expression and enhancing E2 production (Fig.34).

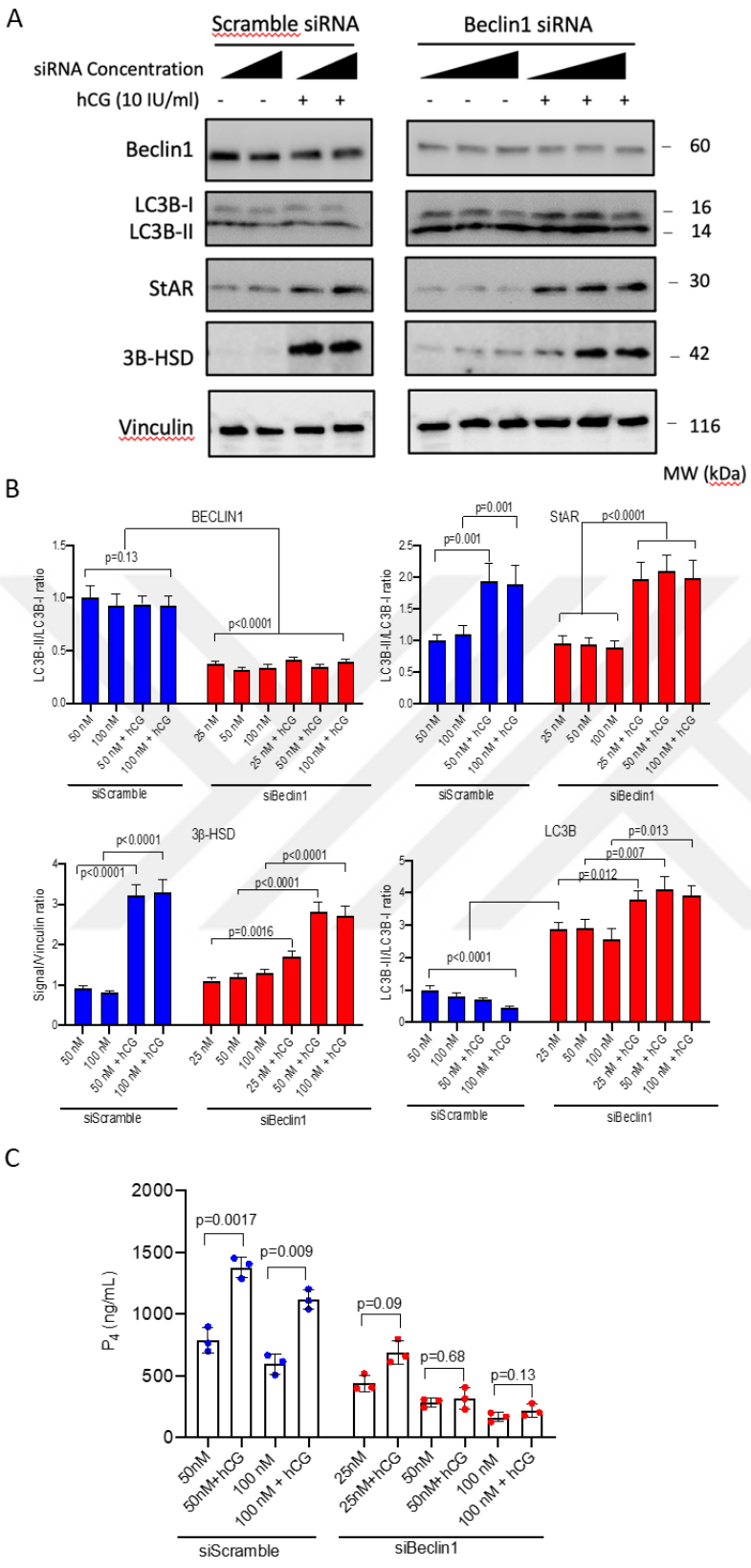

Figure 32. Silencing of Beclin1 in human luteal GCs using siRNA. A) Western Blot analysis of Beclin1 siRNA on luteal GCs. B) Quantification of changes on protein expression on A. C) P4 synthesis change due to the Beclin1 siRNA treatment.

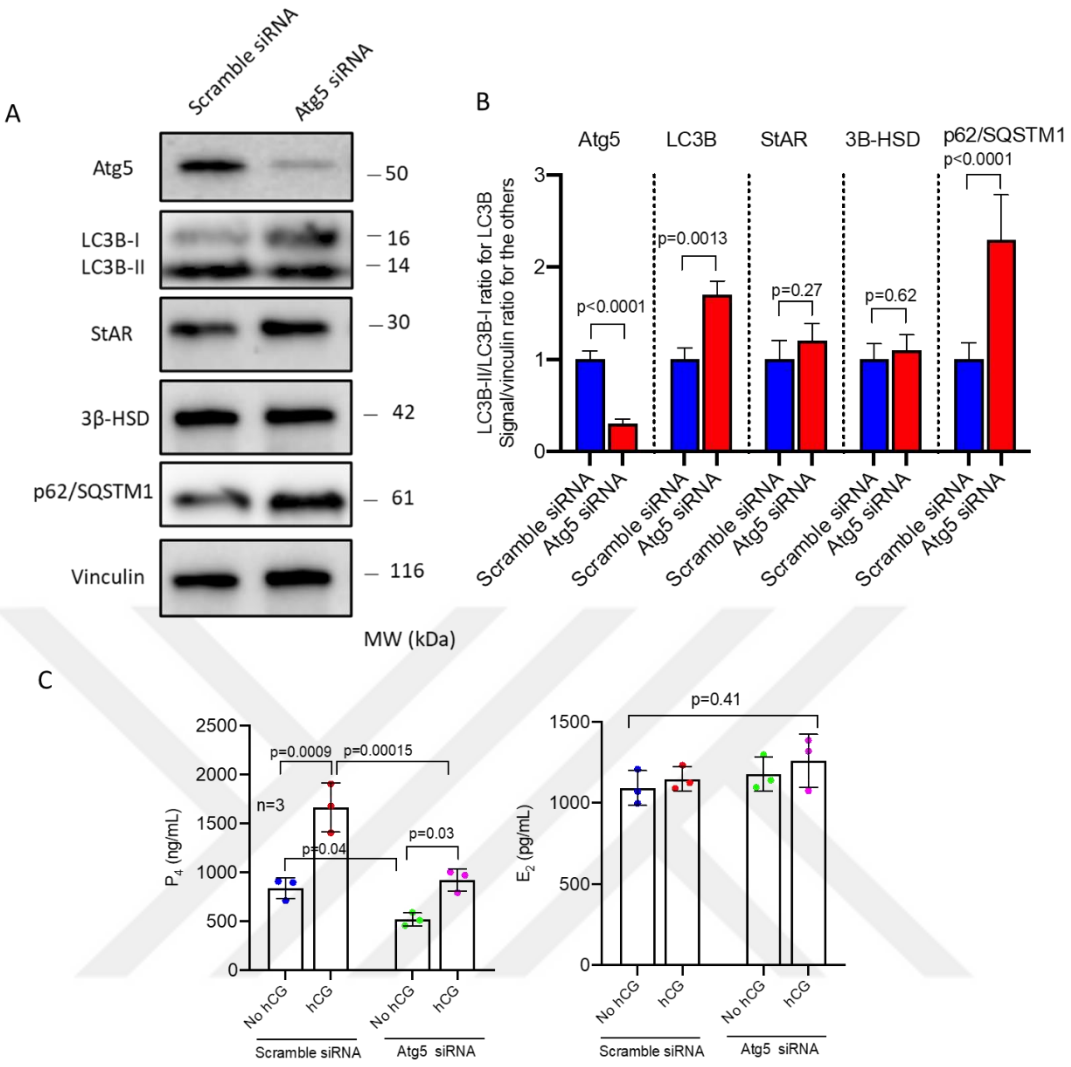

Figure 33. Silencing of Atg5 in human luteal GCs using siRNA. A) Western Blot analysis of ATG5 siRNA, a marker of autophagy, on luteal GCs. B) Quantification of changes on protein expression on A. C) P4 and E2 synthesis change due to the ATG5 siRNA treatment.

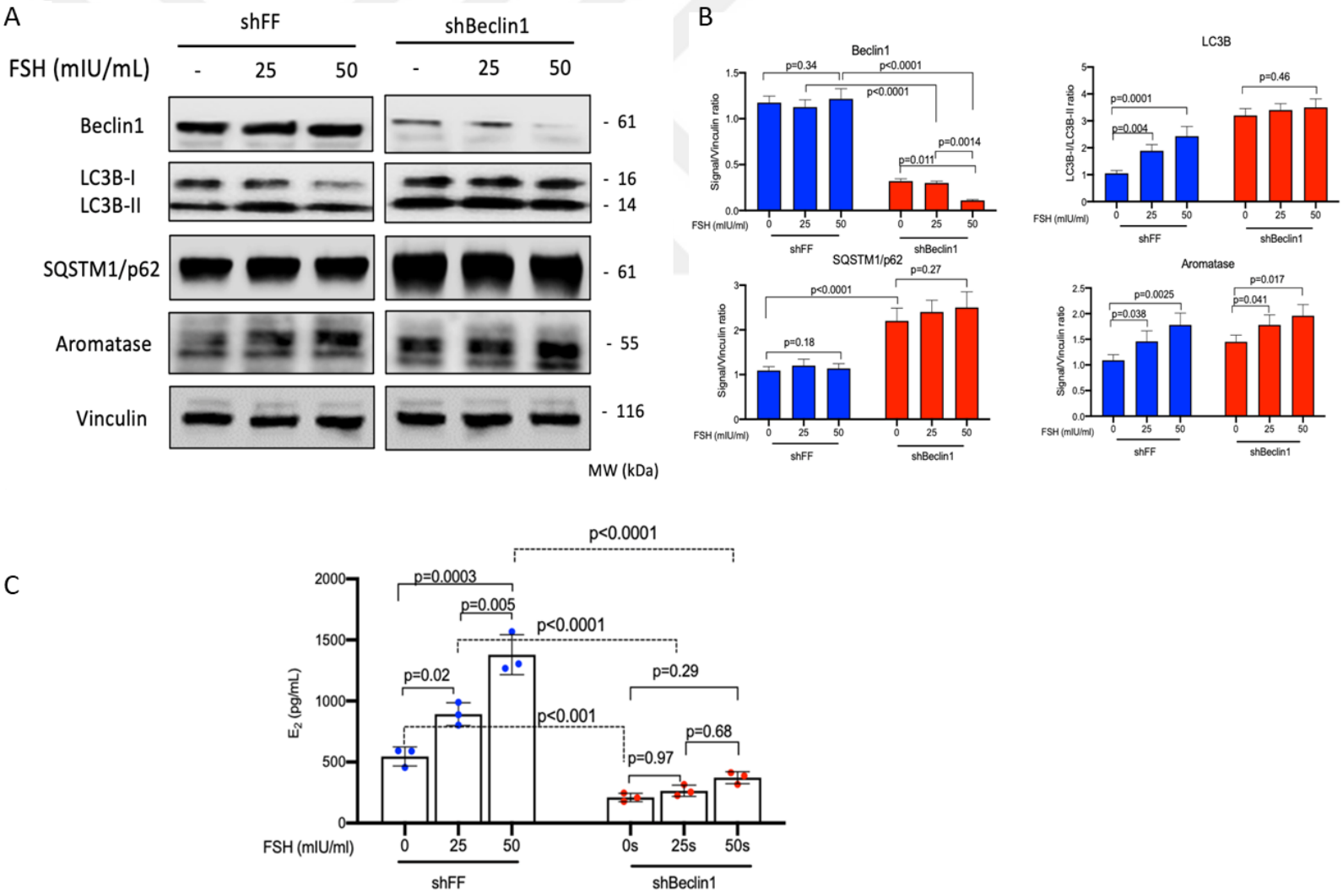

Figure 34. Silencing of Beclin1 in HGrC1 using shRNA. A) Western Blot analysis of Beclin1 shRNA on HGrC1. B) Quantification of changes on protein expression on A. C) E2 synthesis change due to the Beclin1 shRNA treatment.

3.9. Autophagy regulates intracellular lipid trafficking and utilization required for steroid synthesis in granulosa cells

We observed a marked increase in the intensity of Oil Red O staining in the confocal images of the cells treated with chloroquine. By contrast, hCG treatment produced the opposite effect. Chloroquine + hCG combination treatment was associated with less Oil Red O accumulation when compared to the chloroquine treated cells (Fig. 35 A). Oil Red O intensity was also reduced in the rapamycin treated cells compared to the control. And the reduction became more pronounced when rapamycin was combined with hCG (Fig. 35 A). Dual immunofluorescence staining revealed that Oil Red O strongly co-localizes with lipid droplet (LD) associated protein perilipin3 (TIP47) suggesting that lipid accumulation mainly occurs in the form of LDs (Fig.36). We also noticed that Oil Red O co-localizes with autophagy substrates LC3 and SQSTM1/p62 particularly after chloroquine treatment (Fig. 37).

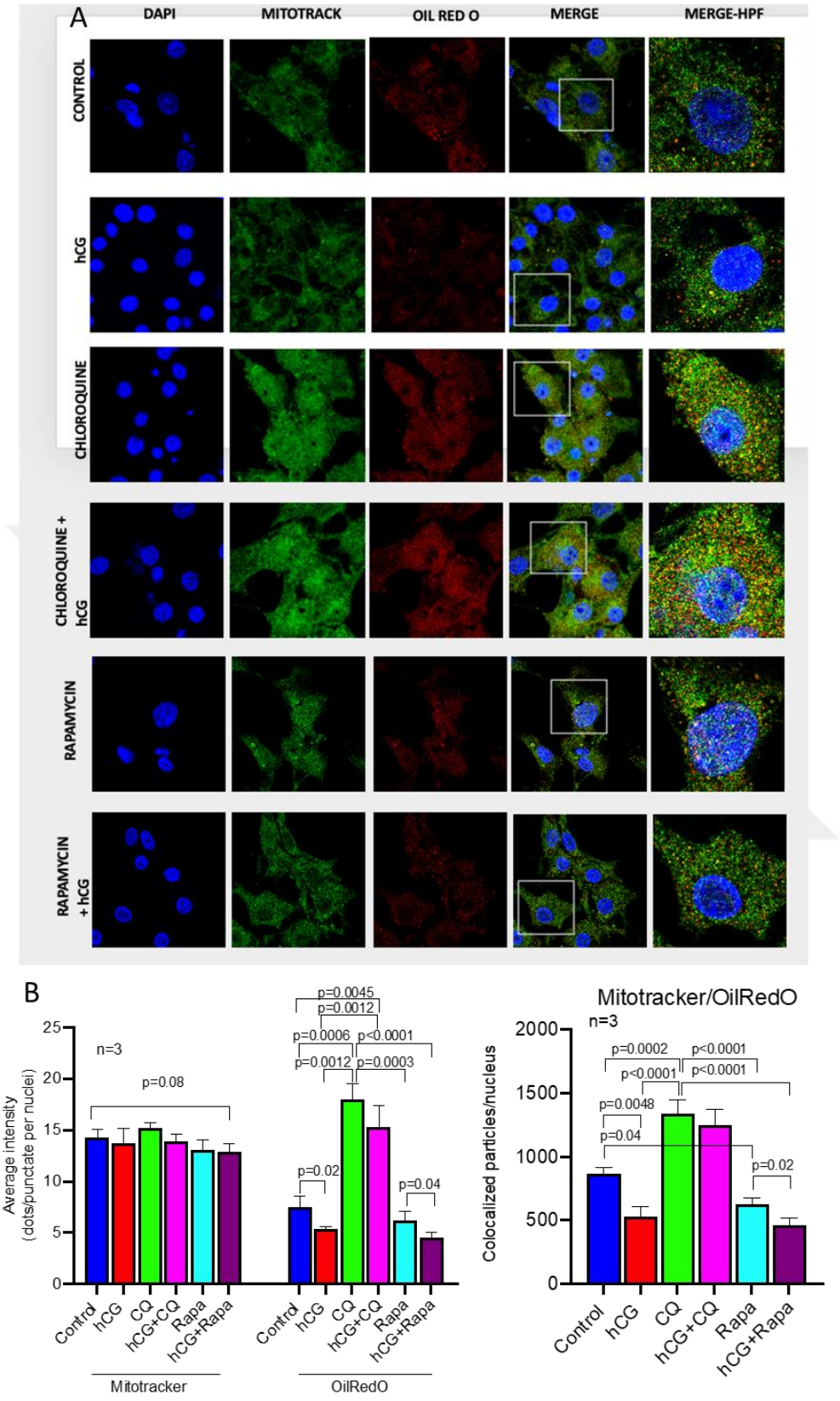

Figure 35. A) Confocal images of hCG ± chloroquine and hCG ± rapamycin treatments on luteal GCs in which changes in Oil Red O and its colocalization with mitochondria is

observed. B) Quantification of Oil Red O dots, mitochondria number and their colocalization.

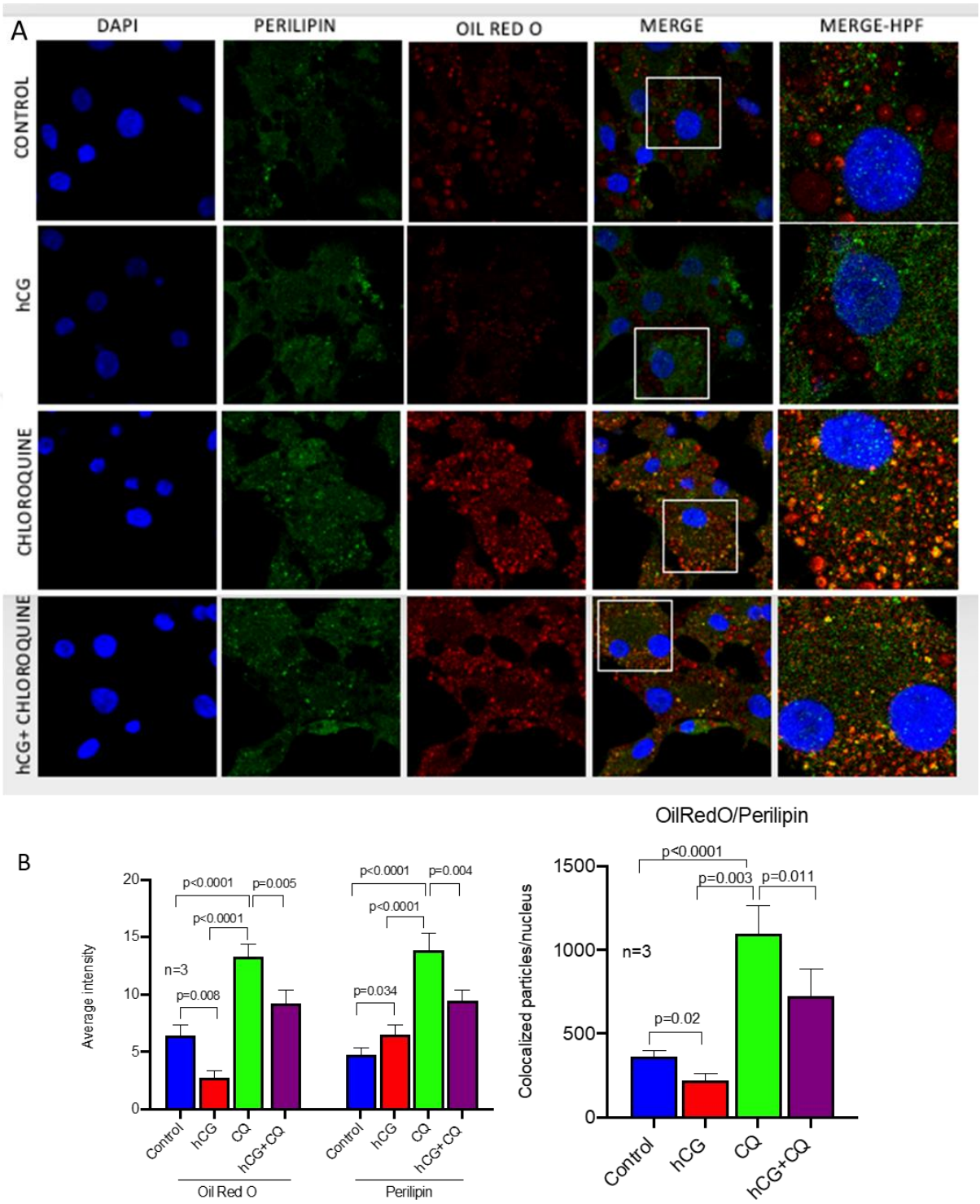

Figure 36. A) Confocal images of hCG ± chloroquine treatments on luteal GCs in which changes in Oil Red O and its colocalization with lipid droplets (Perilipin3/TIP47) is

observed. B) Quantification of Oil Red O dots, Perilipin 3 change in expression and their colocalization.

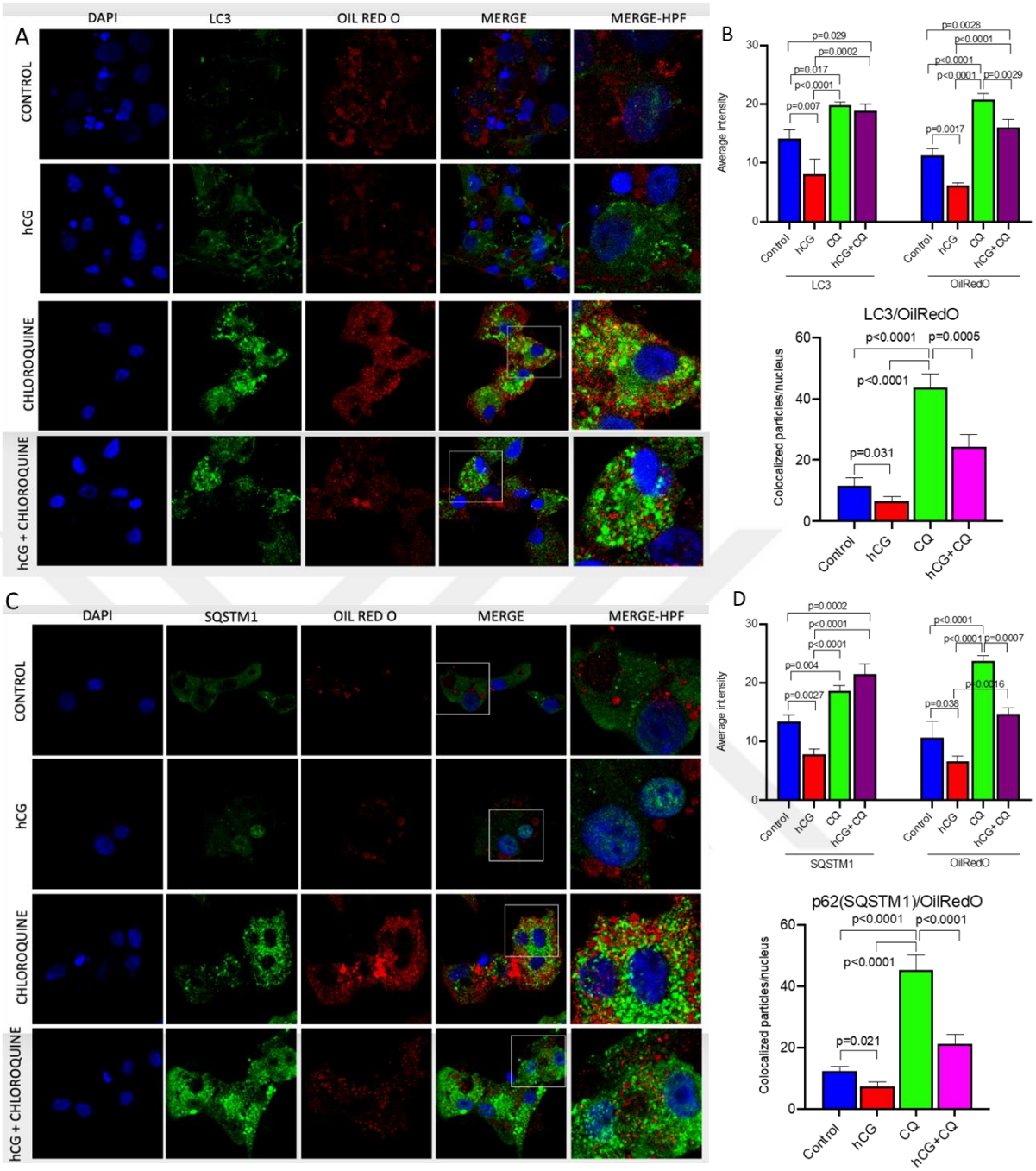

Figure 37. A-C) Confocal images of hCG ± chloroquine treatments on luteal GCs in which changes in Oil Red O and its colocalization with key autophagic proteins LC3 and p62 is observed. B-D) Quantification of Oil Red O dots, LC3 and p62 change in expression and their colocalization.

Taken collectively our findings demonstrate that:

i) the inhibition of autophagy impairs basal and hCG-induced P4 steroidogenesis of the cells and leads to an accumulation of the lipids mainly in the form of LDs, and

ii) the LDs co-localizes with autophagosome markers LC3 and SQSTM1 especially after autophagy was inhibited.

By contrast, autophagy induction with rapamycin produces the opposite effect and improves steroidogenesis particularly in the presence of hCG. Both rapamycin and hCG treatment are associated with the presence of less LDs in the cells, suggesting that autophagy induction and stimulation of steroidogenesis enhance their utilization for steroidogenesis. In the light of these observations we hypothesized that autophagy may play role in the degradation of lipids (lipophagy), which are utilized for steroid hormone synthesis in the steroidogenic cells.

In order to test our hypothesis that autophagic degradation of lipids occurs to provide free cholesterol for steroid hormone synthesis, we next investigated whether or not the LDs co-localize with autophagy markers/substrates and lysosome. We found that the signal intensity of the LD marker perilipin3 and its co-localization with lysosome marker LAMP2 gradually increased in the confocal images of the cells exposed to increasing concentrations of hCG (1-5-10 IU/mL)(Fig. 38). Consistent with this observation, the expression of perilipin3 gradually increased along with StAR and 3β-HSD expression in immunoblot analysis (Fig. 39 A) and P4 production (Fig. 39 C) in a dose dependent manner after treatment with hCG at the indicated concentrations.

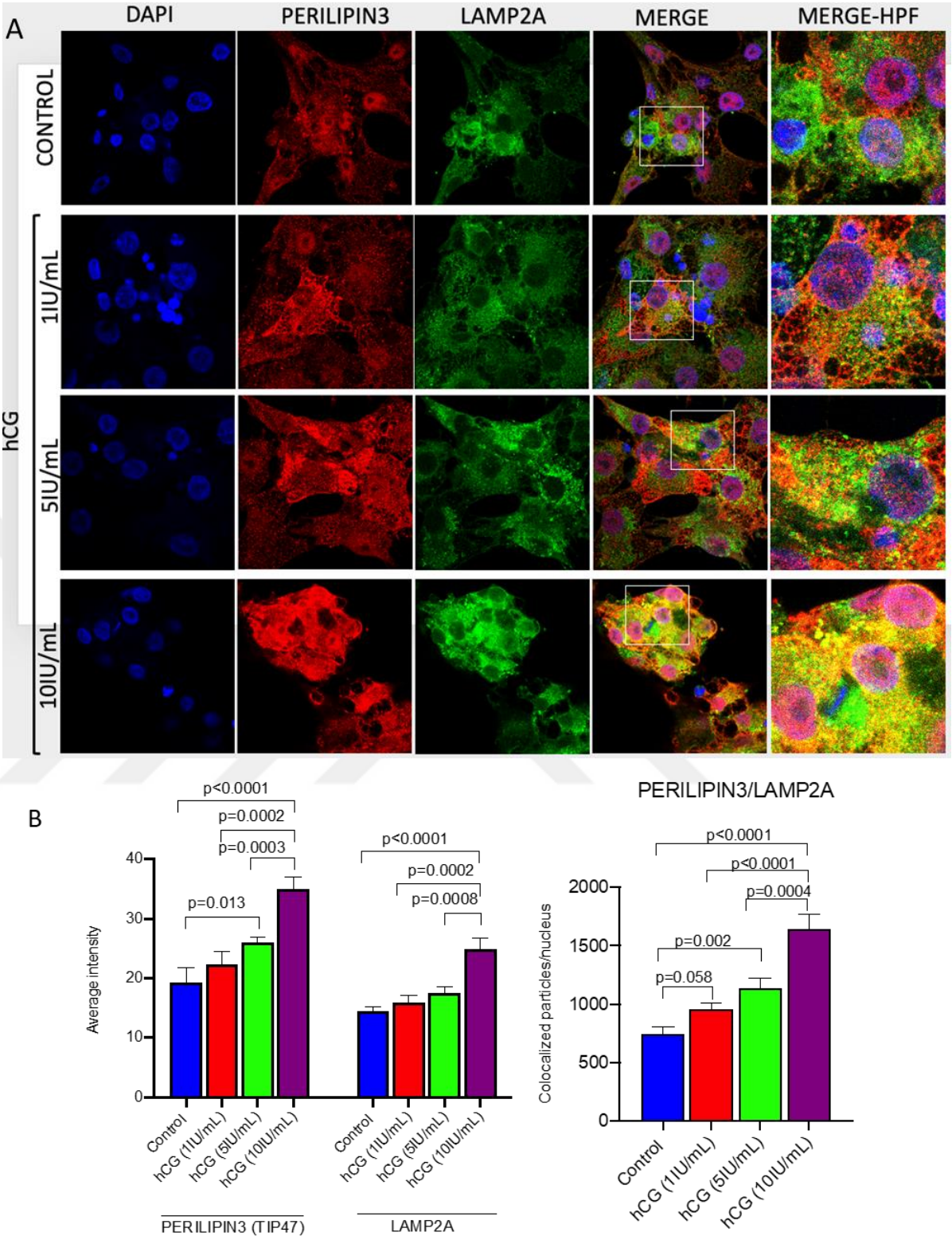

Figure 38. Confocal images of dose dependent hCG treatment of human luteal GCs. A) Changes in LAMP2A and Perilipin 3 expression and their colocalization is observed.

B) Quantification of LAMP2A and Perilipin 3 change in expression and their colocalization.

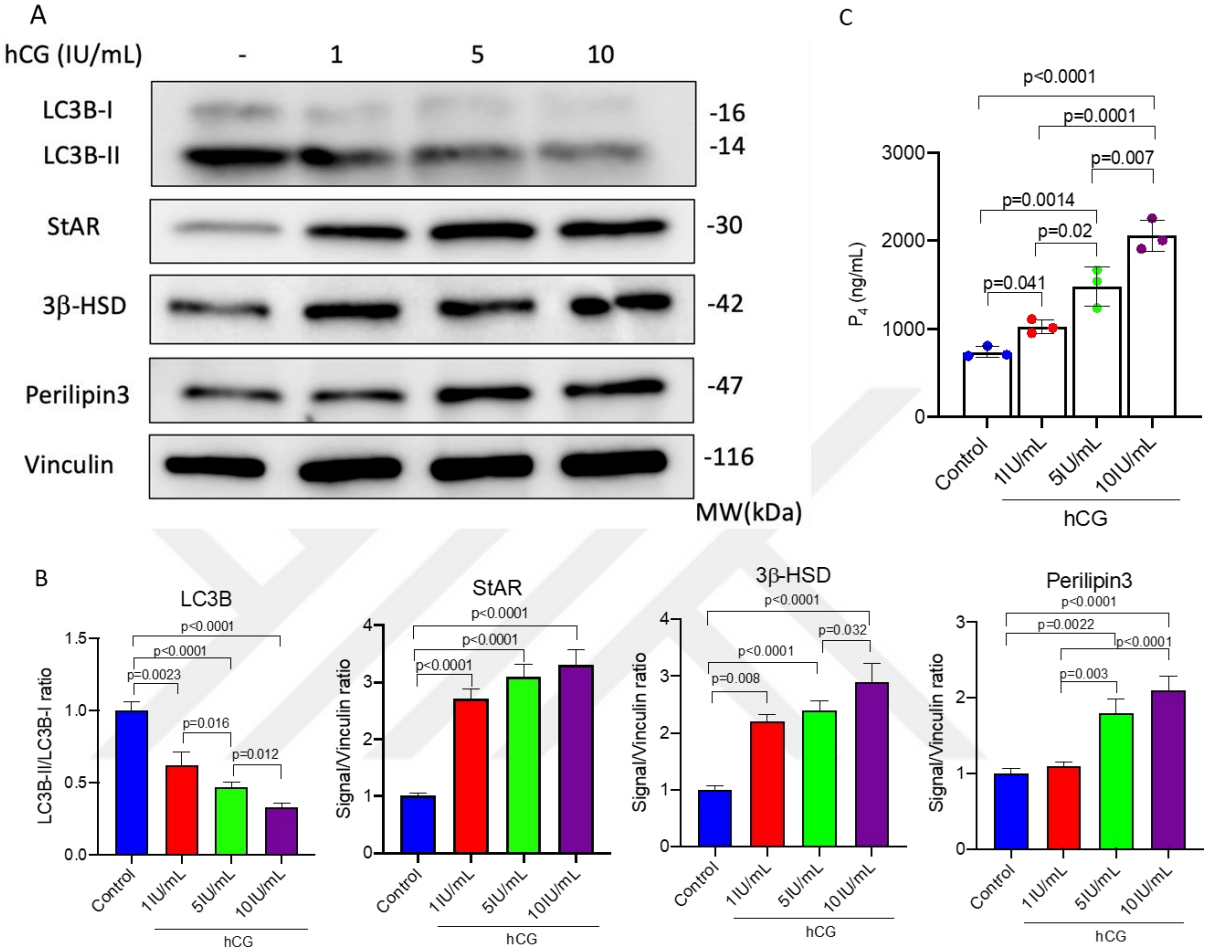

Figure 39. A) Western Blot of hCG dose dependent treatment on luteal GCs. B) Quantification of changes on protein expression on A. C) P4 synthesis change due to the hCG dose dependent treatment.

These findings suggest that hCG appears to stimulate steroid biosynthesis by promoting perilipin production and therefore, the production of the LDs and their association with lysosome in the cells to provide more cholesterol for steroid biosynthesis.

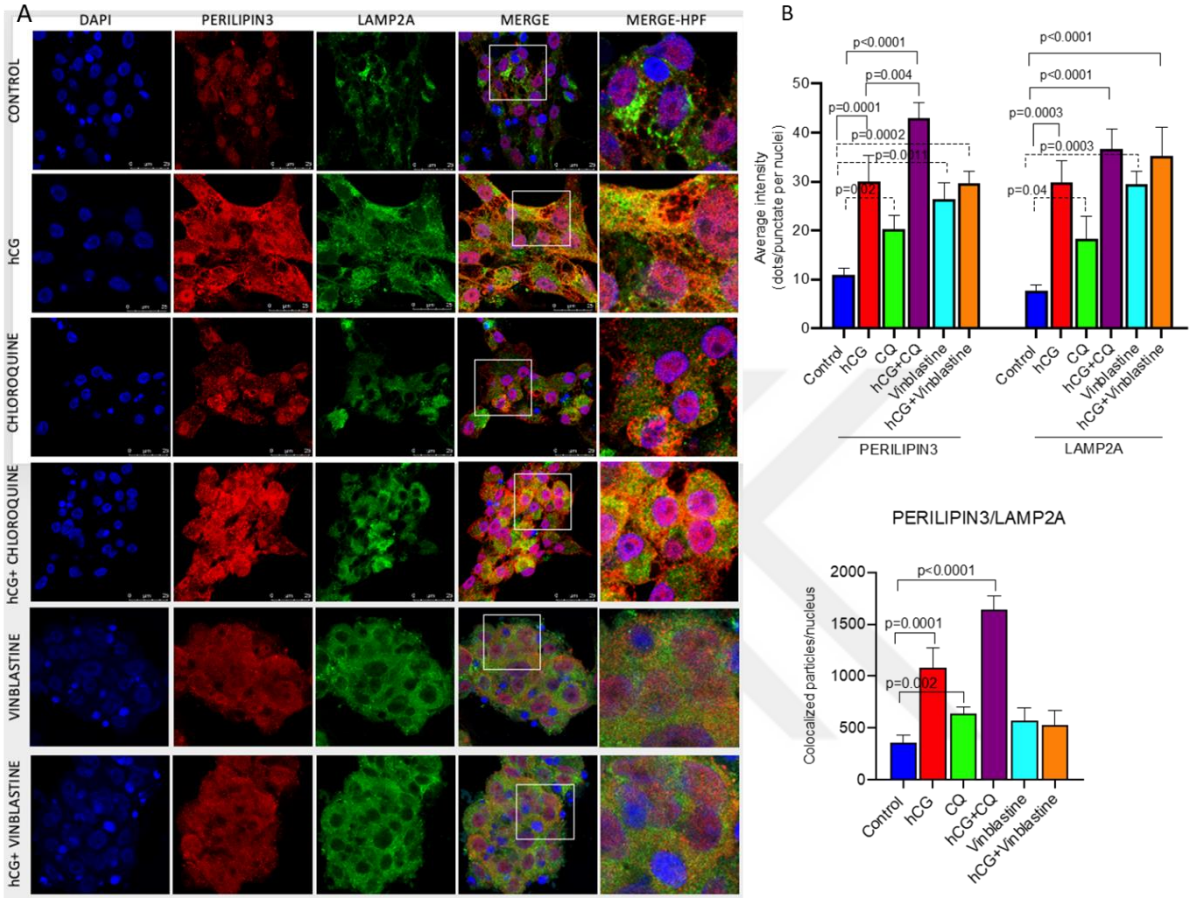

Figure 40. A) Confocal images of hCG ± chloroquine and hCG ± vinblastine treatments on luteal GCs in which changes in expression of Perilipin 3/TIP47, LAMP2A and their colocalization is observed. B) Quantification of perilipin 3/TIP47, LAMP2A and their colocalization.

In order to investigate the possible role of autophagy in this process we next analysed under confocal microscopy how perilipin3/LAMP2 (lysosome-associated membrane protein-2) co-localization change when autophagy is blocked at different stages, namely; with lysosomal hydrolysis stage (chloroquine), autophagosome lysosome

fusion stage (vinblastine) or; genetically interrupted via Atg5 gene knock-down with siRNA (initial stage of autophagosome formation). Chloroquine treatment resulted in a marked perilipin3 accumulation and an increase in the perilipin3/LAMP2 co-localization compared to control cells. And these effects became more evident when chloroquine was combined with hCG. Vinblastine treatment caused perilipin3 accumulation as well. But perilipin3/LAMP2A co-localization was considerably lesser than chloroquine treated cells. Further, hCG addition to vinblastine did not cause such an increase in this co-localization. (Fig. 40).

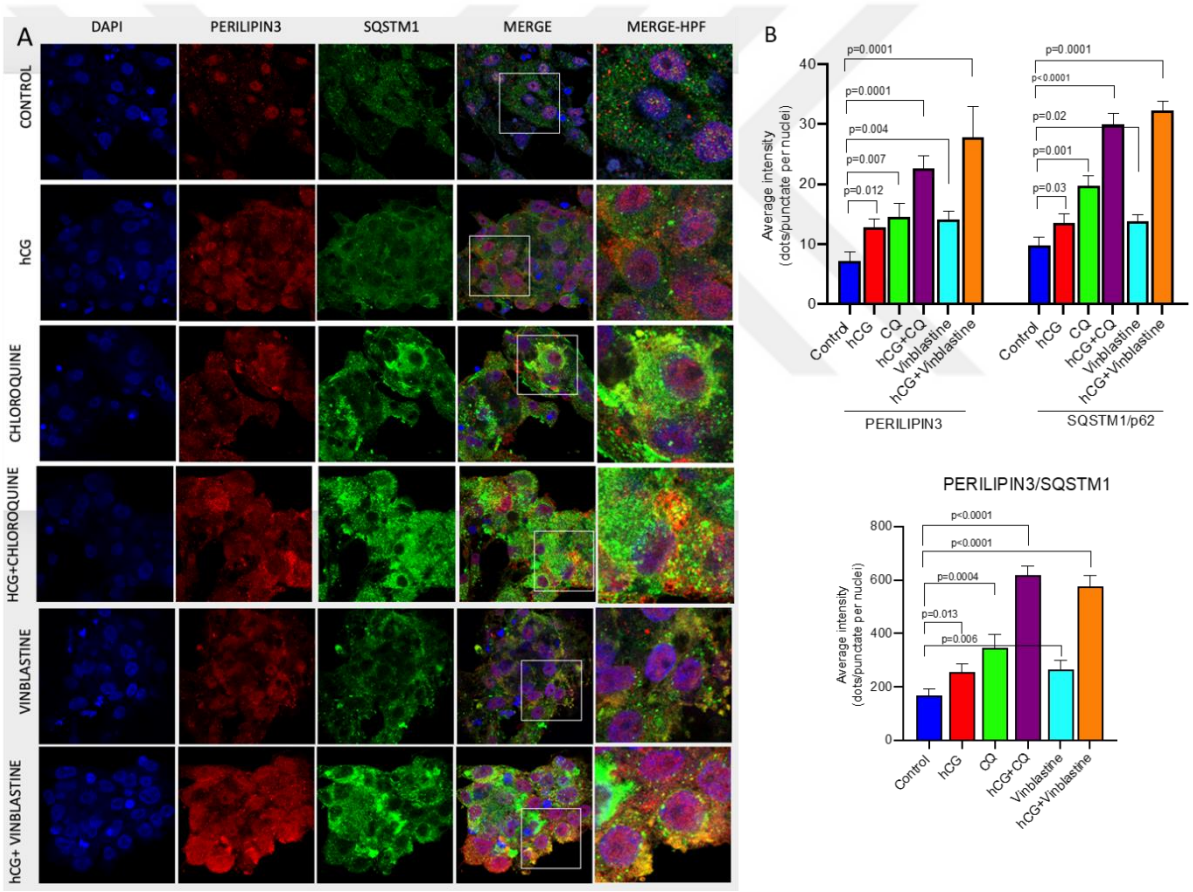

Figure 41. A) Confocal images of hCG ± chloroquine and hCG ± vinblastine treatments on luteal GCs in which changes in expression of Perilipin 3, SQSTM1 and their colocalization is observed. B) Quantification of perilipin 3, SQSTM1 and their colocalization.

3.10. Lipid droplet trafficking to lysosome is mediated by autophagosomes

In support of our hypothesis that autophagosome mediates the delivery of the LDs to lysosome for steroid hormone synthesis we also demonstrated in the confocal images that perilipin3 associates with autophagosome adaptor protein SQSTM1 and perilipin/SQSTM1 co-localization increased after hCG treatment and this association became more evident when hCG was combined with chloroquine or vinblastine (Fig. 41).

In order to see if these observed effects are occurring in a dose-dependent fashion we treated the cells in another set of experiment with chloroquine or vinblastine at different concentrations without hCG co-treatment. We observed a gradual increase in perilipin3 accumulation and its co-localization with LAMP2A along with a progressive decline in P4 output in the cells treated with incremental concentrations of chloroquine. By contrast, vinblastine administration at increasing concentrations did not cause such an increase in perilipin3/LAMP2A co-localization although perilipin3 gradually accumulated and P4 output began to drop in a dose-dependent manner (Fig. 42).

We did not observe any meaningful increase in perilipin3/LAMP2A co-localization even after hCG stimulation when Atg5 gene was knocked-down in the cells compared to control cells transfected with scramble siRNA, signifying the importance of autophagosome formation in the association of the LDs with lysosome (Fig. 43).

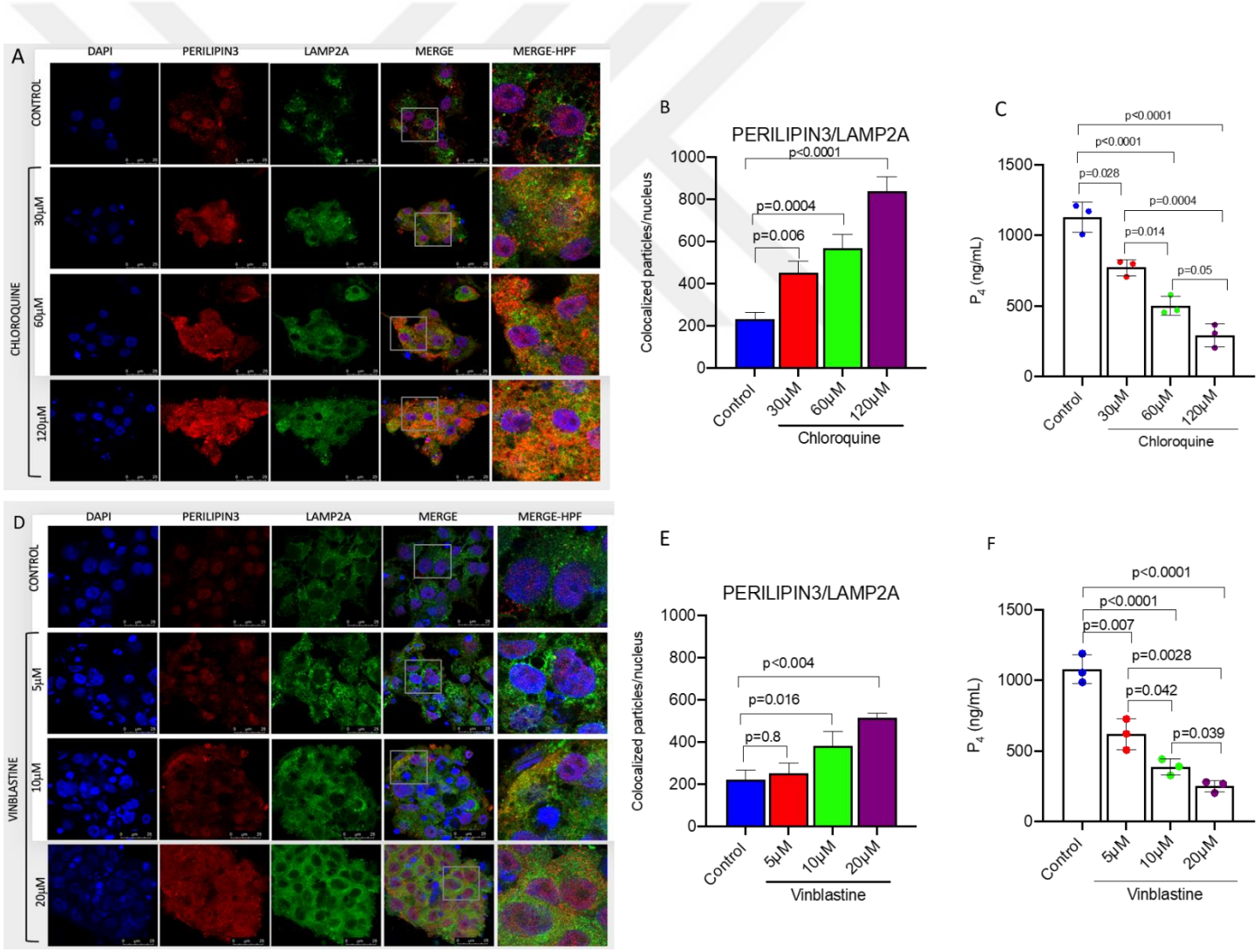

Figure 42. A, D) Confocal images of perilipin3/LAMP2A expression after chloroquine and vinblastine dose dependent treatments of luteal GCs. B, E) Their respective colocalization and C, F) P4 hormone synthesis.

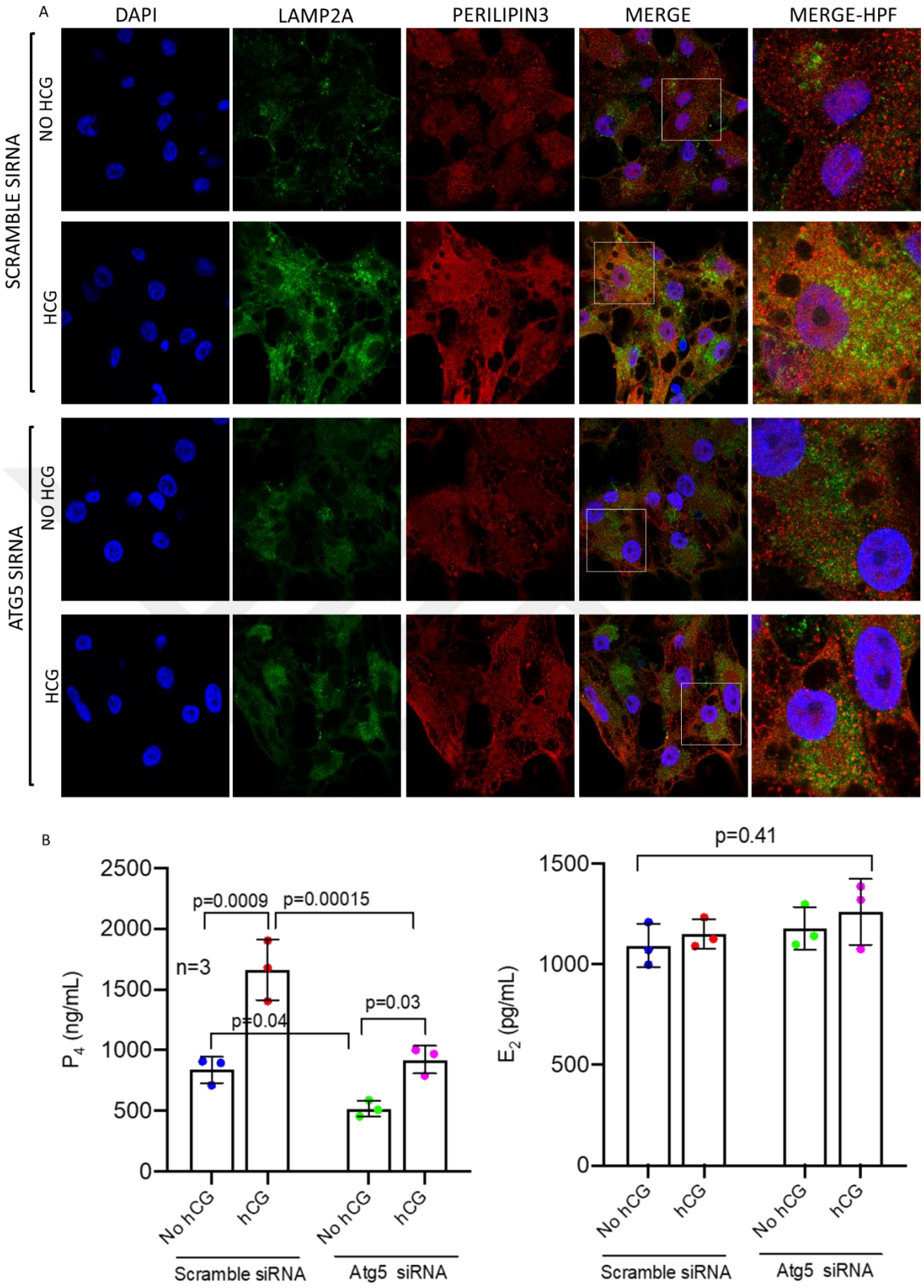

Figure 43. Confocal images of Atg5 siRNA in luteal GCs, combining with hCG treatment. B) Hormone synthesis levels following the treatments in A.

Taken altogether, these observations indicate that autophagy mediates the association of the LDs with lysosome via activating autophagosome formation to deliver the lipid cargo within the LDs to lysosomes for degradation to release free cholesterol required for steroid synthesis and hCG accelerates this process.

Taken collectively these findings indicate that hCG stimulates steroidogenesis by inducing the production of the perilipins and possibly the formation of the LDs and activating autophagosome formation to deliver the lipid cargo within the LDs to lysosomes for degradation to release free cholesterol required for steroid synthesis. The associations of the LDs with autophagosome to fuse with lysosome appears to be operative for basal P4 steroidogenesis that occurs without hCG stimulation because

i) Pharmacological inhibition or genetic disruption of autophagic flux impairs not only hCG-induced but also basal P4 production in the cells and
ii) The co-localization of perilipins with lysosome increases when lysosomal degradation was inhibited chloroquine without hCG co-treatment.

While Atg5 knock down possibly impairs steroidogenesis by disrupting autophagosome formation and therefore the association of the LDs with lysosomes; vinblastine perturbs the process by preventing the fusion of the LDs within the autophagosome with lysosome. Chloroquine disrupts the process by inhibiting lysosomal degradation of the lipid contents in the LDs after the fusion of autophagosome with lysosome.

3.11. Limitations of this study

This study is the first of its kind to be performed in human luteal GCs, at the best of our knowledge. Since our isolated cells are taken after the LH surge, they exhibit only a fraction of general human luteal GCs in terms of molecular characteristics and are closer to a corpus luteum model since they are in the first steps of luteinization. For this reason studies including more general models like 3D culture or organoid models should be employed. This way our findings can be compared in terms of compatibility with these models if this is truly the case for the entire life cycle of human luteal GCs. Another limitation of this study stands in the fact that both pharmacological inhibition/activation of autophagy as a process and/or genetic interruption of autophagic genes cannot be very selective. The reason for this arises from the fact that pharmacological activation/inhibition targets lysosome mostly, a vital organelle which is a crossing point for many important cellular processes or targets master key proteins like mTOR and AMPK, which are crossing points of many cellular pathways. A more selective and efficient targeting solely autophagic process is required in order to get a better grasping of the effect of the autophagy in female reproduction system as a whole.

Chapter 4: Discussion

Bibliography

1- De Duve C, Pressman BC, Gianetto R, Wattiaux R, Appelmans F. Tissue fractionation studies. 6. Intracellular distribution patterns of enzymes in rat-liver tissue. Biochem J. 1955;60(4):604-617.

2- Tsukada M, Ohsumi Y. Isolation and characterization of autophagy-defective mutants of Saccharomyces cerevisiae. FEBS Lett. 1993;333(1-2):169-174.

3- Kawabata T, Yoshimori T. Autophagosome biogenesis and human health. Cell Discov. 2020;6(1):33. Published 2020 Jun 2.

4- Kaushik S, Cuervo AM. Chaperone-mediated autophagy: a unique way to enter the lysosome world. Trends Cell Biol. 2012;22(8):407-417.

5- Hayashi-Nishino M, Fujita N, Noda T, Yamaguchi A, Yoshimori T, Yamamoto A. A subdomain of the endoplasmic reticulum forms a cradle for autophagosome formation. Nat Cell Biol. 2009;11(12):1433-1437.

6- Ravikumar B, Moreau K, Jahreiss L, Puri C, Rubinsztein DC. Plasma membrane contributes to the formation of pre-autophagosomal structures [published correction appears in Nat Cell Biol. 2010 Oct;12(10):1021]. Nat Cell Biol. 2010;12(8):747-757.

7- Hailey DW, Rambold AS, Satpute-Krishnan P, et al. Mitochondria supply membranes for autophagosome biogenesis during starvation. Cell. 2010;141(4):656-667.

8- Dupont N, Chauhan S, Arko-Mensah J, et al. Neutral lipid stores and lipase PNPLA5 contribute to autophagosome biogenesis. Curr Biol. 2014;24(6):609-620.

9- Karanasios E, Walker SA, Okkenhaug H, et al. Autophagy initiation by ULK complex assembly on ER tubulovesicular regions marked by ATG9 vesicles. Nat Commun. 2016; 7:12420.

10- Ge L, Zhang M, Kenny SJ, et al. Remodeling of ER-exit sites initiates a membrane supply pathway for autophagosome biogenesis. EMBO Rep. 2017;18(9):1586-1603.

11- Zhao YG, Liu N, Miao G, Chen Y, Zhao H, Zhang H. The ER Contact Proteins VAPA/B Interact with Multiple Autophagy Proteins to Modulate Autophagosome Biogenesis. Curr Biol. 2018;28(8):1234-1245.

12- Nishimura T, Tooze SA. Emerging roles of ATG proteins and membrane lipids in autophagosome formation. Cell Discov. 2020;6(1):32.
13- Dooley HC, Razi M, Polson HE, Girardin SE, Wilson MI, Tooze SA. WIPI2 links LC3 conjugation with PI3P, autophagosome formation, and pathogen clearance by recruiting Atg12-5-16L1. Mol Cell. 2014;55(2):238-252.
14- Bakula D, Müller AJ, Zuleger T, et al. WIPI3 and WIPI4 β-propellers are scaffolds for LKB1-AMPK-TSC signalling circuits in the control of autophagy. Nat Commun. 2017; 8:15637.
15- Slobodkin MR, Elazar Z. The Atg8 family: multifunctional ubiquitin-like key regulators of autophagy. Essays Biochem. 2013; 55:51-64.
16- Ichimura Y, Kirisako T, Takao T, et al. A ubiquitin-like system mediates protein lipidation. Nature. 2000;408(6811):488-492.
17- Fujita N, Hayashi-Nishino M, Fukumoto H, et al. An Atg4B mutant hampers the lipidation of LC3 paralogues and causes defects in autophagosome closure. Mol Biol Cell. 2008;19(11):4651-4659.
18- Kimura S, Noda T, Yoshimori T. Dynein-dependent movement of autophagosomes mediates efficient encounters with lysosomes. Cell Struct Funct. 2008;33(1):109-122.
19- Koyama-Honda I, Tsuboyama K, Mizushima N. ATG conjugation-dependent degradation of the inner autophagosomal membrane is a key step for autophagosome maturation. Autophagy. 2017;13(7):1252-1253.
20- Klionsky DJ, Abdalla FC, Abeliovich H, et al. Guidelines for the use and interpretation of assays for monitoring autophagy. Autophagy. 2012;8(4):445-544.
21- Romanov J, Walczak M, Ibiricu I, et al. Mechanism and functions of membrane binding by the Atg5-Atg12/Atg16 complex during autophagosome formation. EMBO J. 2012;31(22):4304-4317.
22- Kaufmann A, Beier V, Franquelim HG, Wollert T. Molecular mechanism of autophagic membrane-scaffold assembly and disassembly. Cell. 2014;156(3):469-481.
23- Yamamoto H, Kakuta S, Watanabe TM, et al. Atg9 vesicles are an important membrane source during early steps of autophagosome formation. J Cell Biol. 2012;198(2):219-233.

24- Scherz-Shouval R, Shvets E, Fass E, Shorer H, Gil L, Elazar Z. Reactive oxygen species are essential for autophagy and specifically regulate the activity of Atg4. EMBO J. 2019;38(10): e101812.
25- Cherra SJ 3rd, Kulich SM, Uechi G, et al. Regulation of the autophagy protein LC3 by phosphorylation. J Cell Biol. 2010;190(4):533-539.
26- Diao J, Liu R, Rong Y, et al. ATG14 promotes membrane tethering and fusion of autophagosomes to endolysosomes. Nature. 2015;520(7548):563-566.
27- Olsvik HL, Lamark T, Takagi K, et al. FYCO1 Contains a C-terminally Extended, LC3A/B-preferring LC3-interacting Region (LIR) Motif Required for Efficient Maturation of Autophagosomes during Basal Autophagy. J Biol Chem. 2015;290(49):29361-29374.
28- Wilkinson DS, Jariwala JS, Anderson E, et al. Phosphorylation of LC3 by the Hippo kinases STK3/STK4 is essential for autophagy. Mol Cell. 2015;57(1):55-68.
29- Jordens I, Fernandez-Borja M, Marsman M, et al. The Rab7 effector protein RILP controls lysosomal transport by inducing the recruitment of dynein-dynactin motors. Curr Biol. 2001;11(21):1680-1685.
30- Zhong Y, Wang QJ, Li X, et al. Distinct regulation of autophagic activity by Atg14L and Rubicon associated with Beclin 1-phosphatidylinositol-3-kinase complex. Nat Cell Biol. 2009;11(4):468-476.
31- Wang Z, Miao G, Xue X, et al. The Vici Syndrome Protein EPG5 Is a Rab7 Effector that Determines the Fusion Specificity of Autophagosomes with Late Endosomes/Lysosomes. Mol Cell. 2016;63(5):781-795.
32- Nakamura S, Hasegawa J, Yoshimori T. Regulation of lysosomal phosphoinositide balance by INPP5E is essential for autophagosome-lysosome fusion. Autophagy. 2016;12(12):2500-2501.
33- Abada A, Elazar Z. Getting ready for building: signaling and autophagosome biogenesis. EMBO Rep. 2014;15(8):839-852.
34- Laplante M, Sabatini DM. mTOR signaling in growth control and disease. Cell. 2012;149(2):274-293.
35- Kim DH, Sarbassov DD, Ali SM, et al. GbetaL, a positive regulator of the rapamycin-sensitive pathway required for the nutrient-sensitive interaction between raptor and mTOR. Mol Cell. 2003;11(4):895-904.

36- Peterson TR, Laplante M, Thoreen CC, et al. DEPTOR is an mTOR inhibitor frequently overexpressed in multiple myeloma cells and required for their survival. Cell. 2009;137(5):873-886.
37- Kaizuka T, Hara T, Oshiro N, et al. Tti1 and Tel2 are critical factors in mammalian target of rapamycin complex assembly. J Biol Chem. 2010;285(26):20109-20116.
38- Wang L, Harris TE, Roth RA, Lawrence JC Jr. PRAS40 regulates mTORC1 kinase activity by functioning as a direct inhibitor of substrate binding. J Biol Chem. 2007;282(27):20036-20044.
39- Hara K, Maruki Y, Long X, et al. Raptor, a binding partner of target of rapamycin (TOR), mediates TOR action. Cell. 2002;110(2):177-189.
40- Bonfils G, Jaquenoud M, Bontron S, Ostrowicz C, Ungermann C, De Virgilio C. Leucyl-tRNA synthetase controls TORC1 via the EGO complex. Mol Cell. 2012;46(1):105-110.
41- Wauson EM, Zaganjor E, Lee AY, et al. The G protein-coupled taste receptor T1R1/T1R3 regulates mTORC1 and autophagy. Mol Cell. 2012;47(6):851-862.
42- Sancak Y, Peterson TR, Shaul YD, et al. The Rag GTPases bind raptor and mediate amino acid signaling to mTORC1. Science. 2008;320(5882):1496-1501.
43- Inoki K, Li Y, Xu T, Guan KL. Rheb GTPase is a direct target of TSC2 GAP activity and regulates mTOR signaling. Genes Dev. 2003;17(15):1829-1834.
44- Jung CH, Jun CB, Ro SH, et al. ULK-Atg13-FIP200 complexes mediate mTOR signaling to the autophagy machinery. Mol Biol Cell. 2009;20(7):1992-2003.
45- Duran A, Amanchy R, Linares JF, et al. p62 is a key regulator of nutrient sensing in the mTORC1 pathway. Mol Cell. 2011;44(1):134-146.
46- Manning BD, Tee AR, Logsdon MN, Blenis J, Cantley LC. Identification of the tuberous sclerosis complex-2 tumor suppressor gene product tuberin as a target of the phosphoinositide 3-kinase/akt pathway. Mol Cell. 2002;10(1):151-162.
47- Roberts DJ, Tan-Sah VP, Ding EY, Smith JM, Miyamoto S. Hexokinase-II positively regulates glucose starvation-induced autophagy through TORC1 inhibition. Mol Cell. 2014;53(4):521-533.
48- Wei Y, Zou Z, Becker N, et al. EGFR-mediated Beclin 1 phosphorylation in autophagy suppression, tumor progression, and tumor chemoresistance. Cell. 2013;154(6):1269-1284.
49- Jutten B, Rouschop KM. EGFR signaling and autophagy dependence for growth, survival, and therapy resistance. Cell Cycle. 2014;13(1):42-51.

50- Lin SY, Li TY, Liu Q, et al. GSK3-TIP60-ULK1 signaling pathway links growth factor deprivation to autophagy [published correction appears in Science. 2012 Aug 17;337(6096):799]. Science. 2012;336(6080):477-481.
51- Deretic V, Saitoh T, Akira S. Autophagy in infection, inflammation, and immunity. Nat Rev Immunol. 2013;13(10):722-737.
52- Shi CS, Kehrl JH. TRAF6 and A20 regulate lysine 63-linked ubiquitination of Beclin-1 to control TLR4-induced autophagy. Sci Signal. 2010;3(123):ra42.
53- Shaw RJ, Bardeesy N, Manning BD, et al. The LKB1 tumor suppressor negatively regulates mTOR signaling. Cancer Cell. 2004;6(1):91-99.
54- Gwinn DM, Shackelford DB, Egan DF, et al. AMPK phosphorylation of raptor mediates a metabolic checkpoint. Mol Cell. 2008;30(2):214-226.
55- Kim J, Kim YC, Fang C, et al. Differential regulation of distinct Vps34 complexes by AMPK in nutrient stress and autophagy. Cell. 2013;152(1-2):290-303.
56- Decuypere JP, Welkenhuyzen K, Luyten T, et al. Ins (1,4,5)P3 receptor-mediated Ca2+ signaling and autophagy induction are interrelated. Autophagy. 2011;7(12):1472-1489.
57- Scherz-Shouval R, Shvets E, Fass E, Shorer H, Gil L, Elazar Z. Reactive oxygen species are essential for autophagy and specifically regulate the activity of Atg4. EMBO J. 2019;38(10): e101812.
58- Scherz-Shouval R, Elazar Z. Regulation of autophagy by ROS: physiology and pathology. Trends Biochem Sci. 2011;36(1):30-38.
59- Tang HW, Liao HM, Peng WH, Lin HR, Chen CH, Chen GC. Atg9 interacts with dTRAF2/TRAF6 to regulate oxidative stress induced JNK activation and autophagy induction. Dev Cell. 2013;27(5):489-503.
60- Sarkar S, Korolchuk VI, Renna M, et al. Complex inhibitory effects of nitric oxide on autophagy. Mol Cell. 2011;43(1):19-32.
61- Tripathi DN, Chowdhury R, Trudel LJ, et al. Reactive nitrogen species regulate autophagy through ATM-AMPK-TSC2-mediated suppression of mTORC1. Proc Natl Acad Sci U S A. 2013;110(32): E2950-E2957.
62- Mesmin B, Maxfield FR. Intracellular sterol dynamics. Biochim Biophys Acta. 2009;1791(7):636-645.
63- Steck TL, Lange Y. Cell cholesterol homeostasis: mediation by active cholesterol. Trends Cell Biol. 2010;20(11):680-687.

64- Ikonen E. Cellular cholesterol trafficking and compartmentalization. Nat Rev Mol Cell Biol. 2008;9(2):125-138.
65- Radhakrishnan A, Ikeda Y, Kwon HJ, Brown MS, Goldstein JL. Sterol-regulated transport of SREBPs from endoplasmic reticulum to Golgi: oxysterols block transport by binding to Insig. Proc Natl Acad Sci U S A. 2007;104(16):6511-6518.
66- Song BL, Javitt NB, DeBose-Boyd RA. Insig-mediated degradation of HMG CoA reductase stimulated by lanosterol, an intermediate in the synthesis of cholesterol. Cell Metab. 2005;1(3):179-189.
67- Lusa S, Heino S, Ikonen E. Differential mobilization of newly synthesized cholesterol and biosynthetic sterol precursors from cells. J Biol Chem. 2003;278(22):19844-19851.
68- Grundy SM. Absorption and metabolism of dietary cholesterol. Annu Rev Nutr. 1983; 3:71-96.
69- Miller WL, Bose HS. Early steps in steroidogenesis: intracellular cholesterol trafficking. J Lipid Res. 2011;52(12):2111-2135.
70- Ungewickell EJ, Hinrichsen L. Endocytosis: clathrin-mediated membrane budding. Curr Opin Cell Biol. 2007;19(4):417-425.
71- Jordens I, Marsman M, Kuijl C, Neefjes J. Rab proteins, connecting transport and vesicle fusion. Traffic. 2005;6(12):1070-1077.
72- Anderson RA, Sando GN. Cloning, and expression of cDNA encoding human lysosomal acid lipase/cholesteryl ester hydrolase. Similarities to gastric and lingual lipases. J Biol Chem. 1991;266(33):22479-22484.
73- Chang TY, Chang CC, Cheng D. Acyl-coenzyme A: cholesterol acyltransferase. Annu Rev Biochem. 1997; 66:613-638.
74- Connelly MA, Williams DL. SR-BI and cholesterol uptake into steroidogenic cells. Trends Endocrinol Metab. 2003;14(10):467-472.
75- Kraemer FB, Shen WJ, Harada K, et al. Hormone-sensitive lipase is required for high-density lipoprotein cholesteryl ester-supported adrenal steroidogenesis. Mol Endocrinol. 2004;18(3):549-557.
76- Murphy S, Martin S, Parton RG. Lipid droplet-organelle interactions; sharing the fats. Biochim Biophys Acta. 2009;1791(6):441-447.
77- Liu P, Bartz R, Zehmer JK, et al. Rab-regulated interaction of early endosomes with lipid droplets. Biochim Biophys Acta. 2007;1773(6):784-793.

78- Alpy F, Tomasetto C. Give lipids a START: the StAR-related lipid transfer (START) domain in mammals. J Cell Sci. 2005;118(Pt 13):2791-2801.
79- Strauss JF 3rd, Kishida T, Christenson LK, Fujimoto T, Hiroi H. START domain proteins and the intracellular trafficking of cholesterol in steroidogenic cells. Mol Cell Endocrinol. 2003;202(1-2):59-65.
80- Kallen CB, Billheimer JT, Summers SA, Stayrook SE, Lewis M, Strauss JF 3rd. Steroidogenic acute regulatory protein (StAR) is a sterol transfer protein. J Biol Chem. 1998;273(41):26285-26288.
81- Baker BY, Yaworsky DC, Miller WL. A pH-dependent molten globule transition is required for activity of the steroidogenic acute regulatory protein, StAR. J Biol Chem. 2005;280(50):41753-41760.
82- Moog-Lutz C, Tomasetto C, Régnier CH, et al. MLN64 exhibits homology with the steroidogenic acute regulatory protein (STAR) and is over-expressed in human breast carcinomas. Int J Cancer. 1997;71(2):183-191.
83- Alpy F, Stoeckel ME, Dierich A, et al. The steroidogenic acute regulatory protein homolog MLN64, a late endosomal cholesterol-binding protein. J Biol Chem. 2001;276(6):4261-4269.
84- Strauss JF 3rd, Liu P, Christenson LK, Watari H. Sterols, and intracellular vesicular trafficking: lessons from the study of NPC1. Steroids. 2002;67(12):947-951.
85- Sturley SL, Patterson MC, Balch W, Liscum L. The pathophysiology and mechanisms of NP-C disease. Biochim Biophys Acta. 2004;1685(1-3):83-87.
86- Infante RE, Wang ML, Radhakrishnan A, Kwon HJ, Brown MS, Goldstein JL. NPC2 facilitates bidirectional transfer of cholesterol between NPC1 and lipid bilayers, a step-in cholesterol egress from lysosomes. Proc Natl Acad Sci U S A. 2008;105(40):15287-15292.
87- Watari H, Blanchette-Mackie EJ, Dwyer NK, et al. NPC1-containing compartment of human granulosa-lutein cells: a role in the intracellular trafficking of cholesterol supporting steroidogenesis. Exp Cell Res. 2000;255(1):56-66.
88- Li H, Yao Z, Degenhardt B, Teper G, Papadopoulos V. Cholesterol binding at the cholesterol recognition/ interaction amino acid consensus (CRAC) of the peripheral-type benzodiazepine receptor and inhibition of steroidogenesis by an HIV TAT-CRAC peptide. Proc Natl Acad Sci U S A. 2001;98(3):1267-1272.

89- Rone MB, Fan J, Papadopoulos V. Cholesterol transport in steroid biosynthesis: role of protein-protein interactions and implications in disease states. Biochim Biophys Acta. 2009;1791(7):646-658.
90- Kokoszka JE, Waymire KG, Levy SE, et al. The ADP/ATP translocator is not essential for the mitochondrial permeability transition pore. Nature. 2004;427(6973):461-465.
91- Liu J, Rone MB, Papadopoulos V. Protein-protein interactions mediate mitochondrial cholesterol transport and steroid biosynthesis. J Biol Chem. 2006;281(50):38879-38893.
92- Miller WL, Auchus RJ. The molecular biology, biochemistry, and physiology of human steroidogenesis and its disorders [published correction appears in Endocr Rev. 2011 Aug;32(4):579]. Endocr Rev. 2011;32(1):81-151.
93- Moore CC, Brentano ST, Miller WL. Human P450scc gene transcription is induced by cyclic AMP and repressed by 12-O-tetradecanoylphorbol-13-acetate and A23187 through independent cis elements. Mol Cell Biol. 1990;10(11):6013-6023.
94- Parker KL, Schimmer BP. Steroidogenic factor 1: a key determinant of endocrine development and function. Endocr Rev. 1997;18(3):361-377.
95- Pawlak KJ, Prasad M, Thomas JL, Whittal RM, Bose HS. Inner mitochondrial translocase Tim50 interacts with 3β-hydroxysteroid dehydrogenase type 2 to regulate adrenal and gonadal steroidogenesis. J Biol Chem. 2011;286(45):39130-39140.
96- Edson MA, Nagaraja AK, Matzuk MM. The mammalian ovary from genesis to revelation. Endocr Rev. 2009;30(6):624-712.
97- Kumar TR, Wang Y, Lu N, Matzuk MM. Follicle stimulating hormone is required for ovarian follicle maturation but not male fertility. Nat Genet. 1997;15(2):201-204.
98- Eppig JJ, Wigglesworth K, Pendola FL. The mammalian oocyte orchestrates the rate of ovarian follicular development. Proc Natl Acad Sci U S A. 2002;99(5):2890-2894.
99- Magoffin DA. Ovarian theca cell. Int J Biochem Cell Biol. 2005;37(7):1344-1349.
100- Diaz FJ, Wigglesworth K, Eppig JJ. Oocytes determine cumulus cell lineage in mouse ovarian follicles. J Cell Sci. 2007;120(Pt 8):1330-1340.

101- Richards JS. Hormonal control of gene expression in the ovary. Endocr Rev. 1994;15(6):725-751.

102- Conti M. Specificity of the cyclic adenosine 3',5'-monophosphate signal in granulosa cell function. Biol Reprod. 2002;67(6):1653-1661.

103- Yong EL, Hillier SG, Turner M, et al. Differential regulation of cholesterol side-chain cleavage (P450scc) and aromatase (P450arom) enzyme mRNA expression by gonadotrophins and cyclic AMP in human granulosa cells. J Mol Endocrinol. 1994;12(2):239-249.

104- Young JM, McNeilly AS. Theca: the forgotten cell of the ovarian follicle. Reproduction. 2010;140(4):489-504.

105- Reed BG, Carr BR. The Normal Menstrual Cycle and the Control of Ovulation. In: Feingold KR, Anawalt B, Boyce A, et al., eds. Endotext. South Dartmouth (MA): MDText.com, Inc.; August 5, 2018.

106- Cole LA. Biological functions of hCG and hCG-related molecules. Reprod Biol Endocrinol. 2010; 8:102. Published 2010 Aug 24.

107- Kimmel AR, Sztalryd C. The Perilipins: Major Cytosolic Lipid Droplet-Associated Proteins and Their Roles in Cellular Lipid Storage, Mobilization, and Systemic Homeostasis. Annu Rev Nutr. 2016; 36:471-509.

108- Ong KT, Mashek MT, Bu SY, Greenberg AS, Mashek DG. Adipose triglyceride lipase is a major hepatic lipase that regulates triacylglycerol turnover and fatty acid signaling and partitioning. Hepatology. 2011;53(1):116-126.

109- Singh R, Kaushik S, Wang Y, et al. Autophagy regulates lipid metabolism. Nature. 2009;458(7242):1131-1135.

110- Sathyanarayan A, Mashek MT, Mashek DG. ATGL Promotes Autophagy/Lipophagy via SIRT1 to Control Hepatic Lipid Droplet Catabolism. Cell Rep. 2017;19(1):1-9.

111- Kaushik S, Cuervo AM. Degradation of lipid droplet-associated proteins by chaperone-mediated autophagy facilitates lipolysis. Nat Cell Biol. 2015;17(6):759-770.

112- Zhang H, Yan S, Khambu B, et al. Dynamic MTORC1-TFEB feedback signaling regulates hepatic autophagy, steatosis, and liver injury in long-term nutrient oversupply. Autophagy. 2018;14(10):1779-1795.

113- Seo AY, Lau PW, Feliciano D, et al. AMPK and vacuole-associated Atg14p orchestrate μ-lipophagy for energy production and long-term survival under glucose starvation. Elife. 2017;6: e21690.

114- Seok S, Fu T, Choi SE, et al. Transcriptional regulation of autophagy by an FXR-CREB axis. Nature. 2014;516(7529):108-111.

115- Gao F, Li G, Liu C, et al. Autophagy regulates testosterone synthesis by facilitating cholesterol uptake in Leydig cells. J Cell Biol. 2018;217(6):2103-2119.

116- Galluzzi L, Bravo-San Pedro JM, Levine B, Green DR, Kroemer G. Pharmacological modulation of autophagy: therapeutic potential and persisting obstacles. Nat Rev Drug Discov. 2017;16(7):487-511.

117- Lobb DK, Younglai EV. A simplified method for preparing IVF granulosa cells for culture. J Assist Reprod Genet. 2006;23(2):93-95.

118- Bildik G, Akin N, Esmaeilian Y, et al. hCG Improves Luteal Function and Promotes Progesterone Output through the Activation of JNK Pathway in the Luteal Granulosa Cells of the Stimulated IVF Cycles†. Biol Reprod. 2020;102(6):1270-1280.

119- Bayasula, Iwase A, Kiyono T, et al. Establishment of a human nonluteinized granulosa cell line that transitions from the gonadotropin-independent to the gonadotropin-dependent status. Endocrinology. 2012;153(6):2851-2860.

120- Livak KJ, Schmittgen TD. Analysis of relative gene expression data using real-time quantitative PCR and the 2(-Delta Delta C(T)) Method. Methods. 2001;25(4):402-408.